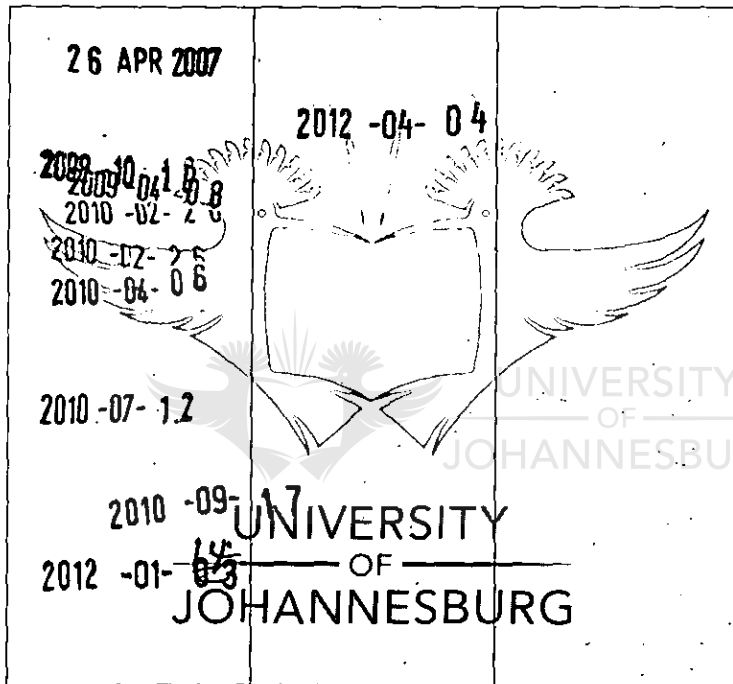


**UNIVERSITY OF JOHANNESBURG
UNIVERSITEIT VAN JOHANNESBURG**

AUCKLAND PARK KINGSWAY CAMPUS / KAMPUS
POSBUS 524 BOX 524
AUCKLAND PARK
2006
Tel: (011) 489-2165



This item must be returned on or before the last date stamped. A renewal for a further period may be granted provided the book is not in demand. Fines are charged on overdue items.

TM10
KRUG

**A NUMERICAL EVALUATION OF NONLINEAR
MATERIAL BEHAVIOUR AND GEOMETRIC
IMPERFECTIONS ON THE BEHAVIOUR OF 3CR12
HOT-ROLLED COLUMNS**

by

SUNITA KRUGER

DISSERTATION

Presented in Partial Fulfilment of the Requirements for the Degree

MAGISTER INGENERIAE



in the

**FACULTY OF ENGINEERING AND THE BUILT
ENVIRONMENT**

at the

UNIVERSITY OF JOHANNESBURG

SUPERVISOR: PROF R.F. LAUBSCHER

MAY 2006

A NUMERICAL EVALUATION OF NONLINEAR MATERIAL BEHAVIOUR AND GEOMETRIC IMPERFECTIONS ON THE BEHAVIOUR OF 3CR12 HOT- ROLLED COLUMNS

Abstract

3CR12 is corrosion-resisting steel containing 12% chrome. The corrosion-resisting characteristics of 3CR12 are between those of carbon steel and existing stainless steels. Since the material properties of 3CR12 differ from carbon steel, the current SABS code of practice cannot be utilized in the design of hot-rolled components.

A numerical investigation into the effect of gradual yielding material behaviour on the buckling strength of 3CR12 columns is presented. The columns under investigation was hot-rolled channel (152×76×18) sections. The influence of material and geometric non-linearities were investigated numerically. The effect of residual stresses was also investigated.

Material data for the Finite Element Model was obtained experimentally via compression tests. The magnitude and distribution of the residual stresses were obtained experimentally by using the sectioning method.

The results obtained from the Finite Element Analysis are compared to the buckling load predictions of the South African Code of Practice (SABS 0162-1:1993). Conclusions are made regarding the applicability to hot-rolled 3CR12 sections.

A NUMERICAL EVALUATION OF NONLINEAR MATERIAL BEHAVIOUR AND GEOMETRIC IMPERFECTIONS ON THE BEHAVIOUR OF 3CR12 HOT- ROLLED COLUMNS

OPSOMMING

3CR12 is 'n korrosie-werende staal wat 12% chroom bevat. Die korrosie-werende eienskappe van 3CR12 is tussen die van koolstof staal en bestaande vlekvrystaal. Omdat die materiaaleienskappe van vlekvrystaal verskil van die van koolstof staal, kan die bestaande kode SABS 0162-1:1993 nie gebruik word vir die ontwerp van 3CR12 komponente nie.

'n Numeriese analise op die invloed van die gelydelik-swiggende gedrag op die klinksterkte van 3CR12 kolumne word in hierdie verhandeling bestudeer. Die spesifieke seksies waarna gekyk word is warmgewalste kanaalseksies (152×76×18). Die invloed van beide materiaal en geometriese nie-lineariteite word numeries bestudeer. Die invloed van residuele spannings word ook na gekyk.

Materiaal data vir gebruik in die numeriese analises is deur middel van samedrukkings toetse bepaal. Die verspreiding en groottes van die residuele spannings is bepaal met behulp van die seksioneringsmetode.

Die resultate van die Eindige Element Analise word vergelyk met die klinksterktes soos voorspel deur die Suid-Afrikaanse ontwerpkode (SABS 0162-1:1993). Gevolgtrekkings word gemaak aangaande die toepasbaarheid van die Suid-Afrikaanse ontwerpkode vir 3CR12 warmgewalste seksies.

A NUMERICAL EVALUATION OF NONLINEAR MATERIAL BEHAVIOUR
AND GEOMETRIC IMPERFECTIONS ON THE BEHAVIOUR OF 3CR12 HOT-
ROLLED COLUMNS

ACKNOWLEDGEMENTS

I would like to thank the following people for their contribution to this thesis:

Prof R.F. Laubscher, my supervisor and Department Head, for his advice and guidance.

Mr. M Goossens and Mr. W. Dott for technical assistance with the experimental work.

The financial support of the Chromium Steel Research Group is gratefully acknowledged.

My husband Julius, for his love, endless encouragement, patience, assistance and understanding.



My parents, for their motivation and support.

A NUMERICAL EVALUATION OF NONLINEAR MATERIAL BEHAVIOUR
AND GEOMETRIC IMPERFECTIONS ON THE BEHAVIOUR OF 3CR12 HOT-
ROLLED COLUMNS

TABLE OF CONTENTS

ACKNOWLEDGEMENTS	4
1 INTRODUCTION	9
1.1 Introduction	9
1.2 Purpose of Investigation	10
1.3 Scope of Work	10
2 LITERATURE REVIEW	12
2.1 Stainless and Corrosion Resisting Steels	12
2.1.1 Introduction	12
2.1.2 Background on Stainless Steels	12
2.1.3 Numbering System for Alloy Identification	15
2.1.4 Physical Properties	15
2.1.5 Alloying Elements	18
2.1.6 Development of 3CR12 Corrosion Resisting Steel	20
2.1.7 Previous Research done on 3CR12	25
2.1.8 Manufacturing of Hot-rolled Sections	28
2.1.9 Code of Practice for Hot-rolled Steel in South Africa	31
2.1.10 Structural Steel Design in South Africa	31
2.2 Theory of Columns and Buckling	36
2.2.1 Introduction	36
2.2.2 Classical Column Theory	37
2.2.3 Inelastic Columns	38
3 FINITE ELEMENT MODELING	56
3.1 Introduction	56
3.1.1 Steady State Problems	56
3.1.2 Eigenvalue Problems	57
3.1.3 Transient Problems	58
3.1.4 General Theory	59
3.1.5 Applications of the Finite Element Method	61
3.1.6 Advantages of the Finite Element Method	67
3.2 Previous Research done on Column Strength using the Finite Element Method	68
3.3 "Abaqus" Finite Element Analysis Software	70
3.3.1 Introduction	70
3.3.2 Components of an ABAQUS Model	72
4 EXPERIMENTAL WORK	79
4.1 Introduction	79
4.2 Compression Tests	79
4.2.1 Theoretical Background	79
4.2.2 Compression Tests: Experimental Program	82
4.2.3 Results	85
4.2.4 Discussion of Compression Test Results	91
4.3 Residual Stresses	92
4.3.1 Introduction	92
4.3.2 Residual Stress Measurement	92
4.3.3 Experimental Procedure	93
4.3.4 Results	97

A NUMERICAL EVALUATION OF NONLINEAR MATERIAL BEHAVIOUR
AND GEOMETRIC IMPERFECTIONS ON THE BEHAVIOUR OF 3CR12 HOT-
ROLLED COLUMNS

4.3.5	Discussion of Results	101
5	FINITE ELEMENT ANALYSIS	102
5.1	Introduction	102
5.2	The Finite Element Model	102
5.2.1	Geometry	102
5.2.2	Material Properties	104
5.2.3	Step/Analysis	105
5.2.4	Interactions	106
5.2.5	Load / Boundary Conditions	107
5.2.6	Mesh	108
5.3	Simulations done in ABAQUS	113
5.3.1	Simulations to Compare with Experimental Work	113
5.3.2	Influence of Gradual Yielding Behaviour on Column Strength	116
5.3.3	Influence of Initial Out-of-Straightness	118
5.3.4	Influence of Eccentric Loading	122
5.3.5	Influence of Both Eccentric Loading and Initial Out-of-Straightness	124
5.3.6	Influence of Residual Stresses on Column Strength	125
5.3.7	Effect of both Residual Stress and Initial Imperfection	127
6	CONCLUSIONS AND RECOMMENDATIONS	129
6.1	General Remarks	129
6.2	Literature Review	129
6.3	Experimental Work	130
6.4	Finite Element Analysis	130
6.5	Overall Conclusion	131
6.6	Recommendations	132
	REFERENCES	133
	APPENDIX A: Derivation of Euler Load	137
	APPENDIX B: Results of Compression Tests	142
	APPENDIX C: Experimental Program	148
	Experimental Work	148
	APPENDIX D: Example Input File	151

A NUMERICAL EVALUATION OF NONLINEAR MATERIAL BEHAVIOUR AND GEOMETRIC IMPERFECTIONS ON THE BEHAVIOUR OF 3CR12 HOT- ROLLED COLUMNS

TABLE OF FIGURES

Figure 2.1: Stress-strain curves for 3CR12 Steel Plates [9]	22
Figure 2.2: Flow chart for various finished and semi-finished steel products [15]	29
Figure 2.3 The hot-rolling process [15]	30
Figure 2.4: Fix-ended Column [18]	33
Figure 2.5: Column Curves [18]	35
Figure 2.6: Engesser's Tangent Modulus Theory [21]	40
Figure 2.7: Reduced Modulus Concept [22]	41
Figure 2.8: Shanley's Column Model [22]	43
Figure 2.9: Column Curves and Imperfection Effects [19]	47
Figure 2.10: Residual Stress Pattern [27]	51
Figure 3.1: Descretization of a region into a number of Finite Elements [29]	60
Figure 3.2: Stress-strain curve for an elastic-plastic material under uniaxial tension.	62
Figure 3.3: Three States Linked Together [30]	71
Figure 3.4: Commonly used Element Families [30]	74
Figure 4.1: Dimensions of Channel Section Cuts (mm)	83
Figure 4.2: Channel Column cut into sections with strain gauges attached	84
Figure 4.3: Test Specimen fastened in the fixture	84
Figure 4.4: Experimental Setup	85
Figure 4.5: Variation of Proportional Limit for each section	88
Figure 4.6: Variation of Modulus of Elasticity	89
Figure 4.7: Variation of Modulus Yield Stress	90
Figure 4.8: Comparator	95
Figure 4.9: Indentations punched into Channel Section	96
Figure 4.10: Channel Section divided into Sections (mm)	96
Figure 4.11: Residual Stress (MPa) Distribution of 3CR12 Channel	99
Figure 4.12: Residual Stress Distribution(MPa) of 300WA Channel	100
Figure 5.1: Dimensions of Channel Section used in Simulations	103
Figure 5.2: Average Material Properties determined from Compression Tests	104
Figure 5.3: Tied interaction between rigid plates and Channel Column	106
Figure 5.4: Boundary Conditions	107
Figure 5.5: Time to Complete vs Element Size	110
Figure 5.6: Buckling Load vs. Element Size	111
Figure 5.7: Number of Elements vs Element Size	111
Figure 5.8: Tetrahedral Mesh	112
Figure 5.9: Comparison of FEM Results with Experimental Results	114
Figure 5.10: Example of a short column failed by yielding followed by Local Buckling	115
Figure 5.11: Example of a Slender Column Failing by Overall Flexural Buckling	115
Figure 5.12: Comparison between 300WA and 3CR12 Stress-Strain Curves	117
Figure 5.13: Column Strength of 3CR12 ($F_y = 300\text{MPa}$)	117
Figure 5.14: Column Curve for $L/500$	119
Figure 5.15: Column Curve for $L/1000$	119
Figure 5.16: Column Curve for $L/1500$	120
Figure 5.17: Column Curve $L/1000$ (300WA)	120
Figure 5.18: Perpendicular view of the thee-dimensional plot	123
Figure 5.19: Three-dimensional plot of Eccentric Applied Load	123
Figure 5.20: Influence of both Initial out-of-straightness and Eccentric Loading	125
Figure 5.21: Influence of Residual Stress on Column Strength	126
Figure 5.22: Columns Containing Residual Stresses and an Initial Curvature	128

A NUMERICAL EVALUATION OF NONLINEAR MATERIAL BEHAVIOUR
AND GEOMETRIC IMPERFECTIONS ON THE BEHAVIOUR OF 3CR12 HOT-
ROLLED COLUMNS

INDEX OF TABLES

<i>Table 2.1: Composition of Stainless Steels</i>	15
<i>Table 2.2: Chemical Composition of 3CR12 Steel(Both Columbus Standard and EN 10088)</i>	20
<i>Table 2.3: Physical Properties of 3CR12 [8]</i>	21
<i>Table 2.4: Mechanical Properties for type 3CR12 plate (1) and hot-rolled Sections (2)[9]</i>	23
<i>Table 3.1: Applications of Equilibrium Problems [29]</i>	57
<i>Table 3.2: Eigenvalue Problems which can be analyzed with FEM [29]</i>	57
<i>Table 3.3: Examples of Transient Problems[29]</i>	58
<i>Table 4.1: Mechanical Properties of 3CR12 as obtained from compression tests for a sectioned 3CR12 152×76×18 structural section</i>	86
<i>Table 4.2: Mechanical Properties categorized into Web and Flanges</i>	87
<i>Table 4.3: Results from 3CR12 Residual Stress Measurement</i>	97
<i>Table 4.4: Results from 300WA Channel Residual stress Measurement</i>	98
<i>Table 5.1: Properties of BS Taper Flange Channel</i>	103
<i>Table 5.2: Slenderness Ratio's for Various Column Lengths</i>	104
<i>Table 5.3: Mesh Size Sensitivity Results (600mm)</i>	109
<i>Table 5.4: Mesh Size Sensitivity Results (1000mm)</i>	109
<i>Table 5.5: Mesh Size Sensitivity Results (1800mm)</i>	109
<i>Table 5.6: Mesh Size Sensitivity Results (2600mm)</i>	110
<i>Table 5.7: Mesh Size Sensitivity Results (3400mm)</i>	110
<i>Table 5.8: Experimental Results</i>	113



UNIVERSITY
OF
JOHANNESBURG

1 INTRODUCTION

1.1 Introduction

In the field of strength of materials, the theory of the buckling strength of compression members in metal structures probably has the most diverse history. This is due to the fact that difficulties were encountered in the research, which can be credited partly to the peculiarities of the problem itself, and partly to the peculiarities of the material used to make these metal structures.

In South Africa structural steel design is usually conducted according to SABS 0162-1:1993-Limit –states design of hot-rolled steelwork. This code provides rules and requirements for the design, fabrication and erection of steel structures based on the limit states design philosophy.

Stainless steel has established itself as a corrosion resistant construction material and it has seen a wide usage in buildings and other structures. The applications of stainless steels as a decorative material have been extended to structural members. This project focuses on the use of hot-rolled 3CR12 corrosion resisting steel in columns.

The SABS code (0162-4 Part 4:1993) includes the specifications for 3CR12 cold-rolled sections, but since hot-rolled sections are relatively new, they are not yet included into this code. Before hot-rolled sections can be added, it is necessary that the 3CR12 hot-rolled sections are tested and evaluated for compliance and inclusion into this code of practice.

Being a new product hot-rolled 3CR12 sections are not covered in the standard code. One reason for the exclusion is because 3CR12 has shown some behavior as a gradually yielding steel [1], which means that there are certain material characteristics that influence the structural behavior differently than those for carbon steel. Hot-rolling introduces residual stresses in the sections. It also introduces geometrical imperfections such as initial out-of-straightness.

It is therefore necessary to investigate the effect of this gradual yielding behaviour, geometric imperfections and residual stresses on the critical axial resistance of the 3CR12 hot-rolled columns.

1.2 Purpose of Investigation

The purpose of this investigation is to determine the effect of non-linear material behavior, geometric imperfections and residual stresses on the structural resistance of hot-rolled 3CR12 sections by using the Finite Element Method. The influence of geometric imperfections on the critical axial resistance of 3CR12 will be determined by investigating the behavior of the following:

- Influence of Gradual Yielding Material Behaviour.
- Eccentrically Loaded Columns
- Initial Crooked Columns
- Columns containing both the above imperfections
- Columns containing Residual Stresses
- Columns containing both Residual Stresses and Initial Imperfections

The section under investigation is a hot-rolled channel section (152 x 76 x 18)

1.3 Scope of Work

In this study, the influence of the gradual yielding behaviour, geometric imperfections and residual stresses on 3CR12 hot-rolled channel sections ((152×76×18)) was investigated by means of the Finite Element Method. Compression tests were also conducted to determine the mechanical properties of the channel sections. The residual stresses contained in the channel sections were obtained experimentally via the sectioning method.

The first part of chapter 2 focuses on stainless steels by briefly discussing the background. The basic metallurgy of steels is investigated, as well as the numbering system used for alloy identification in South Africa. This chapter also discusses the

different components of stainless steel alloys. The history of 3CR12 corrosion resisting steel is discussed in brief. Since the specific sections under investigation in this study are hot-rolled, the manufacturing method of hot-rolled steel is also summarized. Previous research done on hot-rolled 3CR12 sections is briefly discussed. The second part of chapter 2 is devoted to the theory of columns and buckling. Inelastic Column theory are discussed in more detail, as well the factors influencing columns strength such as initial out-of-straightness and eccentricities. A short discussion on the influence of residual stresses is also presented.

Chapter 3 introduces the Finite Element Method by briefly summarizing the most important aspects. Previous studies done on column strength by using the Finite Element Method are discussed, as well as the Finite Element package ABAQUS used in this study.

Chapter 4 discusses the experimental program. This section describes the preparation of the members for compression tests, as well the as experimental procedure and the results. The experimental program for determining the residual stresses are also summarized, as well as the residual stresses obtained from the experiments.

The Finite Element Method is applied in Chapter 5 to determine buckling loads for different situations. The material properties obtained from the compression tests are used in all the simulations, as well as material properties obtained from previous buckling experiments.

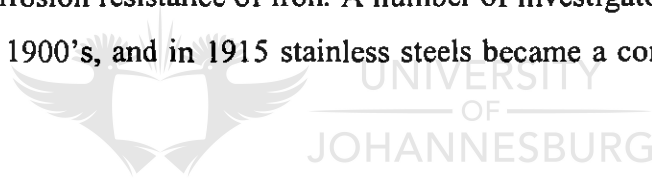
Chapter 6 summarizes the entire study briefly. A detailed discussion is given on the results of the Finite Element Analysis and the experimental program. The chapter concludes by proposing recommendations for future work.

2 LITERATURE REVIEW

2.1 Stainless and Corrosion Resisting Steels

2.1.1 Introduction

This chapter introduces stainless and corrosion resistant steels. The potential for iron-chromium alloys in reducing corrosion weren't noticed until the early part of the 20th century. One reason for this was that sulfuric acid was used to measure the corrosion resistance of metals. Metals were considered corrosion resistant if it did not react with sulfuric acid. Unfortunately, iron/chromium stainless steels are not well suited for used in reducing media such as sulfuric acid. Thus it was decided that chromium does not improve the corrosion resistance of iron. A number of investigators laid this myth to rest in the early 1900's, and in 1915 stainless steels became a commercial reality. [2]



2.1.2 Background on Stainless Steels

Stainless steels can resist corrosion in various situations. They are alloys of iron, chromium and other elements that assist the iron to withstand corrosive environments. To qualify as a stainless steel, the alloy must have a chromium content of at least 10% [2]. The steel alloy must also display passivity in oxidizing environments, i.e. the metal surface must inhibit electrochemical action between the metal and its environment.

2.1.2.1 Metallurgy of Stainless Steels

The major microstructural components available in steels are:

1. Ferrite: BCC iron
2. Cementite: an iron-carbon compound, Fe₃C
3. Pearlite: a lamellar composite of ferrite and cementite
4. Austenite: FCC iron

Hardened steel can also have a martensitic structure, which is a body-centered tetragonal iron. The equilibrium diagram for iron changes as soon as chromium is added, as well as the probable structures.

Stainless steels are categorized into three main categories according to their microstructure. Each group contains a number of alloys with slightly different compositions.[2] The American Iron and Steel Institute (AISI) uses a 3-digit designation number applies to 66 stainless steels. Thirty-nine are austenitic; and the remainder is ferritic or martensitic.

- **Ferritic Stainless Steel**

Ferritic stainless steels are characterized by a body-centered cubic ferrite microstructure, a carbon content less than 0.2%, and chromium contents between 16% and 20% [2]. Due to the higher chromium content, the corrosion resistance of the ferritic grades is superior to the martensitic grades [3]. The equilibrium structure of ferritic stainless steels is ferrite at room temperature, and all temperatures up to the melting point. Therefore these steels will not go through a crystal structure change, and it is not possible to quench harden these steels. Ferritic stainless steels also have poor weldability and notch sensitivity. Brittleness and/or reduced corrosion resistance may occur as a result of welding. [3] The motivation for substituting austenitic stainless steel with ferritic is because ferritic stainless steels are not susceptible to stress corrosion cracking.

Ferritic Stainless Steels are utilized for nitric acid services, water, food processing, automobile trim and for architectural applications.[3]

- **Martensitic Stainless Steel**

This group of stainless steels has a chromium content of approximately 12% to 18%, and their carbon content up to a maximum of 1.2% [2]. The reason for the high carbon content is to ensure on heating that these stainless steels will transform to austenite, enabling quench hardening. For a fully martensitic structure to develop, a carbon content of at least 0.6% is required. Hardenability in martensitic stainless steels is improved by large alloy additions of chromium which makes 100% martensitic structures possible with carbon contents of as low as 0.07%.

The combination of hardenability and stainless properties make these steels ideal for cutlery, turbine blades and high temperature parts. A flaw of the martensitic grades is that they are prone to absorption of atomic hydrogen, which causes hydrogen-assisted cracking (HAC), specifically in sulfide environments [3]. Similar to ferritic grades, they have a low impact resistance at low temperatures.

- **Austenitic Stainless Steels**

The austenitic stainless steels are considerably more complicated than the ferritic and austenitic stainless steels because at least four major alloy elements are present: iron, chromium, carbon and nickel. The carbon content is as low as possible in order to be feasible; chromium range from 16% to 26% and nickel content is typically at least 8% but can be increased up to 24% [2]. The complete austenitic structure is promoted by the presence of the nickel. Austenitic Stainless Steels are also nonmagnetic.

Austenitic stainless steels have a strong inclination to work harden. The transformation of the metastable austenite to martensite is promoted by the

energy of deformation. In commercial forms, austenitic stainless steels are undoubtedly austenitic. Nickel additions, or in some cases manganese, cause the austenite structure to form. Manganese is also an austenitizer.

2.1.3 Numbering System for Alloy Identification

In South Africa, both the European Standard EN 10088 [4] as well as the standards specified by the American Iron and Steel Institute (AISI) are used to identify stainless steels. The latter identifies wrought stainless steels by the three-digit system. The first digit indicates the classification by composition type. Table 2.1 shows the different compositions.

Table 2.1: *Composition of Stainless Steels*

Series	Alloys	Structure
200	Chromium, nickel, manganese or nitrogen	Austenitic
300	Chromium and Nickel	Austenitic
400	Chromium only	Ferritic or Martensitic
500	Low Chromium (<12%)	Martensitic

Low-chromium alloys are in the 500 series, and they do not contain sufficient chromium to be considered as stainless steels. These steels are intended to be heat-resisting steels.

2.1.4 Physical Properties

The properties of the different stainless steels vary from alloy to alloy, but a number of the physical properties are especially important since they can affect many design applications.

➤ Density

The density of stainless steel alloys are approximately the same as low-alloys or carbon steels, since these alloys are all iron based.

➤ Structure

The different structures of stainless steels have already been discussed. Where applications are concerned, the structure is only important as it affects mechanical properties.

Some stainless steels have an austenitic structure, which means that they are not ferromagnetic. Thus they cannot be used anywhere that a material must respond to a magnetic field. Austenitic stainless steels are also difficult to grind on machines with magnetic chucks.

➤ Conductivity

Stainless steels, when compared to carbon steels, are somewhat poor conductors of both heat and electricity [2]. Thermal conductivity is generally less than half than of carbon steels, while the electrical resistance can be as much as six times that of carbon steel.

➤ Expansion

The austenitic alloys have a thermal expansion coefficient that can be 50% higher than that of carbon steel [2]. The ferritics, martensitics, and PH stainless steels have similar expansion characteristics to that of carbon steel.



➤ Modulus of Elasticity

The moduli of elasticity of stainless steels are slightly lower than those carbon and alloy steels. Thus stainless steels will have slightly more elastic deflection than most steel for comparable section sizes. This lower modulus of elasticity often causes problems with coiled or flat springs. When a designer wants to substitute stainless steel for steels where elastic deflection is a consideration, caution must be used.

➤ Mechanical Properties

Since the largest tonnage of stainless steel is used in the chemical industry, the mechanical properties of stainless steels are quite important, and also the utilities industry, where they are used to contain corrosive materials [2].

The stainless steels have a variety of uses: tanks, piping, pressure vessels, stills, valves, and pumps etc, which all require good strength, toughness, and formability. The nuclear industry is one of the largest users of stainless steel, where it is used in piping and heat exchangers, operating at high-stress levels and often at high temperature. The most popular stainless steels used in this industry are the 300-series austenitics, since have better tensile properties, ductility and toughness when compared to mild steel.

Stainless also exhibit good oxidation resistance, and is therefore often used in furnaces where they must carry load at elevated temperatures. Austenitics also have superior creep characteristics than those of carbon steels or the ferritic grades.

The conclusion can be made that one of the definite advantages of stainless steels are their mechanical properties. These steels have the strength, toughness, and formability to meet a wide range of applications [1].

As already mentioned previously, the research done in this dissertation concentrates on columns made from a specific type of stainless steel called 3CR12. The next paragraph discusses the development of this steel.

2.1.5 Alloying Elements

Some of the alloying elements used in stainless steels are discussed below:

➤ Carbon

Carbon is kept to low levels in most stainless steels, except in martensitic stainless steel in which carbon is added in greater quantities to render these steel heat treatable by quenching and tempering to ensure the development of high strength and hardness [5].

➤ Chromium

Chromium is the alloying element responsible for the “stainlessness” of the steel. A minimum of approximately 11% is required, which causes a continuous, stable and inert chromium oxide film to form on the surface. Higher levels of chromium, up to a maximum of 26% will increase the corrosion resistance.

➤ Nickel

If nickel is added to steel in sufficient quantity, a fully austenitic crystal structure develops. These types of stainless steels are most commonly used.

➤ Molybdenum

This element enhances the passivity of the chromium oxide film, and therefore enhances the steels corrosion resistance. The higher the quantity of Molybdenum, the more aggressive corrosive conditions the steel will be able to handle.

➤ Titanium

Titanium acts as a stabilizer, as it is a strong Titanium carbide former, and therefore prevents the formation of Chromium carbides. Thus titanium helps to prevent intergranular corrosion which occurs in the regions adjacent to the weld in welded components.

➤ Manganese

Manganese has the same ability as Nickel as it has the ability to promote the formation of an austenitic crystal structure. Manganese is to partially replace Nickel in the 200 series, and slightly increased in the free machining grades of stainless steel which contains sulphur or selenium [5].

➤ Sulphur

The levels of sulphur in an alloy is usually kept low (0.03% maximum), since it improves the machinability of the steel, but impairs the fabricational and mechanical properties, as well as the corrosion resistance.

➤ Nitrogen

Nitrogen promotes the formation of an austenitic crystal structure, and compliments Nickel in the N-grades of steel. These steel grades have yield strengths at sub-zero temperatures that have been vastly improved. Nitrogen is also used to increase the weldability and austenitic fraction of the crystal structure, in the so-called “second generation” duplex stainless steels.

2.1.6 Development of 3CR12 Corrosion Resisting Steel

3CR12 is also known as DIN 1.4003 and specified in the German standard [4]. Market research showed there was a growing need for a corrosion-resistant steel with a lower chromium content, which is less expensive than the current austenitic stainless steels [6].

To fulfill this need, Middelburg Steel and Alloys started a research program to develop a low cost, weldable stainless steel. This new steel had to have corrosion-resisting characteristics between those of carbon steel and the existing stainless steels.

3CR12 was developed to bridge the gap between carbon steel which is not expensive and rusts easily, and stainless steel, which can cost up to three times that of ordinary carbon steel.

Type 3CR12, which is a modified AISI Type 409 steel, is a corrosion-resisting steel belonging to the group of ferritic stainless steels. The chemical composition can be seen in table 2.2, and the physical properties of 3CR12 are summarized in table 2.3. Each element is discussed briefly on the following pages.

Table 2.2: Chemical Composition of 3CR12 Steel (Both Columbus Standard and EN 10088)

Alloying Element	3CR12 [7]	EN10088 [4]
% Carbon (C)	0.03 max	0.03 max
% Manganese (Mn)	1.50 max	1.50
% Phosphorus (P)	0.04 max	0.04
% Sulphur (S)	0.03 max	≤ 0.015
% Silicon (Si)	1.00 max	1.00
% Nickel (Ni)	1.50 max	0.3-1.
% Nitrogen	-	0.03 max
% Titanium	0.60 max	-
% Chromium	11.00-12.00	10.5 to 12.5

Table 2.3: Physical Properties of 3CR12 [8]

Density		7680	kg/m ³
Elastic Modulus		200	Gpa
Poisson's Ratio		0.3	
Specific Heat Capacity		480	J/kg.K
Thermal Conductivity	200°C	31	W/mK
	300°C	32	W/mK
	400°C	32.1	W/mK
	500°C	31.5	W/mK
Electrical Resistivity		6.60E+10	Ωm
Mean Coefficient of Thermal Expansion	0-100°C	10.8	μm/mK
Expansion	0-300°C	11.3	μm/mK
	0-700°C	12.5	μm/mK
Melting Range		1430-1510°C	
Magnetic Properties		Ferromagnetic	

The mechanical properties (See table 2.2) [7] of stainless steels differ from those of carbon and low alloy steels. Because there is no obvious yield point in the stress-strain curve (See Figure 2.1), the mechanical properties of ordinary steels cannot normally be used in the place of stainless steels.

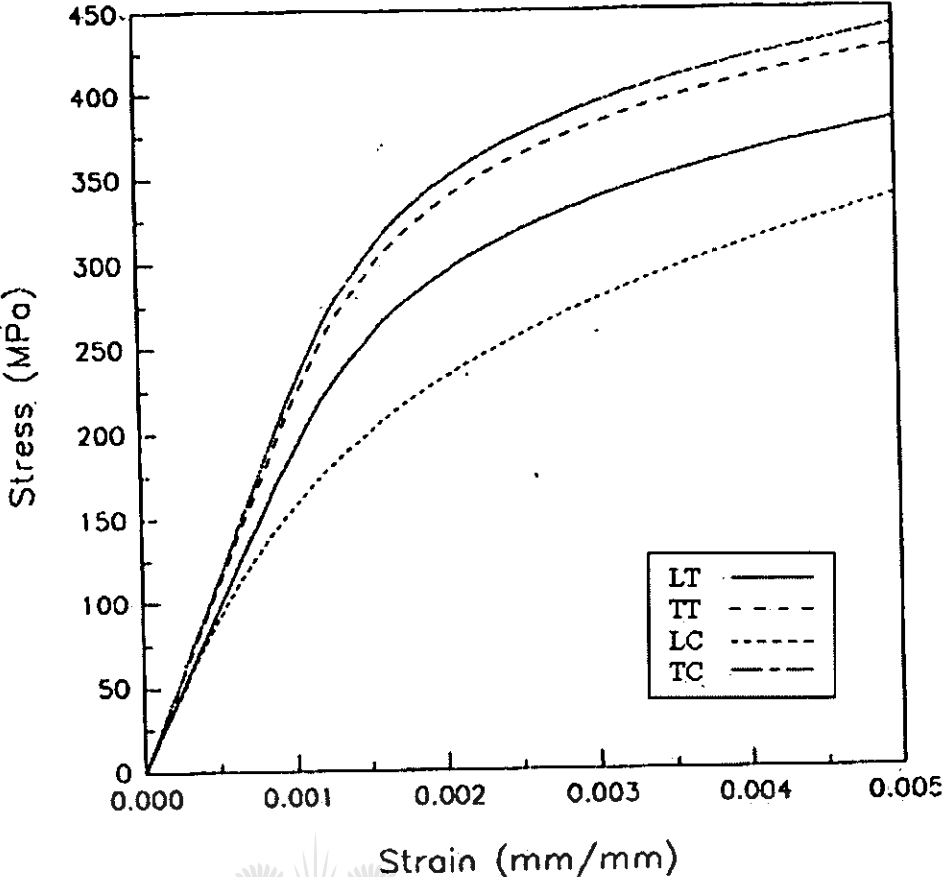


Figure 2.1: Stress-strain curves for 3CR12 Steel Plates [9]

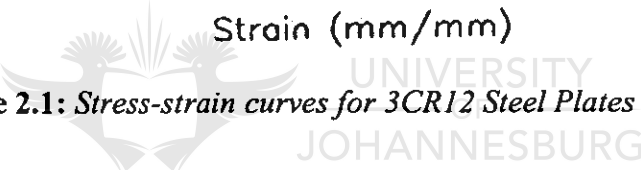


Table 2.4: Mechanical Properties for type 3CR12 plate (1) and hot-rolled Sections (2)[9]

Property	LT	TT#	LC	TC#
Initial Elastic Modulus, E₀ (GPa)				
Plate	194.3	215.2	194.4	225.6
Hot-rolled Section (not annealed)	195.3	-	199.7	-
Hot-rolled Section (annealed)	197.9	-	208.6	-
Yield Strength, F_y (MPa)				
Plate	336.7	375.7	257.4	391.1
Hot-rolled Section (not annealed)	476.8	-	520.9	-
Hot-rolled Section (annealed)	375.2	-	377.7	-
Proportional Limit, F_p (MPa)				
Plate	200.1	252.2	106.2	249.6
Hot-rolled Section (not annealed)	208.2	-	330.6	-
Hot-rolled Section (annealed)	341.5	-	345.7	-
Tensile Strength, F_u (MPa)				
Plate	453.3	506.1	-	-
Hot-rolled Section (not annealed)	615.0	-	-	-
Hot-rolled Section (annealed)	504.1	-	-	-
Elongation, e (%)				
Plate	23.5	20.1*	-	-
Hot-rolled Section (not annealed)	11.6	-	-	-
Hot-rolled Section (annealed)	27.8	-	-	-

LT Longitudinal tension

LC Longitudinal compression

TT Transverse Tension

TC Transverse Compression

(1) Applicable to plates thicker than 3.5mm but less than 12mm

(2) Values listed are the mean of the mechanical properties from experimental tests.

- * Less than the required 15% elongation.
- # Transverse testing on hot-rolled sections not possible due to size limitation.

Stainless steels generally exhibit a more pronounced nonlinearity than the carbon steel equivalent. Stainless steels tend to be more gradual yielding than carbon steels.

The analytical stress-strain curves in figure 2.1 for type 3CR12 corrosion resisting steel plates were produced by using the mechanical properties in table 2.4, together with the following equations:

$$\varepsilon = \frac{F}{E_0} + 0.002 \left(\frac{F}{F_y} \right)^n \quad \text{Eq 2.1}$$

Where

$$n = \frac{1.301}{\log \left(\frac{F_y}{F_p} \right)} \quad \text{Eq 2.2}$$


Where

- ε Strain
- F_y Yield Strength
- F_p Proportional Limit
- F Stress
- E_0 Initial Elastic Modulus
- n constant

The above equations were developed by Ramberg-Osgood [10], and revised by Van der Merwe [11]

2.1.7 Previous Research done on 3CR12

2.1.7.1 Cold-formed Stainless Steel

The behaviour of cold-formed stainless steel structural members was investigated by van den Bergh [12]. It was found that the behaviour of stainless steels differ greatly to that of carbon steels, and warned that special care must be taken when taking into account the inelastic behaviour of stainless steel by using the plasticity reduction factors.

The torsional flexural buckling strength of cold-formed stainless steel axially loaded members was investigated by van den Berg [6]. The sections under investigation were that sections of different stainless steel types (304,409,430) and 3CR12 corrosion resisting steel. It was concluded that:

- The torsional flexural buckling strength predicted by the tangent modulus compared well with the experimental results.
- The effect of cold-forming on the mechanical properties was studied, and it was found that cold-forming increases the yield strength and the maximum strength in the direction of loading, and decreases the ductility.
- Due to cold work, residual stresses developed in the material, and it was concluded that residual stresses influence the structural behavior of stainless steel members.
- The use of the Perry equation in the South African code of Practice was confirmed, since it compared well the experimental results.

A subsequent investigation was conducted into the local buckling of partially stiffened 3CR12 stainless steel compression elements in beam flanges by van den Berg [13]. The steel used in this study was lipped channel sections placed back to back to form a doubly symmetric lipped I-section. From this study it was

concluded that the ASCE (American Society of Civil Engineers) [14] and South African stainless steel design codes overestimates both the buckling stress and the ultimate strength of partially stiffened stainless steel compression members. When the two plasticity reduction factors are used, the experimental results compare well with the theoretical predictions. The author also concludes from the experimental tests that were done, that the elastic theory overestimates the ultimate capacity of a section progressively more as the flat width to thickness ratio (w/t) of the flange increases.

It was also found that an elastic analysis at low w/t ratios underestimates the ultimate capacity of a section, while both the secant and the tangent approaches overestimate the ultimate capacity of a section.

2.1.7.2 Hot-rolled Stainless Steels

Bosch [1] investigated the behavior of 3CR12 hot-rolled corrosion-resistant steel for the use as structural members. He conducted a theoretical study and compared it to experimental values.

Compression and Tensile tests were done in the axial direction of the steel section. These tests showed that there is a variation in the strength of the material. From the tensile tests it was found that the yield stress, proportionality limit and elongation was more at the tips of the section than in the middle, and Young's modulus and the tensile strength were less at the section tips than in the middle of the specimen. The compression tests showed that the yield stress and proportionality limit were less at the tips, and Young's Modulus more than in the middle of the section. This stress distribution can be attributed to uneven cooling after the rolling process.

The experimental behavior of slender columns was determined and compared to the expected results. The experimental results agreed well with the Euler equation without "significant" influence from residual stresses.

He also concluded from the test results that the SSRC (Stainless Steel Research Council) curve and the Euler curve with tangent modulus are sufficient to describe the behavior of the columns. It was observed that these curves described columns with a small eccentricity well.

In an article written by Bredenkamp et al [9], various investigations into the structural performance of hot-rolled and built-up stainless steels were presented. The paper focused on axially loaded compression and flexural members. The required modifications required for built-up and hot-rolled stainless steel design were discussed pertaining specifically to axially loaded compression members. It was found that:

- At stresses above the proportional limit a reduction in stiffness of the member occurs. This is due to the gradual yielding behaviour of stainless steels. Buckling is sensitive to member stiffness, and it was therefore concluded that material non-linearity is the most important factor in buckling analysis of stainless steel columns.
- The tangent modulus equation was suggested to include the effect of the material non-linearity in predicting stainless steel column strength.
- If the critical column buckling stress does not exceed the proportional limit the initial Modulus of elasticity equals the Tangent Modulus of Elasticity. ($E_0 = E_t$). In this case the column strength is governed by slenderness, and material non-linearity have the minimum or no effect at all.
- If the applied critical column stress exceeds the elastic limit, the column stiffness is reduced. This reduction causes the load-carrying capacity of the column to be diminished by an amount proportional to the critical column stress.

2.1.8 Manufacturing of Hot-rolled Sections

The shaping of metal is as old as history itself. In the Chapter of Genesis (Holy Bible, Christian Religion), a metal worker is mentioned, and although his equipment is unknown, it is established that metal forging was practiced before written records. In the middle ages processes such as rolling and wire drawing were common, but probably dated back further. [15]

The equipment utilized in many forming process have evolved over the past centuries, however the basic concepts remained unchanged. Manual processes were converted to machine processes, waterwheels gave way to electricity, and more recently computer controlled, automated processes have emerged.

The popularity of hot-working processes is primarily due to the fact that it is an easy way to produce a desired shape [15]. At high temperatures, metals weaken and become more ductile. Massive deformation can take place without exhausting material plasticity because of dynamic recrystallization. Hot-forming causes the weaker, austenite structure, to cool to the stronger, ferrite structure, or more stronger equilibrium structures.

The process of rolling is usually the first process used to convert material into a finished wrought product. Blooms, billets or slabs (Figure 2.2) are rolled from starting stock. For cold forming or machining, these hot-worked products often form the starting material.

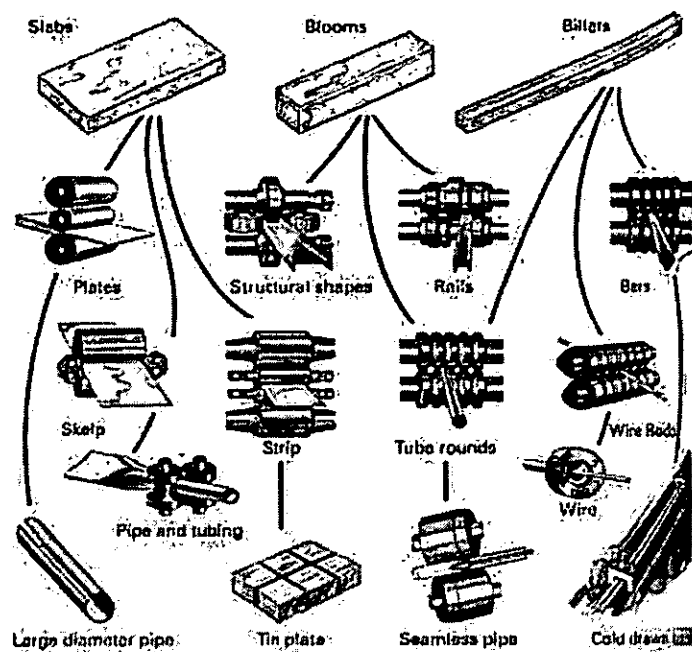


Figure 2.2: Flow chart for various finished and semi-finished steel products [15]

Hot-rolling equipment can produce standardized, uniform-quality products at a relatively low cost. Unfortunately, the shaped rolls are massive and costly, and therefore hot-rolled products can usually only be obtained in standard shapes and sizes for which there is adequate demand to permit cost-effective production.

Figure 2.3 illustrates the basic rolling process. Heated metal is passed between two rolls that rotate in opposite directions. The gap between the rolls is smaller than the thickness of the entering metal. The rolls rotate with a greater surface velocity than the velocity of the incoming metal. The friction created by the difference in velocity along the contact surface causes the metal to move forward. To compensate for the decrease in cross-sectional area, the metal is squeezed and elongates. The friction conditions along the interface determine the amount of deformation that can be achieved in a single pass between a given pair of rolls. If too much deformation is required, the rolls cannot advance the material and just skid over the surface. On the other hand, too little deformation results in a higher production cost.

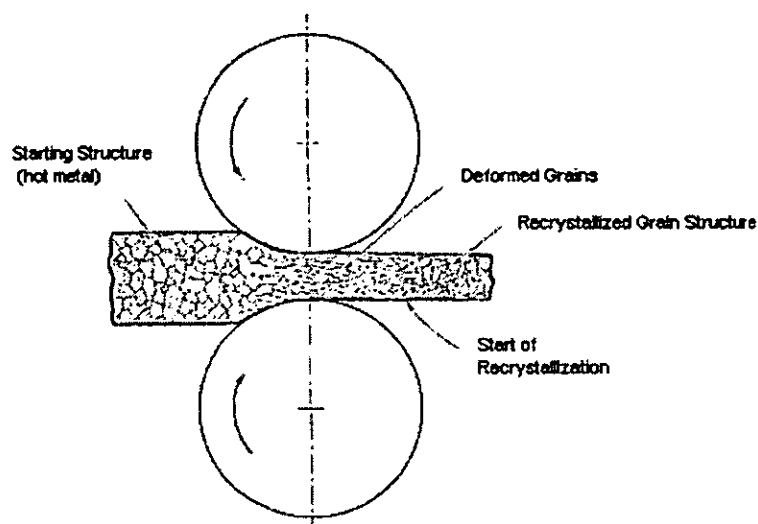


Figure 2.3 *The hot-rolling process [15]*

The success of the hot-rolling process depends largely on temperature control. If possible, the starting material must be heated to a uniform elevated temperature. If the temperature is not uniform, the following deformation will not be uniform.

When the temperature drops to approximately 50 to 100 degrees above the recrystallization temperature, the hot-rolling process is usually terminated. A finishing temperature in this range will ensure a uniform grain size and prevents the risk of unnecessary strain hardening. A period of reheating is required to reestablish hot-working conditions before any subsequent deformation can be performed.

Hot-rolled products are usually devoid of deformation-induced residual stresses, and their properties are independent of direction. However, considerable residual stresses may be induced during cooling after hot working.[15] Normally, hot-rolled products are of good and dependable quality due to the hot deformation and accurate control maintained during the process.

The surfaces of hot-rolled products are usually a bit irregular, and initially covered with a high-temperature oxide, termed mill scale. The mill scale can be removed by an acid pickling process, resulting in a smooth surface finish.

2.1.9 Code of Practice for Hot-rolled Steel in South Africa

The code of practice for hot-rolled steelwork in South Africa is given in the SABS 0162-1 Part 1:1993 [16]. This code is largely based on the Canadian Standard CAN/CSA-S16.1-M89 [17].

The code specifies among others the acceptable material and product standards and specification for hot-rolled steel, the design requirements, as well as the load and limit-states criterion. The code continues by discussing the design lengths of members, slenderness ratios, member resistance, welding and seismic design requirements. The width-thickness ratios for elements in compression are discussed, as well as specifications for members subjected to fatigue loading. Instructions are given for cleaning, preparation of surfaces and protective treatment. Finally the requirements for erection, inspection and testing are discussed.

2.1.10 Structural Steel Design in South Africa

Ultimate failure in a member or unfitness for purpose at serviceability limit states of a structure is avoided by the following criterion [16]:

Factored resistance > effect of ultimate loads or
Serviceability requirements > effect of serviceability loads.

The design code mentions that members in compression should be designed on the basis of their effective length KL . K is the effective length factor, while L is the unbraced length. The unbraced length is the length of the compression member between centers of restraining members.[16]

A reference is made to the slenderness ratio of member in compression, which is defined by the ratio of the effective length factor KL , to the corresponding ratio of gyration. The slenderness ratio of a member in compression is also prohibited to exceed 200 [16].

Guidelines are also laid out as to the classifications of sections for members in compression, as well as the width and thickness of the members, and the gross and net areas of each member.

The code uses the Euler load to define the critical buckling load of a member in compression [18]. This critical load is defined as follows:

$$C_e = \frac{\pi^2 EI}{L^2} \quad \text{Eq 2.3}$$

where

I = moment of inertia, which can also be written as $I = Ar^2$

A = cross-sectional area of strut

r = radius of gyration

E = modulus of elasticity

The effective length of an end-restrained column can be defined as the length of the equivalent pin-ended column that will give the same critical load as the end-restrained column. In a physical sense, the effective length is the distance between the points of inflection of the buckled shape of the end-restrained member (See Figure 2.4).

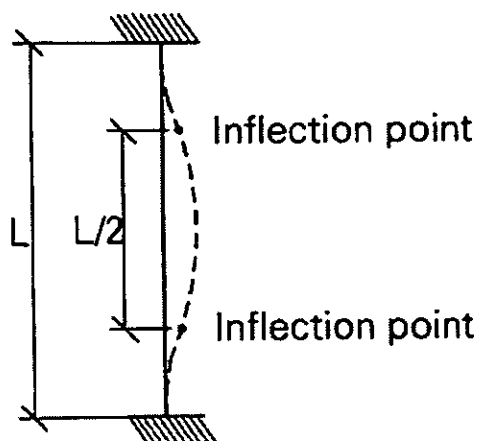


Figure 2.4: Fix-ended Column [18]

The effective length factor is given by:

$$K = \sqrt{\frac{C_e}{C_{cr}}} \tag{Eq. 2.4}$$

where



C_r = critical load of the end-restrained column

C_e = Euler load of the pin-ended column having the same length as the end-restrained column.

Due to geometrical imperfection (initial out-of-straightness) and material nonlinearities a perfectly straight column does not exist in reality.

To account for initial out-of-straightness, the code incorporate into its design curves the Perry-Robertson equation to find the maximum stress, which is given by:

$$\sigma_{\max} = \frac{C}{A} \left(1 + \frac{\delta_0}{r^2} \frac{1}{1 - \frac{C}{C_e}} \right) \tag{Eq. 2.5}$$

where

δ_0 = amplitude of the crookedness at mid-height of the column

C = axial force

To determine the maximum stress in a column subjected to an eccentric loading, the code calculates this stress with the secant formula:

$$\sigma_{\max} = \frac{C}{A} \left[1 + \frac{ea}{r^2} \sec \frac{\pi}{2} \sqrt{\frac{C}{C_e}} \right] \quad \text{Eq. 2.6}$$

where

e = eccentricity

a = distance from neutral axis to extreme fiber of a column.

To account for material non-linearity, the SABS code uses the results of widespread research by Bjorhovde (PhD.1982). He developed column curves representative of the strength of a related category of columns. The column curves were developed for hot-rolled and cold-straightened members, structural hollow sections, wide-flange and box shapes.

For cold-formed, non-stress relieved doubly symmetric sections and hollow sections, the factored axial compressive resistance (C_r) is:

- a) $0 \leq \lambda \leq 0.15$ $C_r = \Phi A F_y$
- b) $0.15 < \lambda \leq 1.0$ $C_r = \Phi A F_y (1.035 - 0.202\lambda - 0.222\lambda^2)$
- c) $1.0 < \lambda \leq 2.0$ $C_r = \Phi A F_y (-0.111 + 0.636\lambda^{-1} + 0.087\lambda^{-2})$
- d) $C_r = \Phi A F_y (0.009 + 0.877\lambda^{-2})$
- e) $C_r = \Phi A F_y \lambda^{-2} = 1970000 \frac{\Phi A}{(KL/r)^2}$

$$\text{where } \lambda = \frac{KL}{r} \sqrt{\frac{F_y}{\pi^2 E}} \text{ and } \Phi = \text{resistance factor} \quad \text{Eq 2.7}$$

For hot-formed or cold-formed stress relieved structural hollow sections, the compressive resistance is given by:

- a) $0 \leq \lambda \leq 0.15$: $C_r = \Phi A F_y$
- b) $0.15 < \lambda \leq 1.2$: $C_r = \Phi A F_y (0.990 + 0.122\lambda - 0.367\lambda^2)$
- c) $1.2 < \lambda \leq 1.8$: $C_r = \Phi A F_y (0.051 + 0.801\lambda^{-2})$
- d) $1.8 < \lambda \leq 2.8$: $C_r = \Phi A F_y (0.008 + 0.942\lambda^{-2})$
- e) $2.8 < \lambda$: $C_r = \Phi A F_y \lambda^{-2} = 1970000 \frac{\Phi A}{(KL/r)^2}$

The sections under investigation in this dissertation are all hot-rolled channel sections. Therefore the above equations for hot-formed sections were used to plot the column curve as prescribed by the SABS code of practice. Figure 2.5 shows the above equations presented as curves.

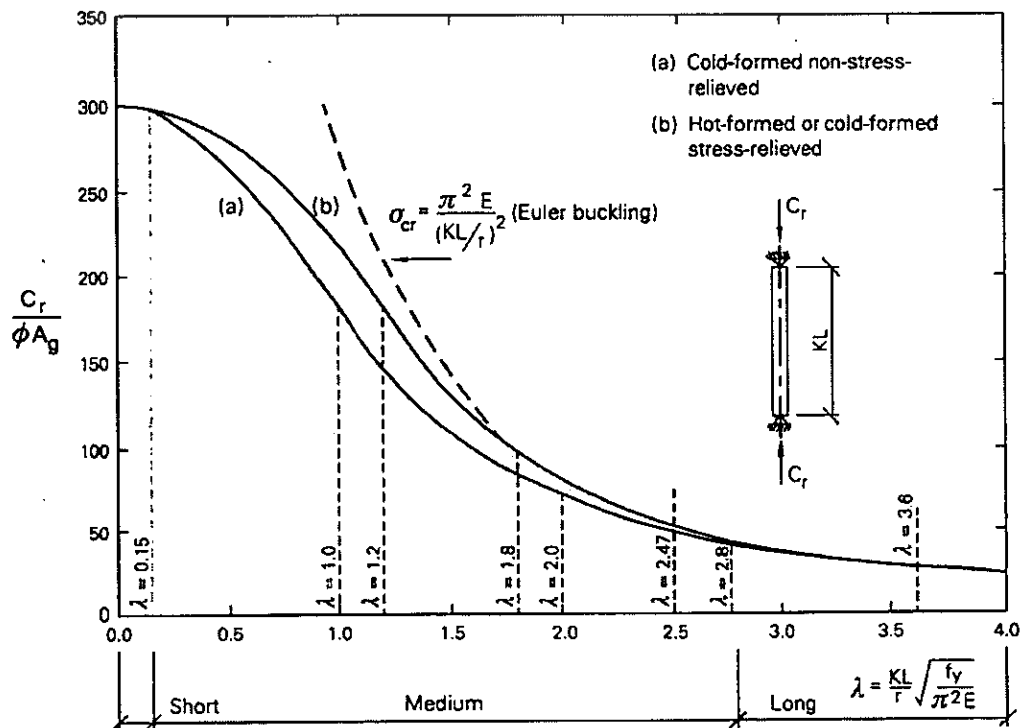


Figure 2.5: Column Curves [18]

2.2 Theory of Columns and Buckling

2.2.1 Introduction

The column or compressive member is one of the basic elements of all structures. The primary function of a column is to transmit a compressive load from one point of the structure to another [19]. Historically used in Greek and Roman temples, these columns were more work of art than true compression members, since little or no engineering design was involved. The columns usually carried loads far below their full capacity.

The failure of a structure can be divided into two categories: Material and Form failure. In material failure, the stresses in the structure exceed the safe limit of the material, resulting in a crack, which ultimately causes the structure to fail. In form failure, the stresses in the structure might still be in the safe limit, but the structure might be unable to retain its original form. In this case, the member may deform to another shape caused by intolerable external disturbance. The geometry and loading of the structure has an influence on the form failure. Form failure occurs in the instance where the conditions of loading are such that compressive stresses are introduced. If the equilibrium of a structure changes from stable to neutral due to the magnitude of the applied load, the load is called the critical load. The change of equilibrium of a structure is termed the buckling of a structure [20]. When the critical load is reached, the ability of the member to withstand increasing loads decreases and the member exhibits a decrease in load-carrying capacity. This condition is called instability.

In structural design, different kinds of sections are utilized. These can broadly be classified as closed sections and open sections. The instability of these sections depends on the following factors:

- Flexural Rigidity EI
- Torsional rigidity GJ
- Position of shear center with respect to the center of gravity
- Symmetry of the cross-section
- Material behavior.

In this section, a summarized background will be given on classical column theory, different theories, buckling modes and factors influencing column strength.

2.2.2 Classical Column Theory

A column is defined as a member that sustains only axial load [20]. The centrally loaded, pinned end column has been studied widely for more than 250 years. [Bjorhovde]. The work of Leonard Euler is generally accepted as the cornerstone of basic column theory. In 1759 the solution defined by Euler indicated that the buckling load of a perfectly straight, pinned-end column manufactured from a linearly elastic material is given by

$$P_{cr} = P_e = \frac{\pi^2 EI}{L^2} \quad \text{Eq. 2.8}$$

Where

P_{cr} = Critical Buckling Load

P_e = Euler Load

He discovered that columns may also fail through bending rather than squashing. His research indicated that a column will remain straight until the critical load is reached. Once this load is reached, the compression member may remain straight or assume the shape of a deflected half-sine wave.

The Euler Equation is derived in Appendix A.

2.2.3 Inelastic Columns

The Euler buckling theory has certain limitations, specifically the fact that it is based on elastic material response. In other words, the Euler solution is only applicable to columns for which the material remains fully elastic and obeys Hooke's law. This assumption is only valid if a column is slender enough so that buckling occurs at a stress level below the proportional limit of the stress-strain relationship of the material. [20] This type of buckling is referred to as elastic buckling.

Certain materials display non-linear material characteristics through a continuously curving stress-strain diagram. [19] Therefore if the material response is inelastic, some of the fibers in the cross-section have yielded prior to buckling. Only the fibers that remain elastic are effective in resisting the additional applied load. Hence the elastic modulus E must be replaced by an effective modulus, since the whole cross-section is not effective in resisting the axial force. The behaviour of the inelastic column is then described by the effective modulus. [20]

The following sections, theories will be discussed which were developed specifically to analyse inelastic columns buckling in the inelastic range: the Tangent Modulus Theory, Double Modulus Theory and Shanley's Inelastic Column Theory.

2.2.3.1 The Tangent Modulus Theory

A theory was developed by Engesser which assumed that the modulus of elasticity at the instant of buckling was equal to the slope of the material stress-strain curve at the level of the buckling stress. This theory described the buckling behaviour of columns whose buckling load was above the proportional limit of the material. [20]. The following assumptions are made in the tangent modulus theory:

- The column is perfectly straight.
- The ends of the column are pinned and the load is applied along the centroidal axis of the column.
- The bending deformation of the column is minimal.
- Plane sections before bending remain plane after bending

- During bending, no strain reversal (i.e. no unloading of fibers) occurs across the cross section of the column.

The theory postulates that the column remain straight up to the instant of buckling, and at failure the modulus of elasticity is equal to the tangent to the stress-strain curve (Figure 2.6). The buckling load corresponding to this stress was defined as the tangent modulus load:

$$P_T = \frac{\pi^2 E_T I}{L} \quad \text{Eq. 2.9}$$

The solution is independent on materials that would behave elastically in agreement with its original properties when used as a structural member. The tangent modulus E_T depends only on the material properties of the column.

The theory also proposed that once buckling have occurred, unloading would take place in the cross-section, and the behaviour of all the fibres within the cross-section are governed by the tangent modulus E_T . [19]. This is also the smallest load for the inelastic range for which bifurcation of equilibrium can take place.[20].

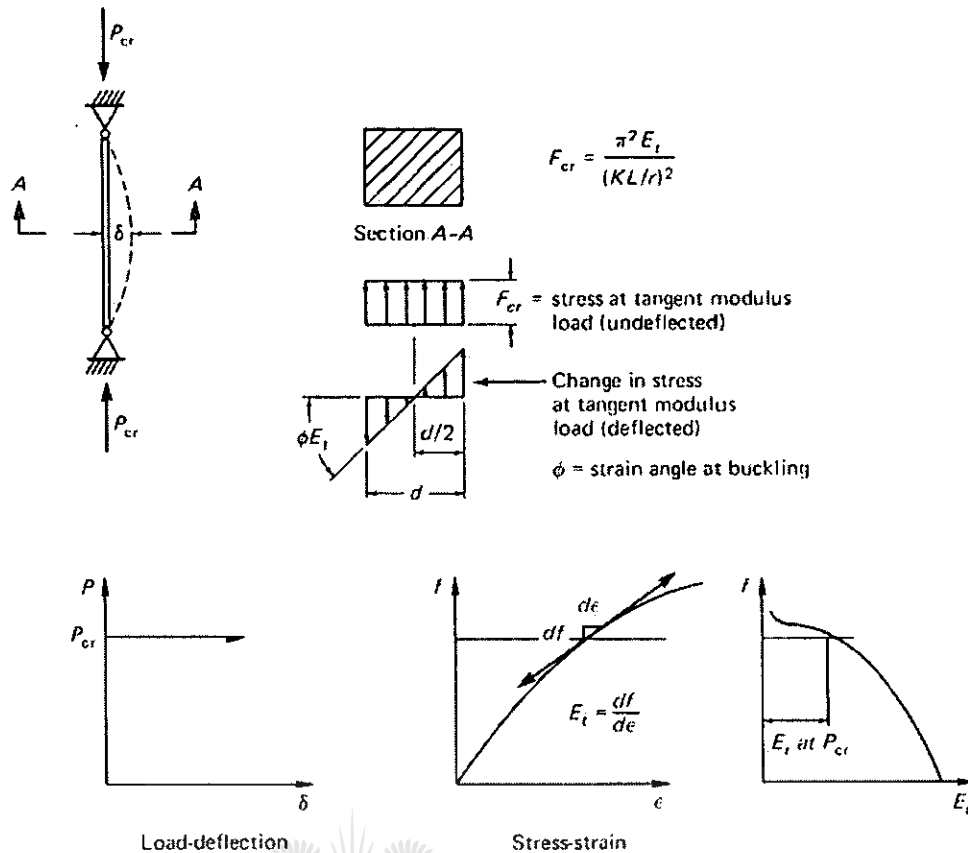


Figure 2.6: Engesser's Tangent Modulus Theory [21]

The buckling loads calculated with the tangent modulus theory still did not agree with the test results. The main reason is because of the 5th assumption, which assumed that as the compression member changes from a straight to a bent configuration, no strain reversal takes place. Therefore Engesser modified his theory, stating that during bending, the strain in certain fibers are increased (lowers the tangent modulus), while other fibers are unloaded (higher modulus at the reduced strain), and concluded that a combined value should be utilized for the modulus. [21]

2.2.3.2 Double Modulus Theory

As previously stated, buckling theories were modified to focus on elastic unloading. In developing the double modulus theory, the same four assumptions as for the tangent modulus theory were made, with the exception of the 5th assumption, which is different. In this case it is assumed that the axial force remains constant during buckling; therefore bending deformation at buckling will induce strain reversal on the

convex side of the column. (Figure 2.7) On the concave side of the column however, the strain will continue to increase. This implies that the stress and strain induced by bending at the buckling load are related by the elastic modulus on the convex side of the column, and the stress-strain increments on the concave side are related by the tangent modulus. The solution involves material in which the fibers can respond both to E and E_T , depending on the location of the fibers in the cross-section. [20] Since two moduli are required to describe the moment-curvature relationship of the cross-section, the name *double modulus* is used. The associated critical load is therefore termed the double modulus load, and defined by

$$P_R = \frac{\pi^2 E_R I}{L^2} \tag{Eq. 2.10}$$

The double modulus load is less than the Euler buckling load, and therefore the double modulus is also referred to as the reduced modulus load P_R . [20]. The reduced/double modulus concept is shown graphically in the Figure below. (Figure)

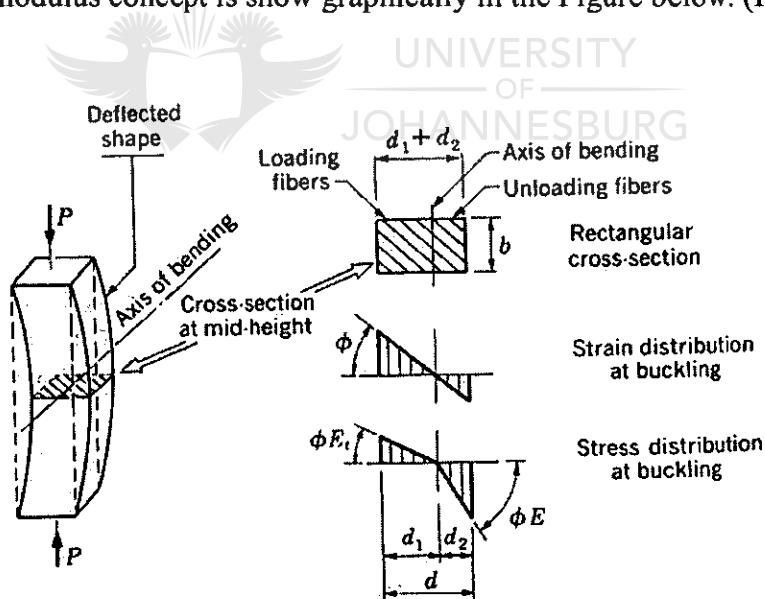


Figure 2.7: Reduced Modulus Concept [22]

2.2.3.3 Shanley's Inelastic Column Theory

Shanley focused on the assumption made in the previous discussed theory that the column remains straight up to the reduced modulus load. His theory, indicated that an

initially straight column will buckle at the tangent modulus load, after which the column will continue to bend with increasing axial load. [22]. Thus, at any instant as the column buckles, the net increase in axial force is given by the difference $\Delta P_{\text{compressive}}$ and $\Delta P_{\text{tensile}}$, and not zero as postulated in the reduced modulus theory. The increase in axial force is of such magnitude that strain reversal may occur at the convex side of the column. It was shown that the relationship between the applied load P and the midheight deflection d can be expressed as: [20]

$$P = P_t \left(1 + \frac{1}{\frac{b}{2d} + \frac{1+\tau}{1-\tau}} \right) \quad \text{Eq. 2.11}$$

Where

P_t = Tangent Modulus Load of the Column

b = width of the column cross section

$\tau = E_t / E$ in which E_t is the tangent modulus.

It was assumed that the column begins to bend at the instant P_t is reached. The above equation therefore describes the postbuckling behaviour of the column, i.e. when the applied load P exceeds P_t .

A simplified column model is used in Shanley's inelastic column theory to explain the postbuckling behaviour of an inelastic column [19]. Shanley used a column model with flexibility shown in Figure 2.8 in order to simplify the analytic considerations. The model consists of two rigid ends of a column connected by springs at the center, therefore only the behaviour of the springs requires investigation in order to study the response of the column [22].

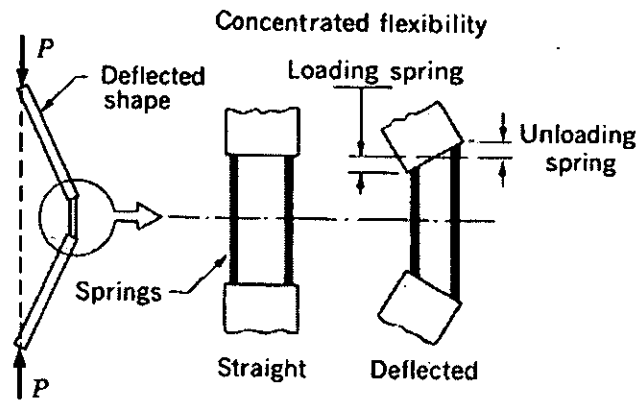


Figure 2.8: *Shanley's Column Model* [22]

The tangent modulus load is the lower limit, which is the load at which an initially straight column will start to bend. The reduced modulus is the upper limit to the strength of a concentrically loaded, perfectly straight inelastic column. This is the load the maximum load that a column will be able to sustain when it is supported for the moment up to that load. [20]

Results from experiments on real columns indicated that their maximum strengths are closer to the lower limit, i.e. the tangent modulus load than to the reduced modulus. This can be attributed to inevitable imperfections existing in real columns as well as unintentional load eccentricities during the experiments. These imperfections tend to lower the strength of real columns. The different factors that can influence the strength of columns will be discussed briefly in the following sections.

2.2.3.4 Factors Influencing Column Strength

In reality, the behaviour of columns are quite complex. Since the behaviour of these structural members depends on responses to a variety of different parameters which include: [19]

- Grade of Steel
 - Stress-Strain Relationship
 - Yield Stress
- Manufacturing Method
- Size of Shape
- Cross-Section Geometry
- Bending Axis (x versus y)
- Initial Curvature
- End Support Conditions.
- Column Length

Some of the above factors specifically pertaining to this investigation will be discussed in more detail below.

Material Properties

The most important is the yield stress of the material F_y . As far as short columns are concerned, the axial resistance is directly proportional to the yield strength. For more slender columns, the influence of the yield strength have a less pronounced influence, since the critical axial resistance is influenced by the magnitudes of the effective modulus, residual stresses, and initial curvature.

Initial Curvature

Columns that are perfectly straight do not exist in reality. Manufactured columns display a form of initial crookedness, which is a consequence from the cooling conditions of the member after rolling. After rolling, the shape is left on a cooling bed

together with other members. Since the heat dissipation is non-uniform throughout the cross-section, the mid-section of the member usually retains the heat longer, as well as the parts closest to the other members [19]. The initial curvature of the columns is caused by this non-uniform cooling process. The curvature may develop in both the principal axes, but this depends on how the member is cooled. The limitation for an initial curvature is usually expressed as a fraction of the length of the member. [20]

The appropriate material delivery specification places a restriction on the amount of initial out-of-straightness allowed [19]. This maximum out-of-straightness is based on the length of the compression member, and most industrialized nations use a maximum allowable value of $e = L/1000$ for wide-flange shapes. Columns not meeting this requirement are either rotorized or gag-straightened to ensure compliance with the code. In South Africa, the design of hot-rolled steelwork is conducted according to the SABS 0163-1:1993 code of practice [16], which is based on the Canadian Standard Association Specification [17]. The Canadian standard specifies the maximum allowable initial-out-of straightness as $L/1000$. Measurements taken by Bjorhovde [23] indicate that wide-flanged shapes have an average initial out-of-straightness of approximately $L/1500$.

For a combination of load eccentricity e'' and initial out-of-straightness e' at midheight of the column, the deflection of any point along the column from the straight position can be expressed as [22]

$$v_0 = e' \left(1 + \frac{1}{2} \cdot \frac{\pi^2}{4} \cdot \frac{P}{P_e} + \frac{5}{24} \cdot \frac{\pi^4}{16} \cdot \frac{P^2}{P_e^2} + \dots \right) + e'' \left(1 + \frac{5}{12} \cdot \frac{\pi^2}{4} \cdot \frac{P}{P_e} + \frac{61}{360} \cdot \frac{\pi^4}{16} \cdot \frac{P^2}{P_e^2} + \dots \right)$$

Eq. 2.12

Where

v_0 = deflection

P_e = elastic/Euler buckling load

P = axial load

If $P/P_e < 1/5$, the following equation can be derived from the previous equation, with a negligible inaccuracy.

$$\nu_0 = (e' + e'') \left(1 + \frac{3P}{2P_e} \right) \quad \text{Eq. 2.13}$$

$$f_{\max} = \frac{P}{A} \left[1 + \left(1 + \frac{3P}{2P_e} \right) \frac{c}{r^2} (e' + e'') \right] \quad \text{Eq. 2.14}$$

Where

f_{\max} = maximum stress

Column Length

The behaviour and strength of compression members vary considerably as a function of length. Bjorhovde [19] subdivided columns into three categories according to their behaviour:

- | | |
|--------------------------------|---|
| 1) Short Columns | Response Mode: <i>Squasing (Yield Load)</i> |
| 2) Intermediate Columns | Response Mode: <i>Inelastic Flexural Buckling</i> |
| 3) Slender Columns | Response Mode: <i>Elastic Flexural Buckling</i> |

Short Columns

These columns are more generally known as stub columns, and fail in purely axial mode, i.e. in squashing of the member. Since the stub column is so short, yielding of the material in the full cross-section takes place before the overall bending occurs. For an applied stress which is less than the proportional limit, the behavior of a column is fully plastic, and the cross-section modulus of Elasticity is E . All responses after the proportional limit has been reached is inelastic. This behavior is attributed to the fact that the applied stress plus the residual stress will equal or exceed the yield stress in some areas of the cross-section. The tangent modulus of elasticity can be applied to the gross cross-section, and is given by:

$$0 \leq E_T \leq E \text{ for } \sigma_{prop} \leq \sigma = (P/A_g) \leq F_y$$

The axial capacity of the short column is exhausted once the yield stress is reached in all fibers. The load at which this occurs is the yield load P_y .

The stub column test can also be used to determine the tangent modulus column curve for a member. This method was utilized before numerical solutions were available. The stub column test determines the variation of the Tangent Modulus as a function of the applied stress. When the level of stress and E_t is combined, the corresponding slenderness ratio at which a perfectly straight column buckles can then be found. But today, with the aid of numerical solutions and if maximum strength forms the basis of for limit states design criteria, this procedure is basically irrelevant.

Intermediate Length Columns

The majority of compression members in structures are represented by this section. The slenderness ratio for these members range from $\lambda = 0.3$ to 1.2, where

$$\lambda = \frac{1}{\pi} \sqrt{\frac{F_y}{E}} \left(\frac{KL}{r} \right) \quad \text{Eq. 2.15}$$

The cut-off from elastic flexural buckling is defined at $\lambda = 1$, for linearly elastic-perfectly plastic steel with no residual stresses. This is the intersection between the Euler curve and the yield plateau. An illustration can be seen in the figure below.

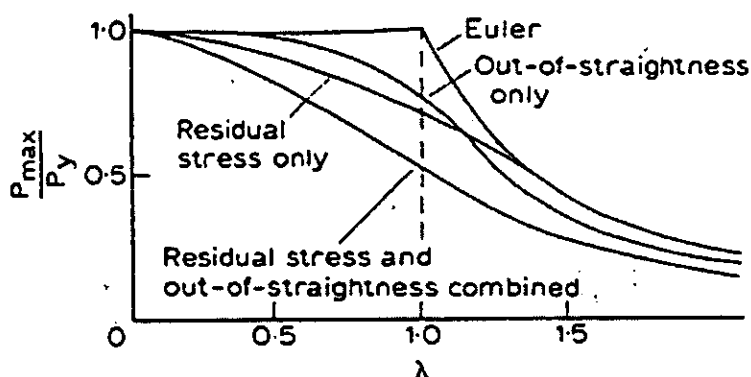


Figure 2.9: Column Curves and Imperfection Effects [19]

The governing ultimate limit state for columns with residual stresses and initial crookedness is the maximum strength. The peak of the load-deflection curve is reached when considerable local yielding has taken place, depending on the yield stress, the residual stress distribution, the crookedness and the slenderness of the column. Therefore intermediate length columns respond primarily by inelastic buckling. In Figure 2.9 maximum strength curves are presented for compression members with different imperfections. It can clearly be seen that the capacity of the columns in the intermediate range is reduced significantly, especially when both initial curvature and residual stresses are present.

Slender Columns

Slender columns fail in elastic flexural buckling, even if residual stresses and initial crookedness are present [19]. This is attributed to the considerable length of the column, and therefore a small critical stress. These factors result in the proportional limit being appreciably higher than the sum of the maximum compressive and residual stresses together. The maximum strength of these slender columns will still be less than the Euler Load because of initial out-of-straightness being present, but for extremely slender columns, this value is close to the Euler Load.

In reality it is quite rare to find slender columns which will fail through elastic buckling.

Different buckling modes will be discussed briefly in the following section.

2.2.3.5 Types of Column Failure

Compression members can fail in different modes, depending on the section, thickness of material and the columns slenderness [24]. Columns can fail by:

- Yielding
- Overall Column Buckling
 - Flexural Buckling
 - Torsional Buckling
 - Torsional Flexural Buckling
- Local Buckling of individual elements

Yielding has already been discussed earlier in this chapter, therefore only the last three buckling modes will be discussed briefly.

2.2.3.6 Flexural Buckling

Hot-rolled sections are susceptible to overall flexural buckling. This is caused by the presence of residual cooling stresses [25]. Slender axially loaded compression members may fail by overall flexural buckling if the cross section of the column is a double symmetric (I-section), closed shape such as a square or rectangular tube, cylindrical shape, or a point-symmetric shape (Z or cruciform) [24]. These sections do not have an inclination to twist.

The average stress of a straight member buckling flexurally is given by: [25]

$$\sigma_c = \frac{\pi^2 E_t}{\left(\frac{KL}{r}\right)^2} \quad \text{Eq. 2.16}$$

Where

σ_c = critical stress

Early Tests indicated that for slender columns, the flexural buckling stress for carbon and low-alloy steel members can be approximated by [25]

$$\sigma_c = \sigma_y - \frac{\sigma_y^2}{4\pi^2 E} \left(\frac{KL}{r} \right)^2 \quad \text{Eq. 2.17}$$

Where

σ_y = yield stress

2.2.3.7 Torsional Buckling

Torsional buckling is reserved for open sections. Closed sections have a large torsional rigidity, and will therefore not buckle torsionally.[24]. Sections inclined to fail by torsional buckling are sections in which the shear center and centroid coincide such as I, Z and cruciforms.[26]

2.2.3.8 Torsional-Flexural Buckling

Certain sections buckle in a combination of twisting and bending. This type of buckling is called Flexural-torsional buckling. Sections that buckle in this mode are sections where the shear center and centroid does not coincide, for example, channel and angle sections. If one axis of symmetry is present in the section, the column can buckle by simple Euler flexural buckling in this plane [26]. If no axis of symmetry is present, only flexural-torsional is possible. Doubly symmetric and point symmetric sections are immune to flexural-torsional buckling, because the shear center and centroid coincide. Closed sections are also not susceptible for this type of buckling.

2.2.3.9 Influence of Residual Stress on Column Strength

Residual stress is defined as stresses that exist in an unloaded member, after it has been manipulated to form the finished product [25]. Research has shown that the magnitude and distribution of residual stresses within the column cross-section is the key factor that influences the strength of straight centrally loaded columns. [22]

Lay and Ward [27] did extensive research on the influence of residual stress on steel sections. They prove that for certain cases, residual stresses have a more detrimental

effect, but in other cases, residual stresses can be used to give a more positive influence. It is shown in this paper that sufficient knowledge of the influence of these stresses can be of significant importance when using steel members.

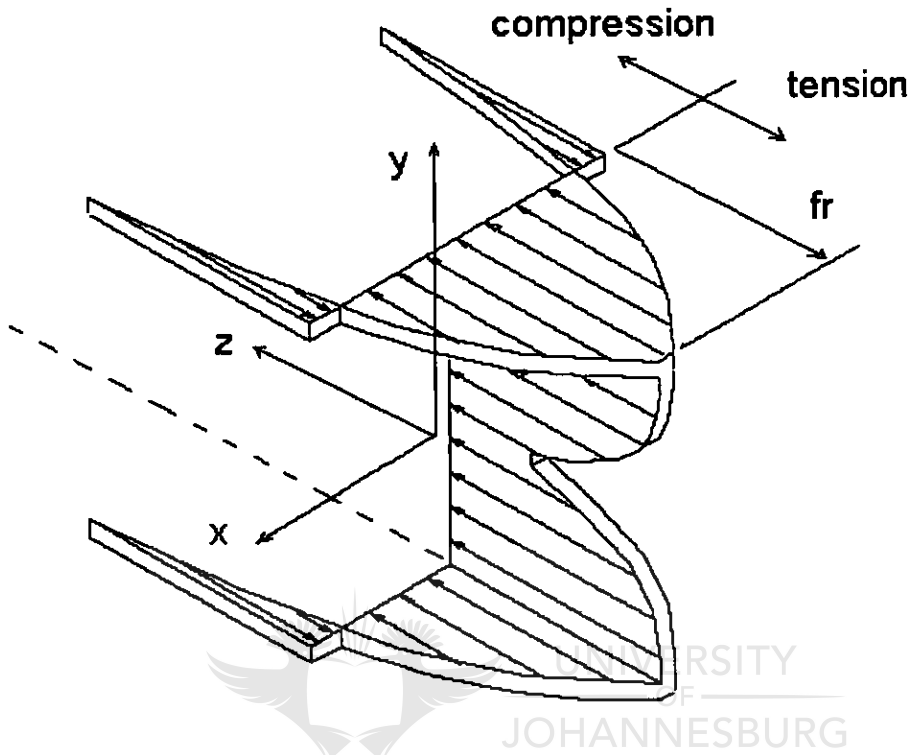


Figure 2.10: Residual Stress Pattern [27]

The distribution of residual stresses throughout a section is governed by the requirement that they be in internal equilibrium at any cross-section. For example, as seen in Figure 2.10, if the residual stresses are denoted as $f_r = f_r(x)$, then the following three equilibrium equations must be satisfied by f_r :

$$\int_A f_r dA = 0$$

$$\int_A f_r x dA = 0$$

$$\int_A f_r y dA = 0$$

Residual stresses in structural steel shapes are mainly due to uneven cooling after the rolling process. In the early part of the 20th century, Howard [25] noted that the cause for reduced column strength in the intermediate slenderness range might be attributed

to the presence of residual stresses. [25]. Where specifically hot-rolled sections are concerned, the type of cross-section, the rolling temperature, cooling conditions, metal properties and the straightening procedures all have an influence on the magnitude and distribution of the residual stresses. [25].

According to Bjorhovde [19], particularly compressive residual stresses have a considerable strength-reducing effect on columns and beam-columns.

The following three main processes cause Residual Stresses to develop:

- thermal
- mechanical or
- metallurgical processes.

Thermally-induced Residual Stresses

Nonuniform permanent or plastic deformations cause thermal residual stresses to develop. These stresses appear when a metal is heated and then cooled under restraint. Residual stresses are not generated by unrestrained expansion and contraction, but rather by restrained expansion and contraction, which induces permanent deformation or strains, and corresponding residual stresses

Lay and Ward [27] defines Thermal residual stresses as stresses that occur due to temperature differences during the manufacturing process. Where specifically hot-rolled sections are concerned, the flange tips will cool down more rapidly than the web-to-flange junction. Strength and stiffness begin to improve when the steel cools, and the varied strength and stiffness properties will create internal strains, which will result in internal residual stresses developing. An example to consider is the production of an I-section. During production, the beam leaves the mill with the web horizontally positioned. This causes the thin web and the flange tips to cool faster compared to the center flange areas and the web-to-flange junction. Therefore, the latter areas are still plastic, which enables them to adjust to the strains formed by the rapid cooling regions. The part that cools last is the body of the flange, which will attempt to contract. The cold web will resist the contraction, and produce line edge

stresses, rendering the flange plate in tension. In reaction to this, a line of compression producing stresses along the web forms.

These differences in temperature are minimized by producing the beams with the web vertical, and by ensuring the flange tips are touching when the beams are packed.

Bjorhovde concluded that in general, tensile residual stresses develop in the metal that cools last. [19]

Mechanically-induced residual stresses

These stresses are caused when a metal is mechanically stretched or compressed under restraint, which causes permanent deformations. Therefore, the occurrence of mechanically-induced residual stresses requires the presence of both permanent and mechanical deformation and restraint that prevents the deformed metal from contracting or expanding to its new unrestrained equilibrium dimension. In general the sign (tension or compression) of the stress is opposite to the sign of the non-uniform plastic strain that produced the residual stress. This process is used to mechanically curve or straighten components. An example is when rolled or built-up structural shapes are bent by means of gaging to remove or introduce camber or sweep. Various mills make use of rotary straightening, which repeatedly bends the shape into opposite directions as it passes through rolls at ambient temperature, eventually rendering the shape straight.

The magnitude of these cold-work stresses resulting from the above process is far more pronounced in the longitudinal direction than in the transverse direction for the shape, except for surface effects [25]. In the case of columns and plate structures built up by welding, longitudinal residual stresses have a significant influence on the behaviour of these members. The longitudinal residual stresses fluctuate through the width and thickness of each plate element comprising the shape. This variation is usually not important when it comes to very thick elements or walls of cold-formed tubular members.

Frey and Alpsten (Alpsten, 1970, Frey, 1969) found that in general, the strength of an as-rolled member is much weaker than its corresponding cold-straightened part. This improvement is due to the less out-of straightens and the redistribution of residual stress. Research done by Alpsten [1970 1972b) also proved that column strength may increase up to 20% when compared to a column of the same length and initial curvature.

In 1964 it was discovered by Tall that the effect of geometry on the residual-stress distribution is more pronounced than that of steel grade. It was found that residual-stress measurements in the flanges of similar shapes made of different steel grades indicates that the distributions and magnitudes of the residual stress are similar.

Extensive research were done by Batterman and Johnston [28] to determine the relation between the residual stresses and initial curvature effects. The obtained results together with research done by Bjorhovde show that [25]:

- Adding the separate effects of initial curvature and residual stresses cannot give an approximation of the combined effect. In some cases the combined effect is less than the sum of the parts, e.g. in intermediate slenderness ratios and low residual stresses, while in other cases the combined effect is more than the sum of the parts. The last case occurs in the intermediate slenderness ratio range for heavy hot-rolled shapes in all steel grades. The research emphasizes the fact that the magnitudes of the maximum compressive residual stresses in a large number of the tested shapes were at 50% or more of the yield stress of the material itself.
- The maximum strength of very slender columns unaffected by the presence of residual stresses, or initial crookedness. However, columns made of higher-strength steels can tolerate much greater deflection before yield or becoming unstable.
- If the assumption is made during a computer analysis that during further loading the initial crookedness of a half-sine wave remains unchanged, the strengths are slightly underestimated.

- The differences in column strength for initially curved columns caused by variations in the shape of the residual stress pattern are smaller than for initially straight columns.

An example of the effect of hot-rolling is when a wide-flange or H shape is hot-rolled. The flanges cool more slowly than the web parts since they are the thicker parts of the shape. The flange tips have a greater exposure to air, and therefore cool more rapidly than the region at the junction of the flange to the web [21]. Accordingly, compressive residual stresses exist in the flange tips, and at mid-depth of the web, while tensile residual stresses are present in the joint region between the flanges and the web.

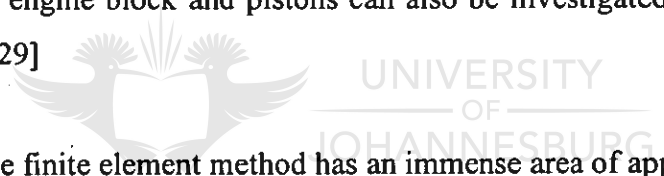
Influence of Residual Stresses on Compression Behaviour

Previously, column behaviour was predicted by taking only the effects of initial curvature and out-of-straightness into account, but nowadays, it is generally accepted that residual stresses as well as the above mentioned imperfections have influences column behaviour. A few cases exist in which residual stresses are the deciding factor. The instance in which residual stresses become critical is when the parts of a section that contributes most to its stiffness contain compressive residual stress. [27].

3 FINITE ELEMENT MODELING

3.1 Introduction

The finite element method is a numeric analysis technique that was first introduced in the 1950's. Since then, the finite element method has been continually developed and improved, and is currently considered an exceptionally refined tool for solving design and analysis problems in various branches of industry. No other numerical analysis procedure has been developed nearly as far, while numerous other numerical analysis techniques and experimental testing methods have been made redundant by its progress. A good example is in the car industry, where the structural integrity and performance of a new car as a whole can be studied using the Finite Element Method. Areas include the car's impact behavior and crash worthiness, the frequency characteristics of the combined structure and its separate components. Temperature distributions in the engine block and pistons can also be investigated, as well as the resulting stresses. [29]



It is obvious that the finite element method has an immense area of application as well as enormous potential. The rapid advances in computer technology has attributed significantly to the growth of the technique over the last decade.

The Finite Element Method is mainly used to investigate three areas that are discussed below.

3.1.1 Steady State Problems

The most widespread use of the Finite Element Method is Steady State or equilibrium analyses. For elasticity problems, the distortion can be predicted for a body under equilibrium conditions. The stresses and strain experienced by the body can then be derived from the calculated values of displacement. This method is also frequently used to perform thermal analysis; it is possible to predict the temperature distribution

and heat flow through a body for a wide variety of boundary conditions. Table 3.1 lists some applications of equilibrium problems.

Table 3.1: Applications of Equilibrium Problems [29]

Area	Typical Application
Aerospace Engineering	Stress analysis of aircraft frames, wings, missile and spacecraft components
Automotive Engineering	Stress analysis of crankshaft, cylinder block, connecting rods, chassis, etc
Biomedical Engineering	Stress analysis of bones, hip replacements, teeth and heart
Civil Engineering	Stress analysis of dams, retaining walls, excavations; soil mechanics.

3.1.2 Eigenvalue Problems

Eigenvalue problems involve the calculation of fundamental characteristics of the body or system being investigated. For example, the mode natural frequencies mode shapes of components and the buckling of loads of structures can be determined by this method. Table 3.2 shows some of the areas where the Finite Element Method is applied to eigenvalue problems

Table 3.2: Eigenvalue Problems which can be analyzed with FEM [29]

Area	Typical Application
Electrical Engineering	Natural Frequencies of printed circuit boards.
Hydraulic Engineering	Natural periods of lakes and harbors, sloshing of liquids.
Mechanical Engineering	Natural Frequencies of components; shafts; critical buckling loads
Nuclear Engineering	Neutron flux distribution; frequency analysis of pressure vessels.

3.1.3 Transient Problems

In eigenvalue problems, time is not present explicitly, although the natural frequency characteristics of a body might be calculated. In transient or propagation problems, however, the loads can be dependant on time, and the forced responses of the body is calculated by the finite element method. The propagation of stress and transient heat flows is also considered as transient problems. In table 3.3 some areas can be seen where the method is applied to transient problems.

Table 3.3: Examples of Transient Problems[29]

Area	Typical Application
Structural Engineering	Shock and earthquake analysis of buildings and bridges
Biomedical Engineering	Impact analysis of skull, dynamic analysis of body and limbs.
Civil Engineering	Stress waves in rock structures
Mechanical Engineering	Analysis of impact problems; dynamic crack propagation

The application of this method is clearly large, and to assist in the analysis using the finite element method, commercial software packages have been developed. Unfortunately, these packages also have a disadvantage. The complexities and the algorithms employed are becoming less perceptible to the user. The important procedures of the method are invariably concealed by complicated pre-and post-processors.

The user is also falsely impressed by the development of pre-and post-processors, which have not only made the user remote from the method, but give the programs an appearance of indisputable accuracy. Complex, visually impressive and evident reliable models can be easily generated by pre-processors with minimum amount of input from the engineer, while equally imposing and credible graphical output are generated by the post-processors.

Accurate and dependable results can be produced by the Finite Element Method if it is utilized correctly, but it must be kept in mind that it is only an approximate technique, and only the correct analysis procedures and an accurate presentation of the problem can produce a valid and accurate model.

In this investigation the ABAQUS [30] range of products were used. This program will be discussed further in the following paragraphs.

3.1.4 General Theory

The Finite Element Method is based on simple principals. As an example, a body in which the distribution of an unknown variable (e.g. temperature or displacement) is required will be investigated.

The first step is to divide the region under investigation into an assembly of subdivisions, called elements. These elements are considered to be interconnected at their joints, which are known as nodes (Figure 3.1).

The unknown variable is assumed to act over each element in a predefined manner. The number and type of elements are the chosen in such a way as to ensure that the combined element presentation adequately represents the variable distribution through the whole body.

Polynomials (for example, linear, quadratic or trigonometric functions) may be used to describe the distribution across each element.

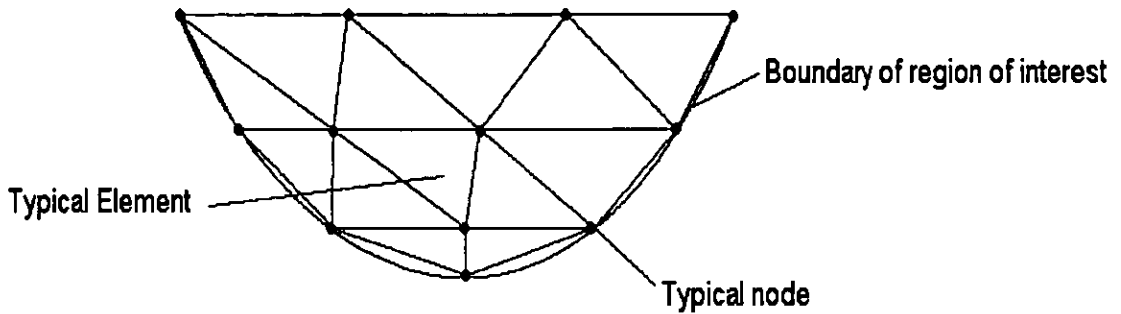


Figure 3.1: *Discretization of a region into a number of Finite Elements [29]*

The second step is to determine the governing equations for each element, which is assembled to provide the system equations. The element equations may be determined in various ways, but generally the equations of a particular type of element for a specific problem areas have a constant format.

Consequently, if the general format of the equations is derived, the nodal coordinates are substituted, along with the material properties and loading conditions into the general equation.

The system equations are obtained by assembling the individual element equations, which describe the behaviour of the entire body. These generally have the following form:

$$[k]\{U\} = \{F\} \qquad \text{Eq 3.1}$$

where $[k]$ is a square matrix, also known as the stiffness matrix; $\{U\}$ is the vector of (unknown) nodal displacements or temperatures; and $\{F\}$ is the vector of applied nodal forces.

Equation 3.1 can be directly compared to the load-displacement relationship for a simple one-dimensional spring, a deflection U in a spring of stiffness k is produced by a force F . The relationship is inverted to obtain the displacement developed by a given force. The same approach is applicable to the finite element method; but before Eq. 3.1 can be inverted and solved for $\{U\}$, a form of boundary condition must be used. In stress problems, the body must be prevented from performing unlimited rigid body motion, and therefore must be constrained.

3.1.5 Applications of the Finite Element Method

3.1.5.1 Linear Problems

A linear problem is where the material properties, geometry and contact conditions are all linear, i.e. the stiffness matrix and force vector are not dependant on the nodal displacements [29]. The Finite Element Method can also be useful in analyzing non-linear static, dynamic and transient problems. The solution to these problems are significantly more complex than that of linear and steady state problems. Complex solutions such as these usually require more than one step.

3.1.5.2 Nonlinear Problems

Non-linear static problems are problems where the stiffness matrix $[k]$ and/or the force vector $\{F\}$ are dependant on the nodal displacements $\{U\}$. This may be attributed to non-linearities present in the material properties, the geometry, combined effects (material and geometry), or the contact conditions of the problem. The different types of non-linearities are discussed below.

➤ Material Nonlinearity

When a linear static analysis is conducted, it is assumed that the material is acting within its elastic limit, and follows a linear stress-strain curve (Figure 3.2). Problems with material non-linearity are those exhibiting plasticity and creep of the material. In this case it is necessary to supply an idealized stress-

strain curve to the Finite Element Program. Depending on the specific material, the stress-strain curve supplied to the program can be approximated in a bilinear or multilinear way.

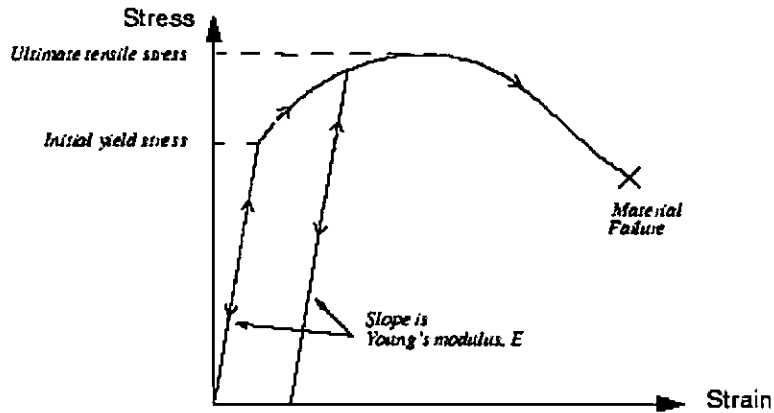


Figure 3.2: *Stress-strain curve for an elastic-plastic material under uniaxial tension.*

➤ Geometric Nonlinearity

When a structure's displacements become so large that the original stiffness matrix is no longer representative of the structure, a large-displacement analysis is required. These types of problems are divided into two groups: those resulting in small strains, and secondly, those resulting in large strains. The small strain conditions implies that the structure return to its original form once the load is removed, and therefore that the material remains elastic.

Elements experiencing large strains undergo permanent deformations, except for hyperelastic materials such as rubber, which remains elastic even if high strains occur. When permanent material deformation occurs, non-linear material properties are required.

Geometric or Stress stiffening is also considered a geometric non-linearity, which occurs when a structure stiffens (or weakens) due to the state of stress. The system equations for such problems are

$$([k] + [k_g])\{U\} = \{F\} \quad \text{Eq. 3.2}$$

where $[k_g]$ is the geometric (or initial) stiffness matrix and is dependant on the state of stress in the structure. Since the state of stress depends on the displacements, the equation is clearly non-linear.

The equations are solved iteratively. In the first iteration a normal static analysis is performed while $[k_g]$ is ignored, and in each subsequent iteration $[k_g]$ is determined from the state of stress of the previous iteration.

➤ Combined Material and Geometric Nonlinearity

The most demanding type of analysis for the Finite Element Method is probably problems containing both material and geometric non-linearities, which includes metal working processes such as forming, rolling and extrusion. The most challenging part of a large deformation analysis is the realization of the boundary conditions, which may include different contact conditions and sliding along curved surfaces with and without friction.

➤ Nonlinear Contact Conditions

Unless special non-linear elements are used, the Finite Element Method assumes that a perfect connection between two parts of a model exists. Generally two types of non-linear contact elements are available: tension-only and gap (compression only) elements. Frictional force as well as a compressive force can be transmitted by these elements, while relative sliding between two contact surfaces are also permitted by some elements. Initial conditions may be specified in two ways: either as an initial gap between the two parts, or a preload, which implies that the two surfaces are pushed against each other.

An iterative solution is required by all non-linear contact conditions. This method examines the state of each element and makes the necessary adjustments after each iteration. It is assumed that the model has converged once the condition of every element remains constant.

➤ Buckling Problems

These types of problems are concerned with determining the critical load at which a structure becomes elastically unstable. A common example is the buckling of a strut, which fails suddenly due to an increasing axial load. Buckling problems are eigenvalue problems, governed by the following equation:

$$([k] + \lambda[k_g])\{U\} = 0 \quad \text{Eq 3.3}$$

where $[k_g]$ is the geometric stiffness matrix, λ is the eigenvalue, related to the buckling load; and $\{U\}$ is the associated vector of nodal displacements describing the mode shape. Sadly, the results rarely agree with those in practice, since this method does not take account of any initial imperfections in the structure or component. A large-displacement analysis should rather be used, since it enables buckling to be detected by the change of displacement at any node.

Therefore the eigenvalue method of solution of buckling is usually approximate, and may produce unsafe answers since it normally overestimates the buckling load, and no information is also given about the post-buckling behaviour of the structure. On the other hand, accurate solutions are produced by a large-displacement analysis, and provide the complete behaviour of the component before and after buckling.

➤ Dynamic Problems

Dynamic analysis include the effects of inertia forces in the calculations. Since these inertia forces are proportional to the accelerations of the body, a time variation is introduced into the system equations. Some form of time varying or dynamic response of the body results from the solution of these equations.

The basic equation for the dynamic behaviour of a structure or component are as follows:

$$[M]\{U''\} + [C]\{U'\} + [k]\{U\} = \{F(t)\} \quad \text{Eq 3.4}$$

Where

[M]	=	Total mass matrix of structure
[C]	=	Structural damping matrix
[k]	=	Stiffness matrix
{U''}	=	Nodal accelerations
{U'}	=	Nodal velocities
{U}	=	Nodal displacements.
{F}	=	Vector of applied forces

A wide range of dynamic problems can be analyzed by the Finite Element Method, a few are briefly discussed below.

Modal Analysis

Modal Analysis is the most frequently performed analysis and is used to predict the natural frequencies and mode shapes of undamped structures subject to free vibrations. It is imperative that the natural frequencies of certain bodies are known to ensure that they are not energized by any applied loading, which would result in high-amplitude vibrations.

Modal Analysis are in general more time consuming and therefore more costly than a static analysis.

Transient Response Analysis

The responses of a structure due to time varying loads are determined by a transient response analysis. These loads can vary with time, or be a time function of displacement, velocity or acceleration.

Transient problems may either be solved by integration over the time domain, or solution in the frequency domain. In the first solution, the forcing function is divided into a series of impulses which can be integrated over time. The second option, which is also known as the Fourier Transform, decomposes the forcing function into its frequency components, and the solution is found in the frequency domain. This approach is not very popular.

Harmonic Response Analysis

Harmonic response analysis is used to determine the steady state response of a structure subjected to a set of harmonic loads of identified amplitude and frequency. Harmonic loads varies sinusoidally in time at a specific frequency) and are usually found in rotating or reciprocating machinery.

Two methods are normally used to obtain the solution of harmonic analysis problems: a direct method and a modal superposition method.

Shock Spectrum Analysis

If it is required to determine the response of a structure to an a foundation shock load, a shock spectrum analysis can be utilized. Since the loading is quite complex, the normal time marching methods can not be employed, and response spectra must be considered instead.

Transient Thermal Analysis

A Transient thermal problem can be described as follows:

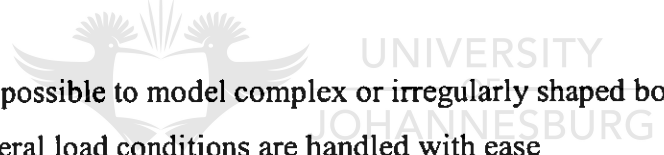
$$[C]\{\dot{\Phi}\} + [k]\{\Phi\} = \{F\} \quad \text{Eq 3.5}$$

where $[C]$ is the specific heat matrix and $[k]$ is the thermal conductivity matrix. Because of the order of the thermal equation is one order less, transient thermal problems are easier to solve than dynamic problems. Temperature is also scalar while structural analyses have three (or possibly six) degrees of freedom to solve for at each node.

3.1.6 Advantages of the Finite Element Method

The popularity of the Finite Element Method are due to the following advantages:

[31]

- 
- It is possible to model complex or irregularly shaped bodies
 - General load conditions are handled with ease
 - It is possible to model bodies consisting of various different materials. This can be done since the element equations are evaluated individually.
 - Unlimited number and types of Boundary Conditions are catered for.
 - The size of the elements can be adjusted when necessary
 - The Finite Element Model can be modified easily.
 - Dynamic effects can be included
 - Large deformations and nonlinear materials resulting in nonlinear behaviour are dealt with easily.

3.2 Previous Research done on Column Strength using the Finite Element Method

B Young and J Yan conducted a finite element analysis of fixed-ended cold-formed plain channel columns [32]. A non-linear model was developed and verified against experimental results. It was found that the finite element model closely predicted the ultimate loads and failure modes of the tested columns. The results from the FEA were also compared to the design column strengths calculated using the Australian/New Zealand, American and European specifications for cold-formed steel structures.

In general, the authors found that the ultimate loads predicted by the FEA slightly overestimated the experimental ultimate loads. Almost all of the axial displacements predicted by the FEA overestimated the experimental values.

The load-displacements curve predicted by the FEA was compared to the experimental curve, and it was found that the two curves were quite similar. The deformed shapes predicted by the FEA closely simulated the experimental buckling modes.

They also investigated the strength and behaviour of cold-formed lipped channel columns using the Finite Element Method [33]. Once again, they developed a non-linear model, and verified it against fix-ended channel column tests. The column strengths obtained from the FEA were compared to with the design column strengths calculated using the American, Australian/New Zealand, and European specifications for cold-formed steel structures.

Their conclusions were that the finite element analysis predictions were generally in good agreement with the experimental ultimate loads and failure modes of the lipped channel columns.

When the column strengths obtained from the FEA compared to the design column strengths calculated from the three specifications, the latter were generally conservative for fix-ended lipped channel columns.

A Liang [34] did research on the distortional buckling of cold-formed stainless steel columns, and also used the finite element method to analyze and calculate the distortional buckling. The results of this analysis were then compared to the experimental results and other theoretical predictions.

The author found that initial imperfections are extremely important in the finite element analysis. Because the pattern modeling of the initial imperfections for various members are not the same, it was found that a thorough analysis should be done on the cold-formed stainless steel structural members before the initial imperfections are designed. For this specific project, the sine curve and the temperature gradient caused by residual stresses were used to model the initial imperfections of the cold-formed steel members.

When the experimental buckling modes were compared to the buckling modes predicted by the Finite Element Method, a good agreement was reached between the finite element method results and those determined experimentally.

3.3 “Abaqus” Finite Element Analysis Software

3.3.1 Introduction

ABAQUS [30] is a collection of engineering simulation programs based on the finite element method. This is a powerful program which is able to solve relatively simple linear problems to the most challenging nonlinear simulations. An extensive library of elements is included in ABAQUS that can model nearly any geometry. The behavior of most common engineering materials can be simulated by the extensive material models, including metals, rubber, polymers, composites, reinforced concrete, crushable and resilient foams, and geotechnical materials such as soils and rock. Since Abaqus is designed as a general-purpose simulation tool, it can be used to simulate problems in such diverse areas as heat transfer, mass diffusion, thermal management of electrical components (coupled thermal-electrical analyses), acoustics, soil mechanics (coupled pore fluid-stress analyses), and piezoelectric analysis.

ABAQUS is not difficult to use, even though a extensive range of capabilities are available to the user. Modeling complicated problems are accomplished easily.

If the simulation is highly nonlinear, only the engineering data such as the geometry of the structure, the material behaviour, boundary conditions and the loads applied need to specified by the user. ABAQUS chooses the appropriate load increments and convergence tolerances automatically. ABAQUS decides on values for these parameters, and continually adjusts them during an analysis to guarantee that the most accurate solution is obtained.

A complete ABAQUS/Standard analysis generally consists of three stages: preprocessing, simulation, and postprocessing. These three stages are linked together by files as shown in Figure 3.3:

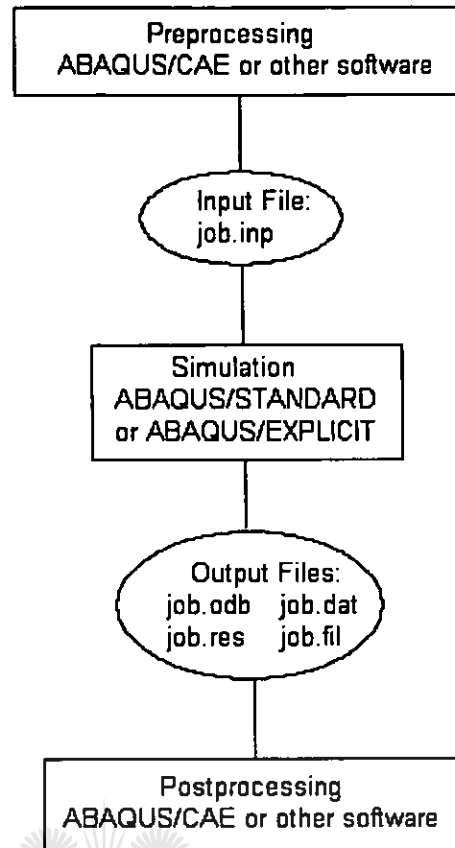


Figure 3.3: Three States Linked Together [30]

3.3.1.1 Preprocessing(Abaqus/CAE)

In the first step, the model of the physical problem is defined and an ABAQUS input file is generated. It is possible to create the model in ABAQUS/CAE, or by using another design package and importing the model. If the analysis is not too complicated, it can be created directly using a text editor.

ABAQUS/CAE (Complete ABAQUS Environment) is a complete environment in ABAQUS which allows the user to create, submit monitor, and evaluate results from ABAQUS/STANDARD and ABAQUS/Explicit. ABAQUS/CAE is divided into several modules, where module defines a logical aspect of the modelling process. ABAQUS/CAE allows the user to import the geometry, or it can be created in the program itself. Physical and material properties can be assigned, as

well as the loads and boundary conditions. Powerful mesh options are available, and the resulting mesh can be verified. After completing the model, it can be submitted by ABAQUS/CAE,. The progress of the simulation can be monitored and controlled. Lastly, the visualization mode is utilized to interpret the results.

3.3.1.2 Simulation (Abaqus/Standard)

The simulation is the stage in which ABAQUS/Standard solves the numerical problem which is defined in the model. This process usually runs in the background. The analysis may take anything from a few seconds up to several days to complete, depending on the complexity of the problem being analyzed and the power of the computer being used.

3.3.1.3 Postprocessing (Abaqus/Viewer)

Once the simulation has been completed, and the fundamental variables have been calculated, the results can be viewed in ABAQUS/Viewer. ABAQUS/Viewer reads the neutral binary output database file, and has different options for displaying the results.

3.3.2 Components of an ABAQUS Model

An ABAQUS model consists of various different components that combined describe the physical problem to be analyzed and the results to be obtained. At the least the analysis model consists of the following information: discretized geometry, element section properties, material data, loads and boundary conditions, analysis type, and output requests.

3.3.2.1 Descretized Geometry

The basic geometry of the physical structure being modelled in ABAQUS are defined by finite elements and nodes. Each discrete portion of the physical structure is represented by interconnected elements.

A discrete portion of the physical geometry is represented by an element, which in turn consists of many interconnected elements. The elements are connected to each other by shared nodes. The model geometry consists of the coordinates of the nodes and the connectivity of the elements (which nodes belong to which elements). The collection of all the elements and nodes in a model is termed the mesh. Usually, the mesh will be only an approximation of the actual geometry of the structure.

The results obtained from a simulation are influenced by the element type, shape, and location, as well as the overall number of elements used in the mesh. By increasing the number of elements (mesh density), the accuracy of the simulation are improved. An increased mesh density causes the analysis results to converge to a unique solution, and the computer time required for the analysis also increases. Generally, the solution obtained from the numerical model is only an approximation to the solution of the physical problem being simulated. The accuracy of extent to which the numerical simulation matches the physical problem depends on the approximations made in the model's geometry, material behavior, boundary conditions, and loading.

3.3.2.2 Element Section Properties

ABAQUS has an extensive library of elements which is a powerful set of tools for solving different problems. Many of the elements have geometry not defined entirely by the coordinates of their nodes. An example is the layers of a composite shell or the dimensions of an I-beam section which are not defined by the nodes of the element. To define the model completely, additional geometric data are required in order to define as physical properties of the element.

Each element in the library is characterized by the following:

- Family
- Degrees of freedom (directly related to the element family)
- Number of nodes
- Formulation
- Integration

Each element in ABAQUS is identified by a unique name, such as T2D2, S4R, or C3D8I. The element name identifies each of the five aspects of an element, discussed briefly below.

Family

Figure 3.4 illustrates the most commonly used element families in a stress analysis. An important feature that characterizes the different element families is the geometry type that each family assumes. The first letter or letters of an element's name indicate to which family the element belongs.

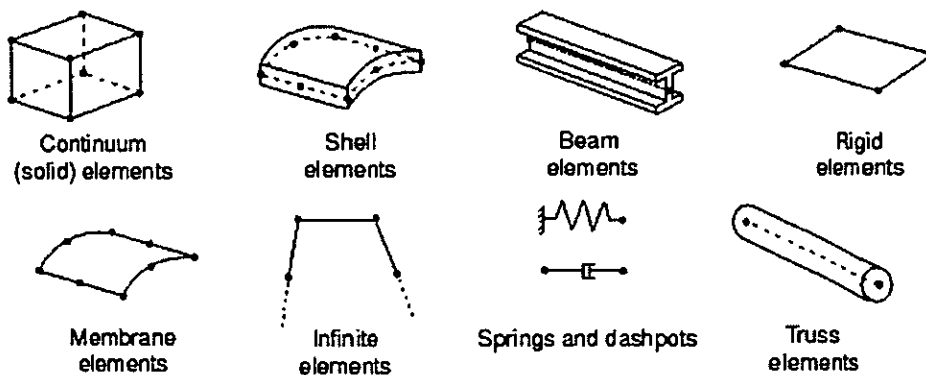


Figure 3.4: *Commonly used Element Families [30]*

Degrees of Freedom

The degrees of freedom (DOF) are the elementary variables calculated during the analysis. For a stress/displacement simulation the degrees of freedom are the translations as well as, for shell and beam elements, the rotation for each node. The degrees of freedom in a heat transfer analysis are the temperatures at each node; therefore a heat transfer analysis requires the use of different elements than a stress analysis, since the degrees of freedom are not the same. In ABAQUS, the following numbering convention is used (shown on the next page):

1. Translation in direction 1
2. Translation in direction 2
3. Translation in direction 3
4. Rotation about the 1-axis
5. Rotation about the 2-axis
6. Rotation about the 3-axis
7. Warping in open-section beam elements
8. Acoustic pressure or pore pressure
9. Electric potential
10. Temperature (or normalized concentration in mass diffusion analysis) for continuum elements or temperature at first point through the thickness of beams and shells
11. Temperature at other points through the thickness of beams and shells

Number of Nodes – order of interpolation

The degrees of freedom mentioned previously are calculated only at the nodes of the element. To obtain the displacements at any other point in the element, the nodal displacements are interpolated. The interpolation order is determined by the number of nodes used in the element. Elements with only corner nodes use linear interpolation in each direction and are frequently called linear elements or first order elements. Quadratic interpolation is used for elements with midside nodes and is often called quadratic or second-order elements.

Formulation

The mathematical theory used to define the element's behaviour is referred to as the elements' formulation. The stress/displacement elements in ABAQUS are based on the Lagrangian or material description of behaviour, which implies that the material associated with an element remains associated with the element throughout the analysis, and material cannot move among elements. Alternatively, Eulerian or spatial description, elements are fixed in space as the material flows through them. Eulerian methods are used generally in fluid mechanics simulations. In ABAQUS convective heat transfer are modelled using Eulerian elements. In ABAQUS, some element families include elements with several different formulations to accommodate different types of behaviour.

Integration

Numerical techniques are used in ABAQUS to integrate various quantities over the volume of each element. ABAQUS evaluates the material response at each integration point in each element by using Gaussian quadrature for most of the elements in the library. When continuum elements are used in a simulation, the user has a choice between full or reduced integration. This can have a considerable influence on the accuracy of the element.

3.3.2.3 Material Data

Material properties for all the elements must be specified. The accuracy and validity of the ABAQUS results are directly dependant on the accuracy and extent of the material data that is supplied.

3.3.2.4 Loads and Boundary Conditions

Stresses in the structure are caused by loads acting on the structure. The most general forms of loading include:

- point loads;
- pressure loads on surfaces;
- body forces, such as the force of gravity; and
- thermal loads.

To constrain parts of the model to be fixed (zero displacements), or to move by a prescribed amount (nonzero displacements), boundary conditions are used. In a static analysis it is essential that sufficient boundary conditions are used to prevent the model from moving as a rigid body in any direction. If this precaution is not adhered to, unrestrained rigid body motion causes the stiffness matrix to be singular. If this is encountered, a solver problem will occur during the solution stage and may cause the simulation to stop prematurely.

If ABAQUS detects a solver problem, it will issue a warning message. Inertia forces prevent the model from undergoing infinite motion instantaneously in a dynamic analysis. This will only occur as long as all separate parts in the model have some mass.

3.3.2.5 Analysis Type

A static analysis is the most common type of simulation, where the long-term response of the structure to the applied loads is obtained. But in other cases the dynamic response of a structure to the loads may be required: for example, the effect of a sudden load on a component, such as occurs during an impact, or the response of a building in an earthquake.

ABAQUS includes various types of analysis steps. The specific type of analysis used in this investigation are discussed in more detail in chapter 5.

3.3.2.6 Output Requests

If care is not taken, an ABAQUS simulation can generate a large amount of output. Therefore options are available that limits the output to only that required for interpreting the results.

Generally a preprocessor such as ABAQUS/CAE is used to define the necessary components of the model.

Output is available in four different files:

- the output database (.odb) file, which contains data in a neutral binary format necessary to postprocess the results with ABAQUS/Viewer;
- the data (.dat) file, which contains printed tables of selected results;
- the restart (.res) file, which is used to continue the analysis; and
- the results (.fil) file, which is used with third-party postprocessors.



4 EXPERIMENTAL WORK

4.1 Introduction

In this section the mechanical properties of 3CR12 steel, as related to the section under investigation, are investigated with compression tests. The specimens are cut from channel sections ($152 \times 76 \times 18$). The residual stresses in the channel are also investigated. This chapter documents the procedures and results for each experiment.

4.2 Compression Tests

4.2.1 Theoretical Background

Compression tests are conducted by applying a stress to a material and recording the response of the material to this applied stress [2]. One of the most important material characteristics determined by compression tests, are the Compressive Yield Strength. This indicates where the material starts to behave inelastically or deviates from the proportionality of stress and strain [2]. Compressive tests are usually conducted on a universal testing machine, or more commonly, a tensile tester. These machines can perform, tensile, compressive and shear tests. Compressive tests are done in an analogous manner to tensile tests, except a compressive force is used, and the specimen contracts along the direction of the applied stress [35].

A compressive test is done by applying a compressive load to a specimen, of which one end is attached to a movable cross-head, while the other is fixed to a stationary crosshead. The movable cross-head is then moved towards the stationary cross-head, in order to compress the specimen.

The test is performed by attaching an electrical device to measure strain, which is called an extensometer, or alternatively strain gauges can be used. The specimen is then compressed until it yields, or starts to behave inelastically. When a shape is deformed elastically, it will return to its original shape once unloaded, but an inelastic/plastic deformation is irrecoverable.

Since convention indicates a compressive stress as negative, compression tests yields negative stresses, which in turn leads to negative compression strain. Compression strain can be calculated with the following formula:

$$\varepsilon = \frac{l_i - l_0}{l_0} = \frac{\Delta l}{l_0} \quad \text{Eq. 4.1}$$

where ε = engineering strain

l_f = the final length of the test specimen

l_0 = initial length of the test specimen

The original cross-sectional area of the specimen is used to convert the load into stress, and a stress strain diagram is obtained. From this diagram three important mechanical properties are determined:

- Yield Strength
- Modulus of Elasticity
- Proportional Limit

Compressive tests are mainly used when a material is subjected to large and permanent strains, for example in manufacturing applications, or in the case of materials that are brittle in tension [35].

Below some definitions pertaining to mechanical properties are discussed.

4.2.1.1 Yield Strength

This is the stress level at which a material will deform plastically, i.e it will stretch permanently [2]. In most design situations, this property is considered more important than the ultimate strength, since it is not desirable for a structural component to permanently deform or bend under service loads.

For gradual yielding materials F_y is found at 0.2% strain or 0.002 strain by constructing a straight line parallel to the elastic part of the stress-strain curve at the 0.2% offset. The stress found at the intersection of the line with the stress-strain graph is then defined as the yield strength. [35]

4.2.1.2 Modulus of Elasticity

This property is given by the slope of the elastic portion of the stress-strain diagram. In this portion, the material is stretching elastically, and therefore will return to its original shape [2]. The modulus of elasticity is a measure of the rigidity of a material, used to determine the elastic deflection of a material under a load.

4.2.1.3 Proportional Limit

The proportional limit is the stress at which the material ceases to behave elastically, or where stress and strain are no longer proportional. In some cases, this point cannot be determined precisely, and therefore a convention has been established to determine this point. The method used is similar to the method described above to determine the yield strength, except that an offset of 0.01% strain is used to determine the intersection between the line and the stress-strain graph.

4.2.1.4 Work Hardening

This phenomenon is also known as strain-hardening. This is the process where a ductile material, as it is plastically deformed, becomes harder and stronger. Unfortunately, this process has a negative effect on the ductility of the material. When a part is loaded beyond the elastic limit of the material, the part undergoes a small amount of permanent deformation.

This phenomenon can be explained on the basis of dislocation-dislocation strain field interactions [35]. Cold work increases the dislocation density in a metal, because of dislocation multiplication or the formation of new dislocations. Consequently the dislocations are positioned closer together. Generally, these type of strain interactions are repulsive and the result of this repulsiveness is that the dislocations hinder the movement of other dislocations. The resistance to the movement of dislocations increases as the dislocation density increases.

4.2.2 Compression Tests: Experimental Program

4.2.2.1 Specimen Preparation

The channel sections were neatly cut into 20cm stub columns and the ends of each section were then machined square. The channel columns were then cut into 13 specimens as shown in Figure 4.1. The ASTM Book of Standards [36] does not specify dimensions for compression test specimens, but only gives a general outline. According to ASTM, all specimens must be flat and contain the full thickness of the material if possible. It further states that the length must be sufficient to allow enough shortening in order to define the yield stress of the material. But the length must not be of such dimensions as to induce buckling in the unsupported portion of the specimen. As far as machining is concerned, it is specified that the ends of specimens must be flat and parallel (within 0.0005mm/mm), and perpendicular to the lateral surfaces with no more than 3° of an arc.

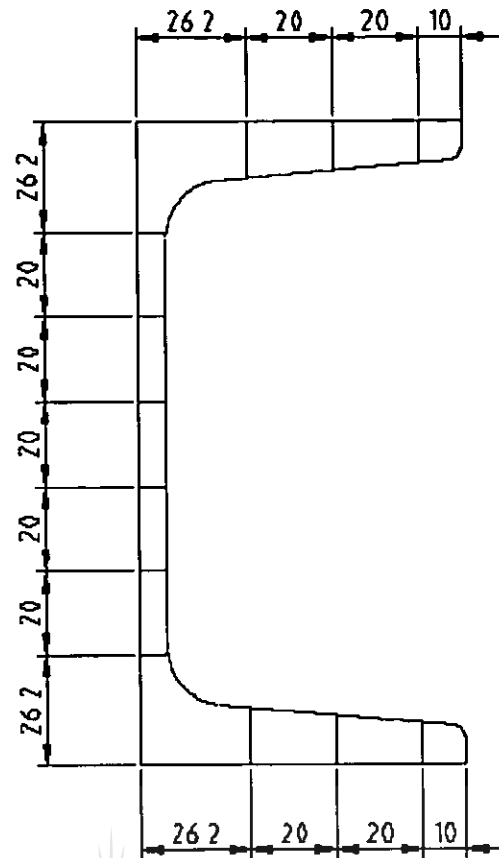


Figure 4.1: *Dimensions of Channel Section Cuts (mm)*

4.2.2.2 Experimental Setup and Procedure

Once the specimens were machined, both surfaces of each specimen were cleaned with alcohol to ensure that the strain gauges attaches properly. The 4 wires of the Wheatstone bridge were soldered onto the four terminals of the strain gauges (Figure 4.2), and the specimen was fastened in the fixture (Figure 4.3) the width and thickness of the specimen were entered into the control program, as well as the specimen name. The experimental setup can be seen in Figure 4.4. The computer then calculates the area automatically, and use the result to convert the applied load into stress. The initial speed was set to 1 mm/min, but once 2% strain was reached, the speed was adjusted to 10mm/min. The results of each compression test is a stress-strain graph, together with a detailed excel file, containing all the relevant information.

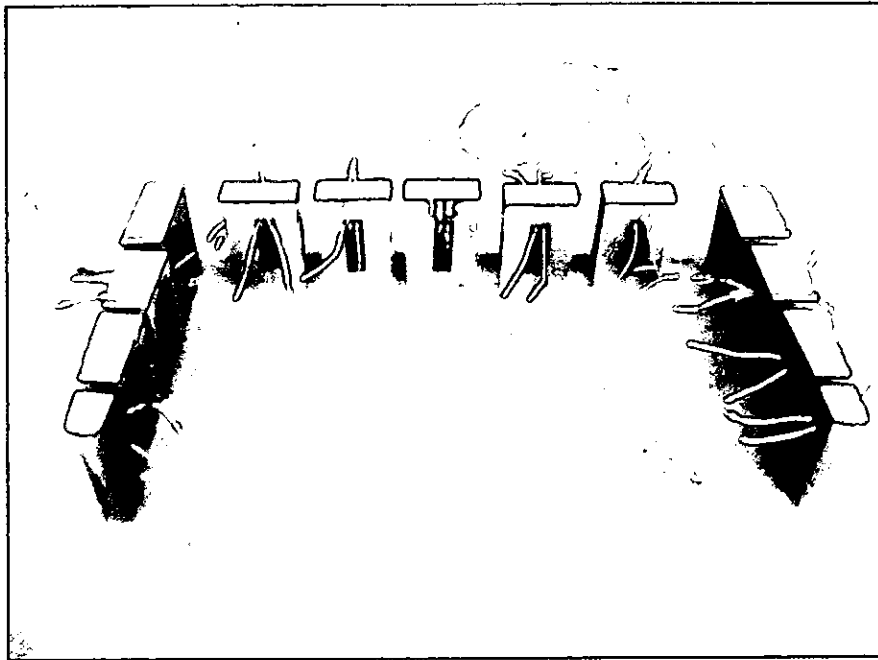


Figure 4.2: *Channel Column cut into sections with strain gauges attached*

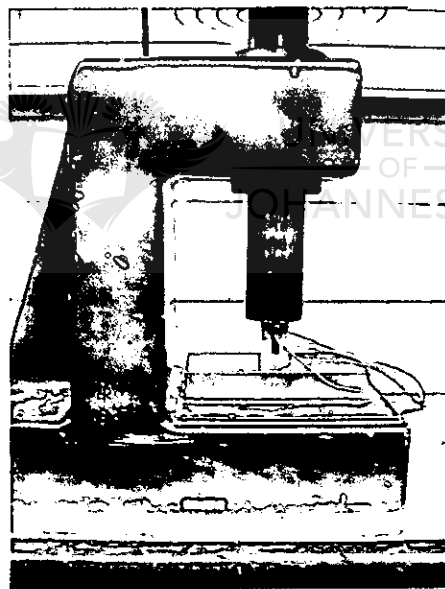


Figure 4.3: *Test Specimen fastened in the fixture*

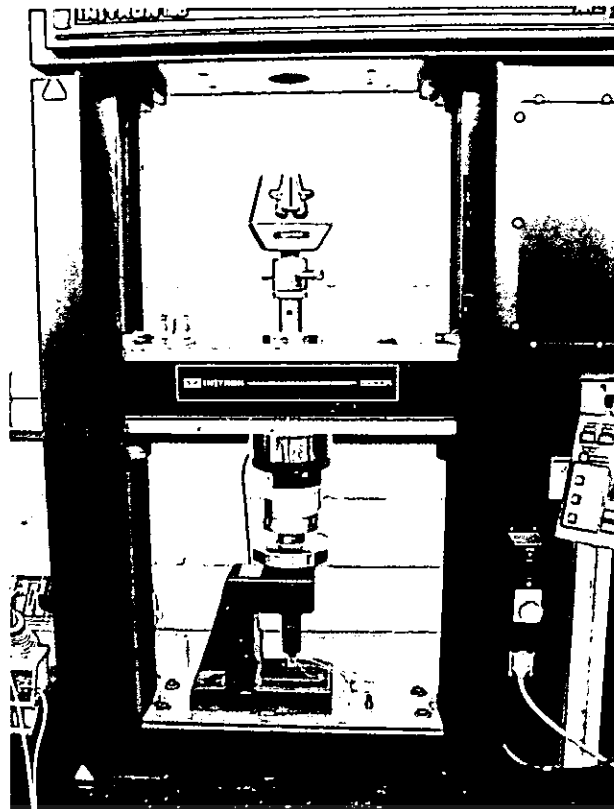


Figure 4.4: *Experimental Setup*

4.2.3 Results

The individual graph for each section can be seen in Appendix B. Table 4.1 page tabulates the mechanical properties obtained from the compression tests. In figure 4.5, 4.6 and 4.7 the distribution of each of these material properties are graphically illustrated.

Table 4.1: *Mechanical Properties of 3CR12 as obtained from compression tests for a sectioned 3CR12 152×76×18 structural section*

	Proportional Limit	Modulus of Elasticity	Yield Stress
	MPa	GPa	MPa
1	198.0	192.1	353.0
2	229.3	198.9	333.2
3	214.0	201.6	320.7
4	198.6	205.0	334.3
5	251.3	209.7	355.5
6	249.3	205.9	350.2
7	267.7	201.9	356.3
8	237.6	199.7	355.5
9	252.5	204.6	346.7
10	244.0	191.5	357.5
11	231.1	188.9	312.0
12	200.5	192.7	322.7
13	208.9	180.0	349.1
Average	229.5	197.9	342.0

Table 4.2: Mechanical Properties categorized into Web and Flanges

	Upper Flange (Incl. Corner)	Web	Bottom Flange (Incl. Corner)
Average Yield Stress (MPa)	335.3	354.4	335.3
Coeff of Variation (%)	2.0	0.7	3.2
Average Modulus of Elasticity (GPa)	199.4	204.3	188.3
Coeff of Variation (%)	1.4	1.1	1.5
Average Proportional Limit (MPa)	210.0	251.5	221.1
Coeff of Variation (%)	3.5	2.5	4.5



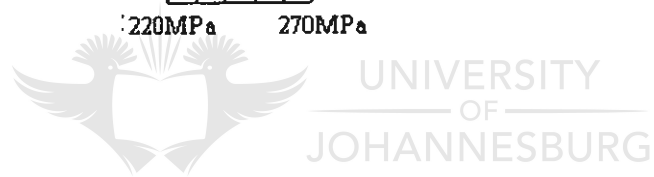
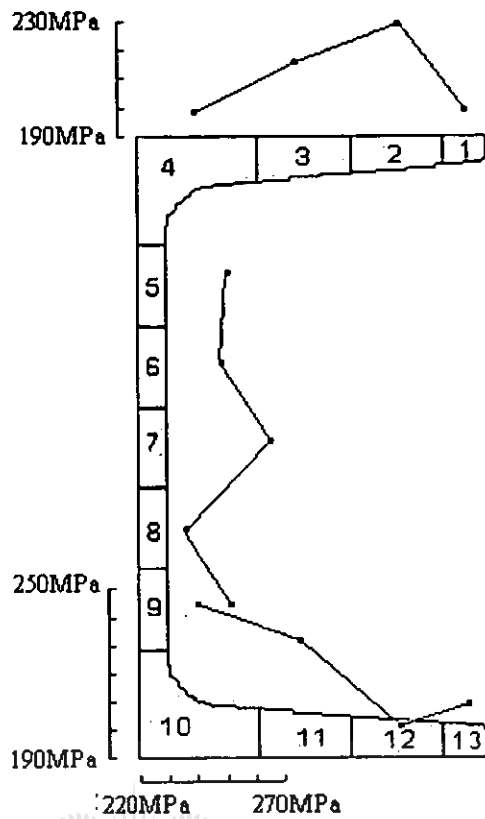


Figure 4.5: Variation of Proportional Limit for each section

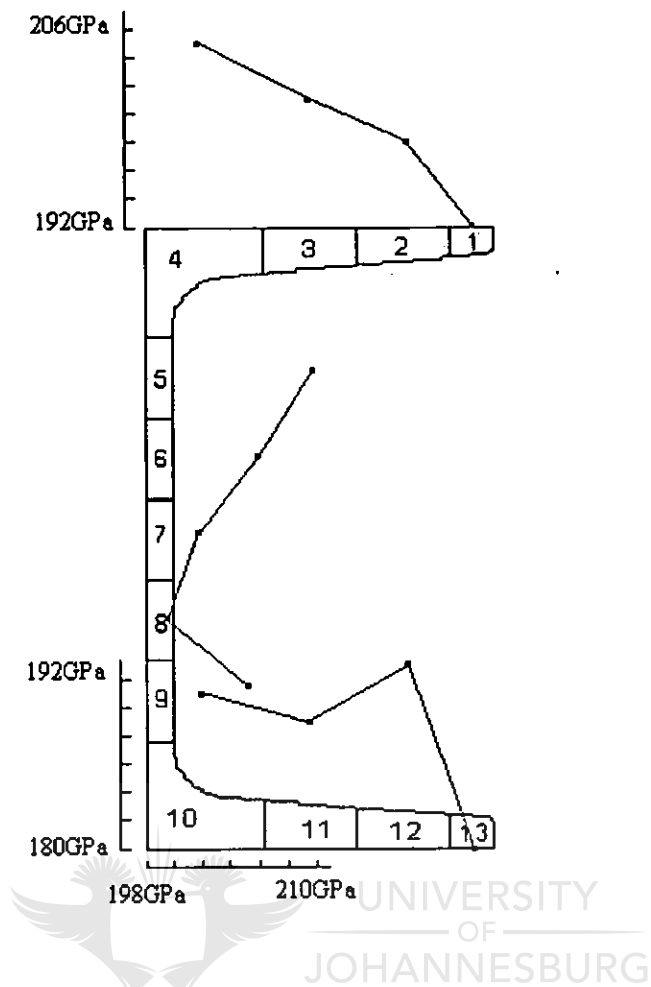


Figure 4.6: Variation of Modulus of Elasticity

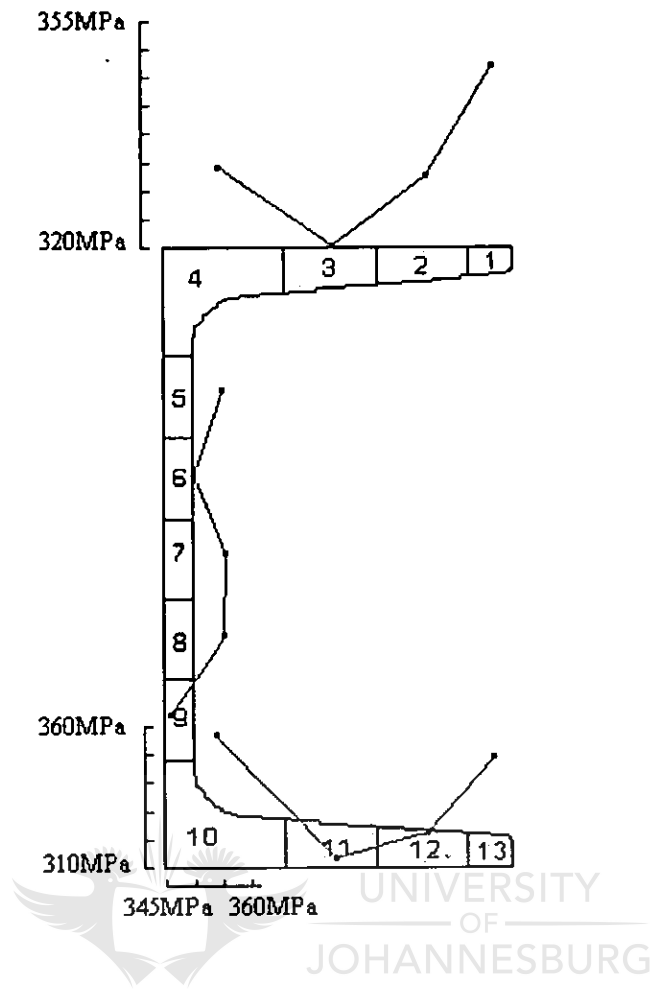


Figure 4.7: Variation of Modulus Yield Stress

4.2.4 Discussion of Compression Test Results

The results of the compression tests indicate clearly that the material properties vary throughout the channel section. This variation is an indication of the variation in strength of the material.

Table 4.1 tabulates the results obtained from the compression tests. The Proportional Limit, Modulus of Elasticity and Yield Strength for each of the 13 sections tested are shown. The proportional limit has the lowest value at section 1 and 4, which is a flange tip and corner section respectively. The highest value is section 9, which is a section adjacent to a corner section in the web. As far as the Modulus of Elasticity is concerned, the lowest value is that of section 13, which is the tip of the bottom flange. Section 5 has the highest value of 209.7 GPa. Section 10 has the highest value for the Yield Stress of 357.5 MPa. Once again section ten is one of the corner sections. The section with the lowest Yield Stress is section 11, adjoining section 10 in the flange plate. Each of these sections also experienced strain-hardening, since they were all deformed past their elastic limit.



When the average mechanical properties between the two flanges are compared, it is clear that on average the yield stress is higher in the web than in the two flanges of the channel section. The same holds true for the Modulus of Elasticity, which is also slightly higher than those in the flanges. As far as the proportional limit is concerned, the value determined by the compression tests in the upper flange is considerably lower than that of the bottom flange as well as the web. This variation in material properties can be attributed to uneven cooling after rolling. This will be discussed in more detail in the next section.

4.3 Residual Stresses

4.3.1 Introduction

Residual stress is defined as stresses that exist in an unloaded member, after it has been manipulated to form the finished product [25]. Research has shown that the magnitude and distribution of residual stresses within the column cross-section is the key factor that influences the strength of straight centrally loaded columns. [22]

In this section, the residual stresses are measured in both 3CR12 and Carbon channel sections, and compared. Simulations were also run in ABAQUS with the residual stress data to determine the influence of residual stress on column strength.

4.3.2 Residual Stress Measurement

Three techniques exist to determine residual stresses, and are classified as nondestructive, semidestructive and destructive [25]. Methods using X-rays and ultrasonic methods are termed nondestructive, but unfortunately, these methods are also the most impractical for determining residual stresses in structural members.

When semidestructive and destructive techniques are used, the residual stresses are determined from the removal of material which causes distortions. A relaxation in stress is caused when the equilibrium in the shape is disturbed by cutting, planing, drilling, grooving or etching. The strain is then measured, and the relaxation of stress is calculated using Hooke's law. A technique is termed semidestructive if the amount of material is minute compared to the original volume of the specimen, and if the specimen can be put together again, as by welding. Destructive techniques remove so much material that the entire specimen is destroyed.

The most widely used method to determine residual stresses in a shape is the destructive method, which was also the method chosen for this particular study. This method is performed by locating a suitable portion of the specimen to be investigated. The second step is to divide the specimen into strips, after which gauge marks are drilled in the middle of each strip. Once this is done, the longitudinal spacing is

measured. The strips are then cold-sawed from the test piece using either a thin milling cutter or a band saw. The change in length between the two gauge marks on each test piece are measured. The average value of residual stress present in the test piece is determined by the change in length and Hooke's law.

4.3.3 Experimental Procedure

The method chosen to determine the residual stresses was the sectioning method, which is a destructive technique, but also the most widely used [25]

Four channel sections (76x18x152) manufactured from both 3CR12 and Carbon, were divided into 13 sections. The thickness of the sections was chosen as 20mm. The length was chosen in accordance with the method used by Bosch [1]. The ends of the columns were machined flat, without allowing the columns to absorb heat.

After the ends of the columns were machined flat, reference indentations were punched into the steel as shown in Figure 4.9. A 5mm center drill were then used to enlarge the indentations. The reason for the indentations was to assist the measuring of the strips. The columns were taken to a room with a constant temperature, and left for approximately 24 hours. This was done to ensure the temperature stabilized since sunlight may cause uncontrollable heat distributions [1]. The distance between the punched indentations was then measured using a digital comparator (Mitutoyo) with a measuring range of 25mm and an accuracy of 0.01mm (Figure 4.8). To ensure that the measurements before and after partitioning were taking in the exact same position, a 6mm diameter ball bearing was attached to both ends of the measuring device. The ball bearings fitted perfectly into the top and bottom indentations made by the center drill. The comparator was calibrated by using a standard gauge length of 203.2mm (8 inches). Subsequent measurements were then either above or below the gauge length. The indentations in the sections caused the true length to be less than the gauge length. Since only the difference in length was important, this did not have an influence on the measurements. Each specimen was measured five times. The extreme readings were ignored and the final measured length consists of the average of the remaining three values.

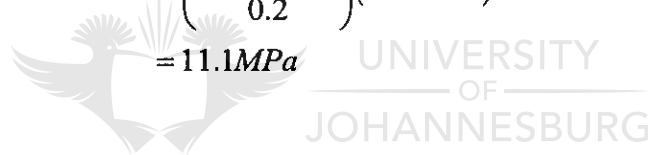
A constant temperature is essential during residual stress measurement. This statement can be proved as follows: [37]

If a temperature difference of 5 degrees centigrade is assumed, and the length of the specimen to be 200mm, the thermal expansion/contraction can be calculated: [35]

$$\begin{aligned}\Delta L &= L\alpha\Delta T \\ &= (0.2)(11.1\times 10^{-6})(5) \\ &= 11.1\mu m\end{aligned}$$

Hooke's Law is used to relate the above contraction/expansion to stress:

$$\begin{aligned}\sigma &= \varepsilon E \\ &= \left(\frac{\Delta L}{L}\right)E \\ &= \left(\frac{11.1\times 10^{-6}}{0.2}\right)(200\times 10^9) \\ &= 11.1MPa\end{aligned}$$



The previous calculation indicates that a temperature difference of 5 degrees can lead to an over/under estimation may occur of approximately 3-4% of the magnitude of the Yield Strength (in this case assumed to be 300MPa). It is therefore concluded that the experiments should be conducted at a constant temperature.

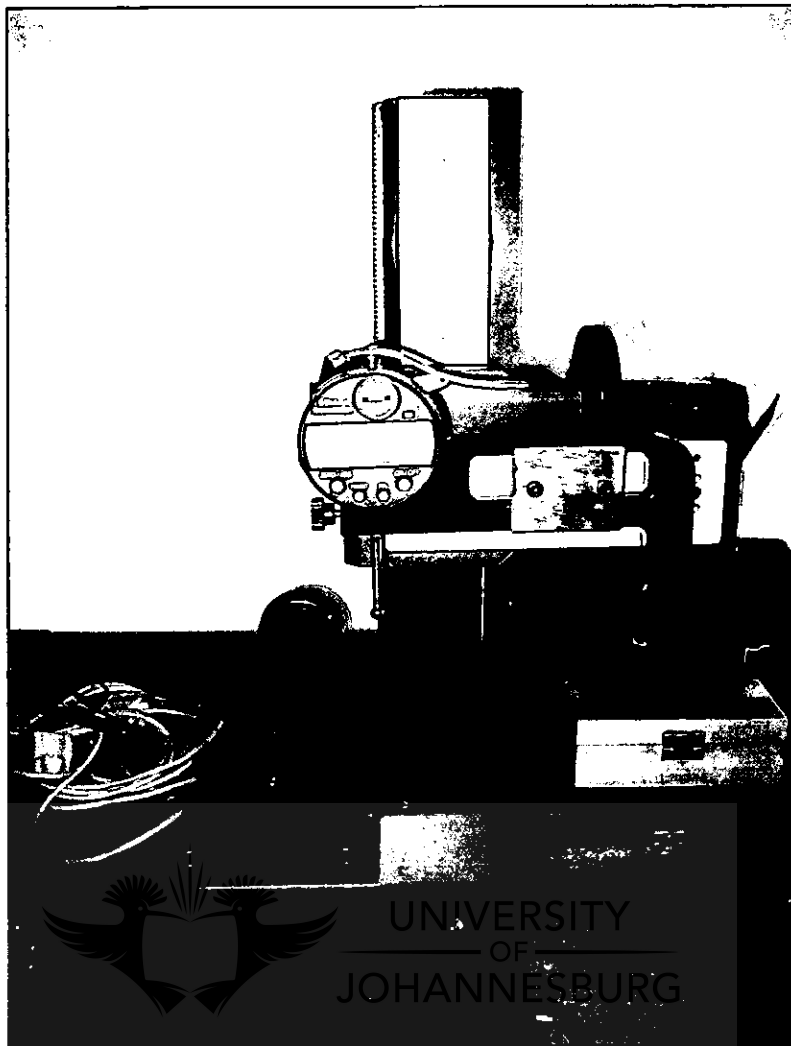


Figure 4.8: *Comparator*

Once the measurements were obtained, the specimens were cut into strips, as indicated in Figure 4.10. This was done carefully with an air cooled band saw, to ensure the metal does not absorb too much heat. The same method as mentioned above were used to measure the distances between the punched holes on the two ends of each section.

The maximum standard deviation for the profile measurements were 0.01, and for the partitioned profiles, 0.002345.

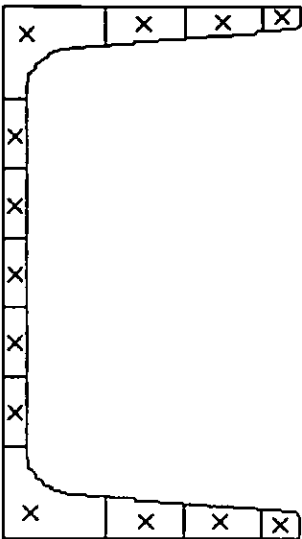


Figure 4.9: Indentations punched into Channel Section

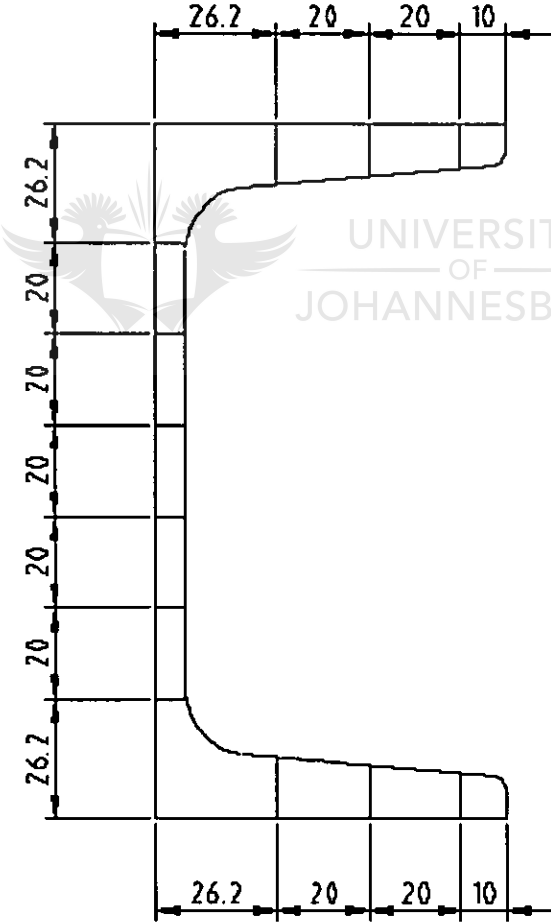


Figure 4.10: Channel Section divided into Sections (mm)

4.3.4 Results

The differences obtained in length from before and after the specimens were cut into strips, are used to determine the residual stresses. The internal Residual Stresses are calculated using the following equation, better known as Hooke's Law:

$$\sigma = E\varepsilon$$

where σ = stress (Pa)

ε = strain

E = Modulus of Elasticity (200 GPa)

The results from the 3CR12 Channel Sections are shown in table 1 and 300W in table 2. The results are presented graphically in Figure 4.11 and Figure 4.12.

Table 4.3: Results from 3CR12 Residual Stress Measurement

	Length(Profile)	Length(Strip)	DI	Strain	Stress
	(mm)	(mm)	(mm)	($\mu\text{m}/\text{m}$)	(MPa)
1	205.833	205.819	0.0140	86.0	13.6
2	205.883	205.900	-0.0177	-8.58	-17.2
3	205.758	205.774	-0.0163	-79.4	-15.9
4	205.764	205.774	-0.0100	-48.6	-9.7
5	205.744	205.706	0.0377	183.1	36.6
6	205.669	205.670	-0.0017	-8.1	-1.6
7	205.719	205.725	-0.0060	-29.2	-5.8
8	205.774	205.771	0.0027	13.0	2.6
9	205.793	205.778	0.0153	74.5	14.9
10	205.779	205.797	-0.0177	-85.9	-17.2
11	205.862	205.856	0.0060	29.1	5.8
12	205.896	205.893	0.0033	16.2	3.2
13	205.937	205.958	-0.0210	-102.0	-20.4

Table 4.4: Results from 300WA Channel Residual stress Measurement

	Length(Profile)	Length(Strip)	dl	Strain	Stress
	(mm)	(mm)	(mm)	($\mu\text{m}/\text{m}$)	(MPa)
1	205.618	205.616	0.00133	6.5	1.3
2	205.477	205.478	-0.00167	-8.1	-1.6
3	205.448	205.436	0.01133	55.2	11.0
4	205.467	205.443	0.02400	116.8	23.4
5	205.480	205.466	0.01433	69.8	14.0
6	205.400	205.396	0.00400	19.5	3.9
7	205.417	205.403	0.01433	69.8	14.0
8	205.420	205.416	0.00400	19.5	3.9
9	205.416	205.408	0.00767	37.3	7.5
10	205.437	205.432	0.00500	24.3	4.9
11	205.464	205.437	0.02700	131.4	26.3
12	205.476	205.467	0.00933	45.4	9.1
13	205.548	205.562	-0.01367	-66.5	-13.3

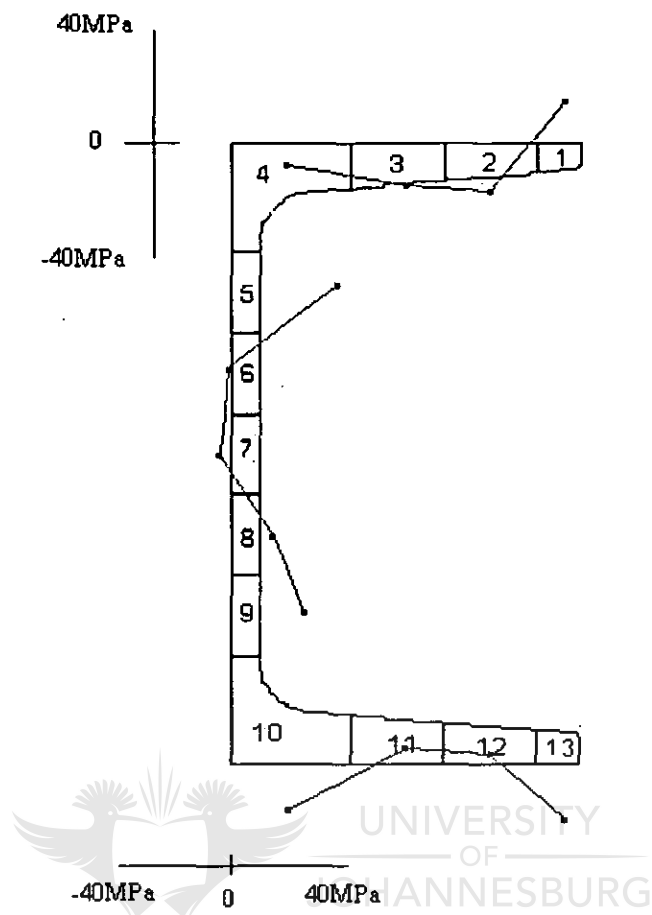


Figure 4.11: *Residual Stress (MPa) Distribution of 3CR12 Channel*

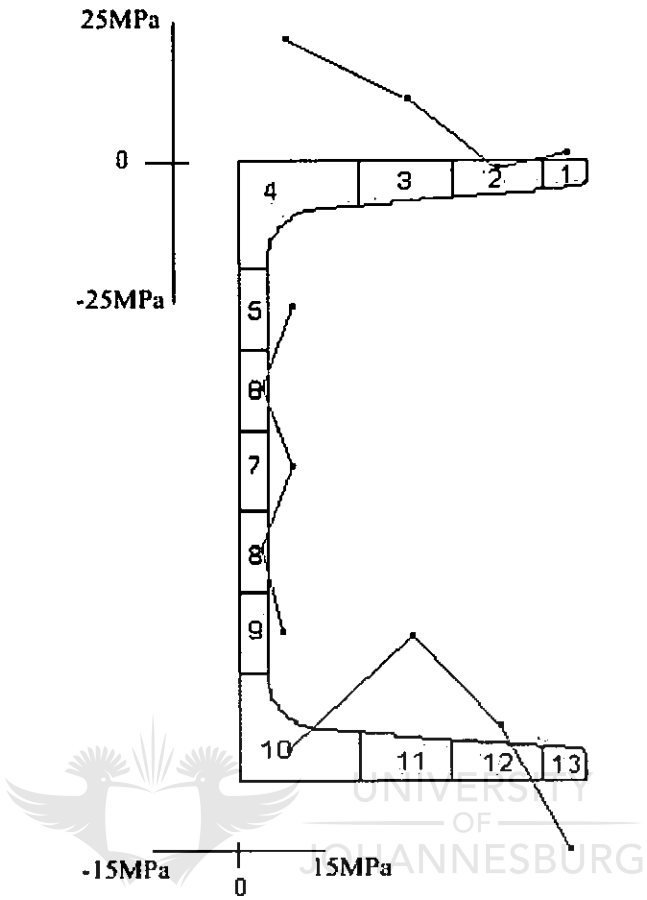


Figure 4.12: Residual Stress Distribution(MPa) of 300WA Channel

4.3.5 Discussion of Results

The results from the residual stress measurements seem to indicate that the residual stresses are relatively small when compared to the results published by Bosch [1]. The maximum measured tensile stress in the 3CR12 channel section was approximately 37MPa, while the largest compression stress was 20MPa. The average tensile residual stress in the channel section was found to be 12.8MPa, while the average compression residual stress was 12.5 MPa.

When the results are compared to that predicted by the literature, the channel sections does not quite follow the theoretical predictions. For both sections, it can be seen that only the bottom flanges behave as predicted, while the top flanges act almost the opposite. The bottom flanges have the tip in compression, while the middle section (the flange plate) is in tension as described by theory.

Both the corner sections are in compression. This is a concern, in view of the fact that in an article published by Lay and Ward [27], it is mentioned that the influence of residual stresses on column strength becomes critical when the parts that contributes most to the stiffness of the section are in compression.

Bjorhovde [19] predicts that the parts that cool last should contain tensile residual stresses. It is assumed that sections 4 and 10 are the thickest, and should therefore take the longest to cool down. For 3CR12, this is not the case, since these two sections are in compression.

Comparing the 3CR12 residual stresses to the residual stresses measured in the 300WA columns, it is noted that the entire web section is in tension, while part of the web in the 3CR12 channel is in compression. The 300WA exhibits the exact behaviour predicted by Bjorhovde, since both the thickest parts (sections 4 and 10) of the 300WA channel are tension.

5 FINITE ELEMENT ANALYSIS

5.1 Introduction

The current chapter discusses Finite Element Analysis that was conducted to investigate the buckling behaviour of channel sections. The ABAQUS finite element code was used. The effect of eccentric loadings, initial imperfections, and the influence of residual stresses were investigated.

A sensitivity analysis was done to ascertain the most suitable element type and size to use in the Finite Element models.

Simulations were done with both Carbon (300WA) and 3CR12 material properties in order to compare the results of a gradual yielding material (3CR12) to that of a less gradual yielding material (300WA). The main focus of all the simulations was to determine the extent of the influence of gradual yielding behaviour, geometric imperfections and residual stresses on the critical axial resistance on the 3CR12 hot-rolled columns. For each series of simulations a graph was obtained, comparing the buckling loads with the minimum prescribed by the relevant SABS Code of practice [16].

5.2 The Finite Element Model

The non-linear Finite Element program ABAQUS (Version 6.5) [30] was used to simulate the behaviour of the channel columns subjected to different imperfections and material properties. The model used in the simulations is discussed in more detail in the following sections.

5.2.1 Geometry

The dimensions of the channel section used in the simulations are presented in the Figure 5.1. The geometry of the channel columns were modeled in SolidWorks, after

which it was converted to an ACIS format (*.sat) file to enable importing into ABAQUS.

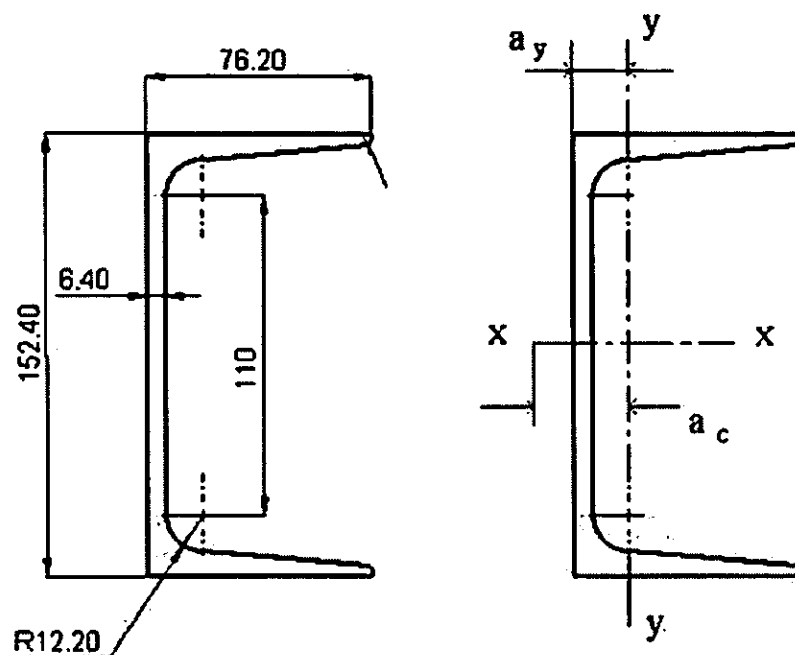


Figure 5.1: Dimensions of Channel Section used in Simulations

Table 5.1: Properties of BS Taper Flange Channel

m	A	a_c	a_y	About x-x			About y-y		
				I	Z_e	r	I	Z_e	I
kg/m	10^3 mm^2	mm	mm	10^6 mm^4	10^3 mm^3	mm	10^6 mm^4	10^3 mm^3	Mm
17.9	2.28	47.8	22.1	8.51	112	61.1	1.14	21.0	22.3

Two discreet rigid plates, one for each end of the column, were created in the Part Module. The main reason for this was to model pinned-ended boundary conditions at the two column ends. The second reason was to simplify the model. Instead of applying the Boundary Conditions to the complex geometry of the channel section, the boundary conditions are applied to one single node on the rigid body plate. The interaction between the rigid body and the channel column will be described later in this chapter.

Various analyses were conducted at different slenderness ratio's. The implied that models were created for different column lengths. Typical models analysed are shown in Table 5.2

Table 5.2: Slenderness Ratio's for Various Column Lengths

Length	0.2	0.6	1	1.4	1.8	2.2	2.6	3	3.4	4.2
Slenderness Ratio (L/r)	9.0	26.9	44.8	62.8	80.7	98.7	116.6	134.5	152.5	188.3

5.2.2 Material Properties

The material properties that were used in the simulations were obtained by conducting compression tests as described in the previous chapter. To obtain representative stress values for a constant set of strain values for the various experimental sets linear interpolation was utilized. These sets were then normalized to an average yield stress of 342MPa. These normal interpolated sets were then averaged to obtain a single representative stress-strain set, which can be seen in Figure 5.2.

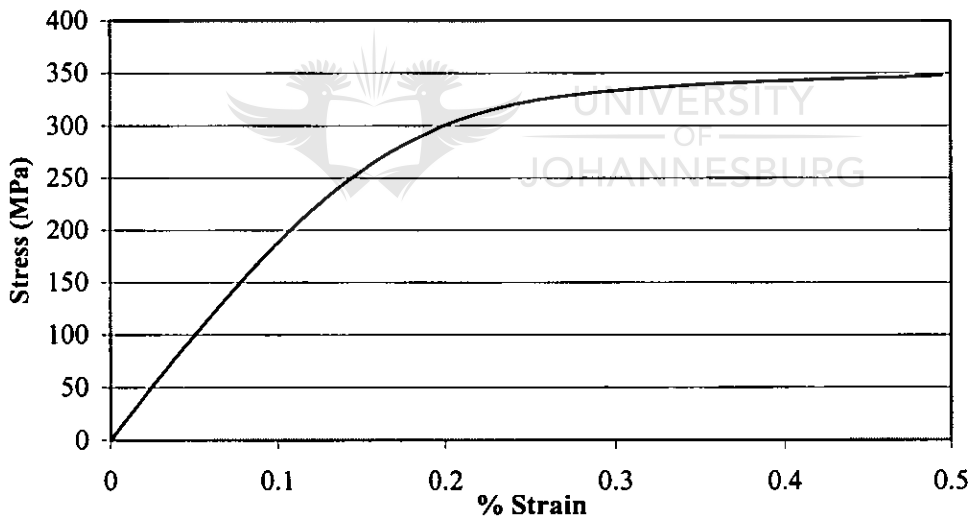


Figure 5.2: Average Material Properties determined from Compression Tests

The material data was first normalized to a yield stress of 327MPa at 0.2% strain to facilitate a comparison between the Finite Element Results and the SABS code of practice prescribed values. A representative stress-strain data set had to be produced from the different stress-strain data sets obtained experimentally. Simple averaging was not possible because the data set were not represented by a constant varying set of either stress or strain variations.

5.2.3 Step/Analysis

Each model was analyzed by using a dynamic implicit step. This type of step was used to conduct a nonlinear direct-integration dynamic analysis. Since this is a general nonlinear procedure, ABAQUS/Standard utilizes implicit time integration to determine the dynamic response of a system.

A dynamic analysis was chosen because nonlinearities are easier accounted for in a dynamic situation than in a static situation, in view of the fact that mathematical stability is provided to the system by the inertia terms in a dynamic analysis. Therefore, except for extreme cases, this method usually proves to be more successful.

ABAQUS/Standard uses time integration to calculate a model's dynamic response in a nonlinear analysis. The method provided by ABAQUS is called the Hilber-Huges-Taylor operator, which is an extension of the trapezoidal rule. This operator ensures that the integration operator matrix is inverted, and at each time increment, a set of simultaneous nonlinear dynamic equilibrium equations must be solved. Using Newton's method, this solution is done iteratively.

The main advantage of using the Hilber-Huges-Taylor operator is that it is unconditionally stable for linear systems. This is based on the fact that no mathematical limit is imposed on the size of the time increment used in a linear system. For practical purposes, an adequate indication of the integration method's properties for nonlinear systems is provided by the linear stability results.

When studying structural systems, an unconditionally stable operator is of essential importance, since a conditionally stable integration operator may lead to impractical small step, which will result in an expensive analysis.

To ensure an accurate solution, automatic incrementation in a general, implicit dynamic integrations scheme uses a half-step residual control. The half step residual is defined as the equilibrium residual error or the out-of-balance forces halfway through

a time increment. The adaptive time incrementation scheme is based on the half-step residual check. High accuracy of the solution is indicated by a small half-step residual, while a large half-step residual indicates that the time step should be reduced.

To specify an appropriate half-step residual tolerance, the `*HALFTOL` parameter on the `*DYNAMIC` option is used (See sample input file – Appendix C). The dimensions of the `HALFTOL` parameter is that of force, and should therefore be chosen by comparison to actual force values, e.g. applied forces or expected reaction forces.

5.2.4 Interactions

The interaction between the discrete rigid plates and the bottom and top of the channel were modelled by creating a “tie-connection” between the two surfaces (see Figure 5.3) ABAQUS utilized a master-slave surface relationship for defining interactions. The slave surface cannot penetrate the master surface although limited penetration the other way around is possible.

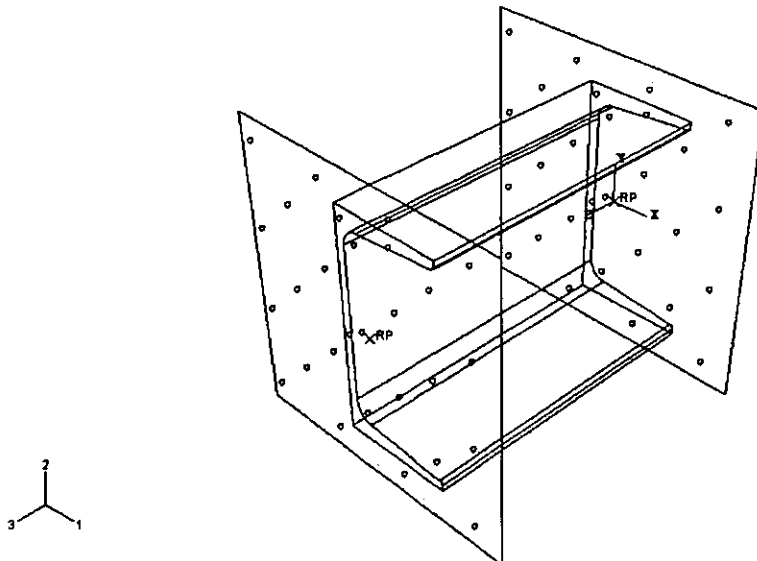


Figure 5.3: *Tied interaction between rigid plates and Channel Column*

5.2.5 Load / Boundary Conditions

The finite element model simulated the column compressed between pinned ends. The pinned-ended boundary condition was simulated by restraining all the translating degrees of freedom at both ends of the column, except for the translational degree of freedom in the axial direction at the top, due to the applied load. Here, an appropriate displacement was specified in the negative z-direction. The rotational degree of freedom in the z-direction at the top was also restrained to prevent the column from spinning. These boundary conditions were applied to the reference nodes on the plates at the ends of the column (Figure 5.4). The reference point or point of rotation corresponded with the centroid.

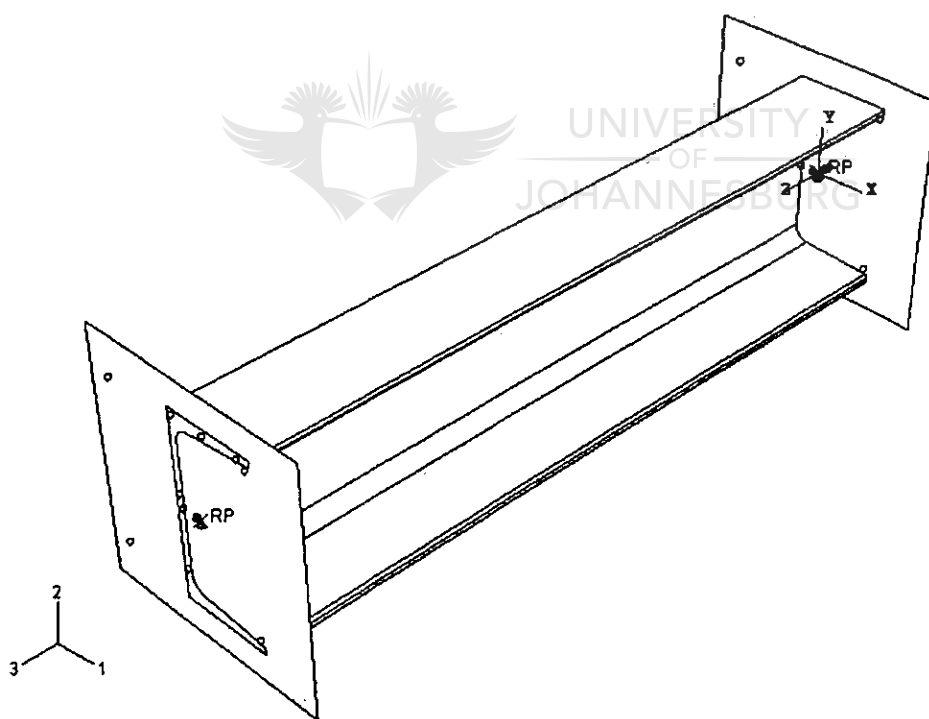


Figure 5.4: *Boundary Conditions*

5.2.6 Mesh

Two types of elements were investigated to be used to mesh the channel sections. The channel column was mesh with C3D10M elements, which are 10-node modified quadratic tetrahedral elements. Tetrahedral elements are less sensitive to distortion, and for problems not involving complex contact conditions, impact or severe element distortions, the second-order (quadratic) elements provide higher accuracy than their first-order counterparts. The reason for the increased accuracy is that first-order tetrahedral elements are usually overly stiff, and to obtain accurate results, extremely fine meshes are required, which in turn increases the running time. First-order elements are also prone to volumetric locking in incompressible problems.

The discrete rigid plates on the ends of the channel were meshed using R3D4 elements. The R3D4 element is a four-node three-dimensional, bilinear rigid quadrilateral element. An example of the meshed column and end plates are shown in Figure 5.8.



5.2.6.1 Mesh Sensitivity Analysis

The first step in the Finite Element Analysis is to divide the model under examination into an assembly of subdivisions called elements. This is done in such a way that the unknown field variable is adequately represented throughout the model.

Since the finite element method is only an approximate method, the way in which the problem is discretized affects the accuracy of the final answer [29].

The accuracy of the model can be increased in two ways.

- 1) The geometry can be divided into smaller elements, so that the mesh density is increased (h-refinement).
- 2) The accuracy of the elements themselves can be improved by using higher order interpolation functions (p-refinement)

To investigate the increasing accuracy of a model by h-refinement, all previous meshes should be contained in the finer meshes, i.e. a reducible net should be used [29]. It was decided to conduct simulations in which the columns are meshed with 10mm,15mm,20mm, 25mm and 30mm Quadratic Tetrahedral Elements respectively. The results for selected column lengths are tabulated below, specifically pertaining to running time, number of elements and buckling load. The columns analyzed below are 600mm, 1000mm, 1800mm, 2600mm and 3400mm. Tables 5.3 – 5.7 summarizes the analysis for each column length in table format.

Table 5.3: Mesh Size Sensitivity Results (600mm)

Element Size(mm)	Buckling Load	Time to Complete (hh:mm:ss)	Number of Elements
10	698.2	02:00:21	14367
15	698.0	00:49:45	6150
20	692.6	00:33:33	3791
25	691.6	00:23:04	2740
30	696.0	00:19:05	2247

Table 5.4: Mesh Size Sensitivity Results (1000mm)

Element Size(mm)	Buckling Load	Time to Complete (hh:mm:ss)	Number of Elements
10	660.9	02:48:52	24221
15	656.2	01:00:36	9461
20	654.2	00:33:29	6004
25	627.0	00:23:46	3262
30	626.8	00:20:00	2676

Table 5.5: Mesh Size Sensitivity Results (1800mm)

Element Size(mm)	Buckling Load	Time to Complete (hh:min:ss)	Number of Elements
10	500.0	13:45:44	43825
15	487.7	03:43:45	16951
20	487.1	01:48:22	10775
25	460.4	00:57:09	5766
30	462.2	00:47:14	4768

Table 5.6: Mesh Size Sensitivity Results (2600mm)

Element Size(mm)	Buckling Load	Time to Complete (hh:min:ss)	Number of Elements
10	351.2	*	46170
15	350.7	*	24180
20	350.3	03:46:50	15249
25	323.4	01:29:03	8210
30	328.4	01:22:19	6811

Table 5.7: Mesh Size Sensitivity Results (3400mm)

Element Size(mm)	Buckling Load	Time to Complete (hh:min:ss)	Number of Elements
10	#	#	#
15	#	#	#
20	206.1	02:10:36	17367
25	210.6	01:19:50	10423
30	203.1	01:06:54	8403

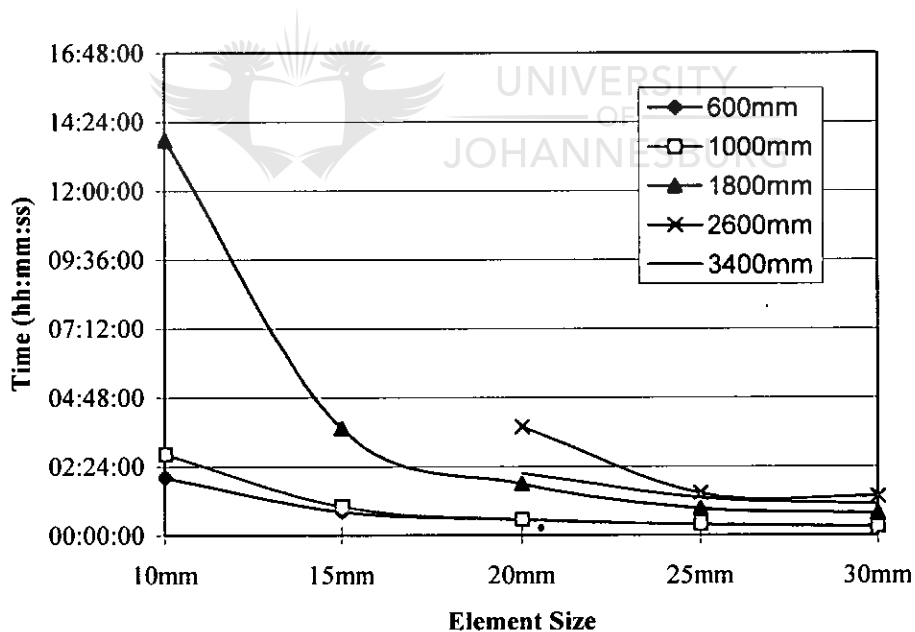


Figure 5.5: Time to Complete vs Element Size*

* Due to limited hard drive space, these simulations aborted before it completed.

These simulations aborted before the column could buckle.

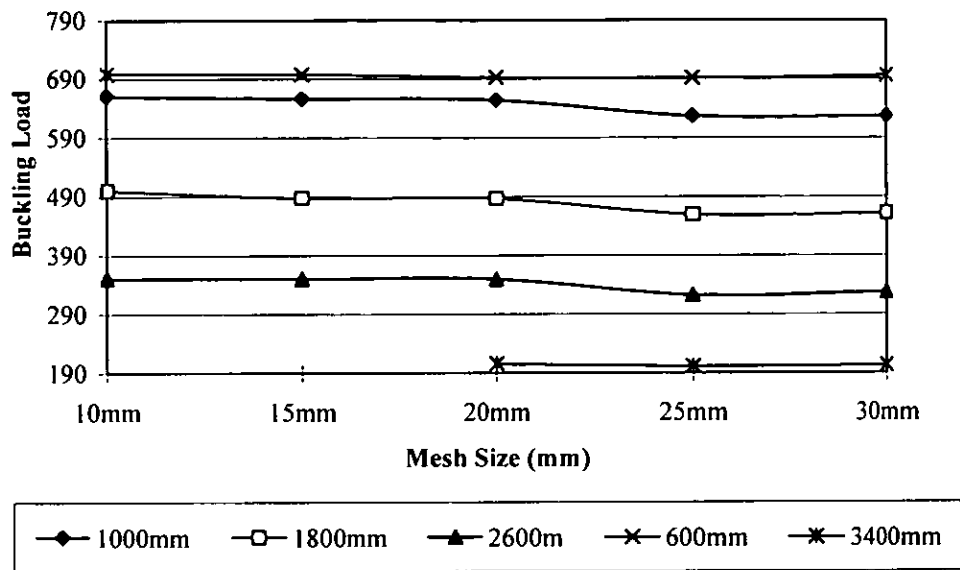


Figure 5.6: Buckling Load vs. Element Size

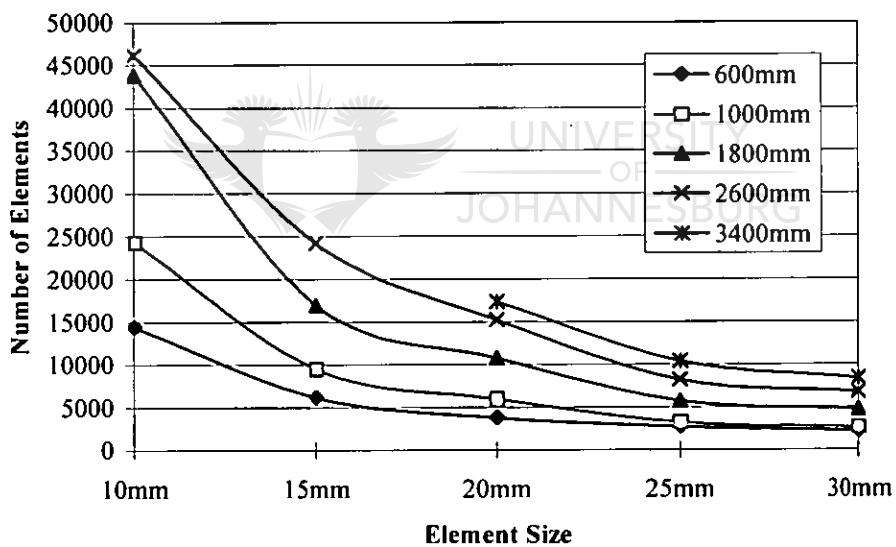


Figure 5.7: Number of Elements vs. Element Size

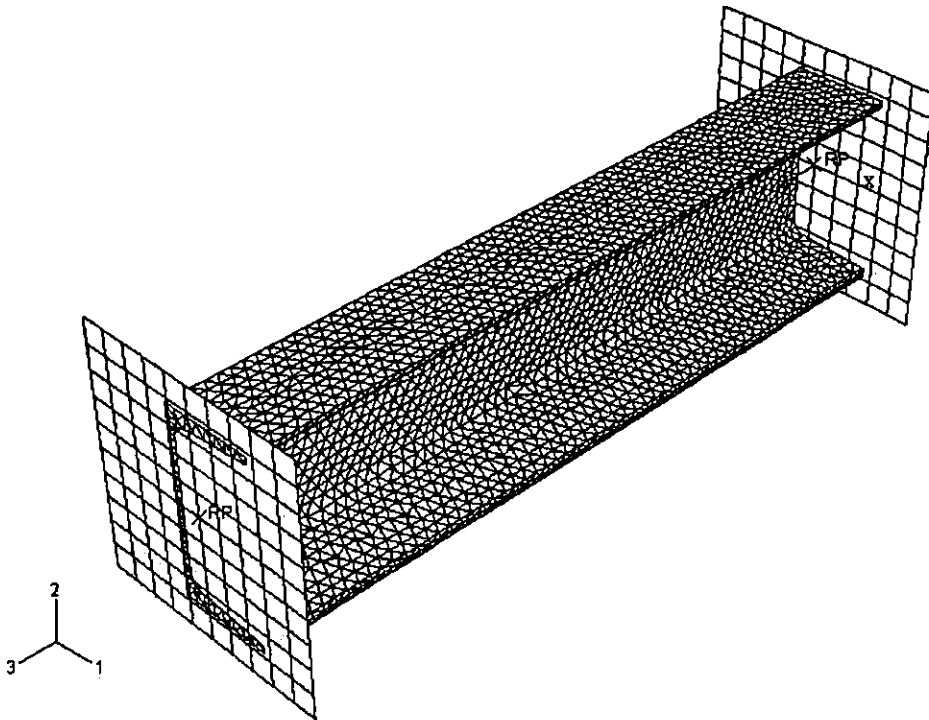


Figure 5.8: *Tetrahedral Mesh*

Discussion of Mesh Analysis Results

All of the above tables and graphs clearly indicates that meshing the column with different element sizes have a notable effect on the time it takes to complete the simulation, the number of elements, and most importantly, the buckling load. Figure 5.5 illustrates that the time ABAQUS takes to complete a simulation increases drastically if the element size is decreased from 30mm to 10mm. For example, a column of length 1800mm will take only 47 minutes to complete if the column is meshed with 30mm elements. If the size is reduced to 10mm, the running time increases to approximately 13 hours and 45 minutes. This could be attributed to the fact that as the element size is reduced, the number of elements increases (Figure 5.7), and therefore the number of nodes that needs to be integrated increases accordingly.

Most important is the effect of the element size on the buckling load. Figure 5.6 indicates that as the element size is increased, the buckling load is reduced. This is more pronounced for columns in the intermediate slenderness range (1000mm, 1800mm and 2600mm) than for the shorter 600mm column and the slender 3400mm column.

Overall it was concluded that 10mm quadratic tetrahedral elements should be used for all the columns except the most slender columns, as these elements were the smallest elements that approached convergence. The two slender columns (3400mm and 4200mm) should be meshed with 20mm Quadratic Tetrahedral elements in order to reduce the file size (*.stt) and the running time.

5.3 Simulations done in ABAQUS

5.3.1 Simulations to Compare with Experimental Work

Experimental tests were done on 3CR12 hot-rolled channel sections by Laubscher [38] to determine the buckling loads of the columns. The experimental procedure is discussed in Appendix C. To determine the accuracy of the developed Finite Element Model, simulations were done on channel sections using the physical geometry from the channels used in the tests, but using the material properties obtained from the compression tests as described earlier. The average curve was normalized to a yield stress of 327 MPa to make it possible to directly compare the ABAQUS results with the experimental results.

The overall effective length of the axial compression members was adjusted by taking the end-fixtures into account as described by Osgood [39]. This was achieved by adding the thickness of the end fixtures (adjustable plates and steel balls) to the length of each member. The results of the channel column tests are shown in Table 5.8.

Table 5.8: Experimental Results

	3CR12				
<i>L/r</i>	T1	T2	T3	<i>Avg (kN)</i>	SD
9.91	863	873	863	866	5.8
58.56	585.7	622.7	642.7	617.0	28.9
94.59	501	513.5	526	513.5	12.5
184.7	141	128	124	131.0	8.9

The critical buckling loads as obtained from the numerical analysis are presented in Figure 5.9, as well as a plot of the column curve prescribed by the SABS 0162-1:1993 Code of practice, and the experimental results.

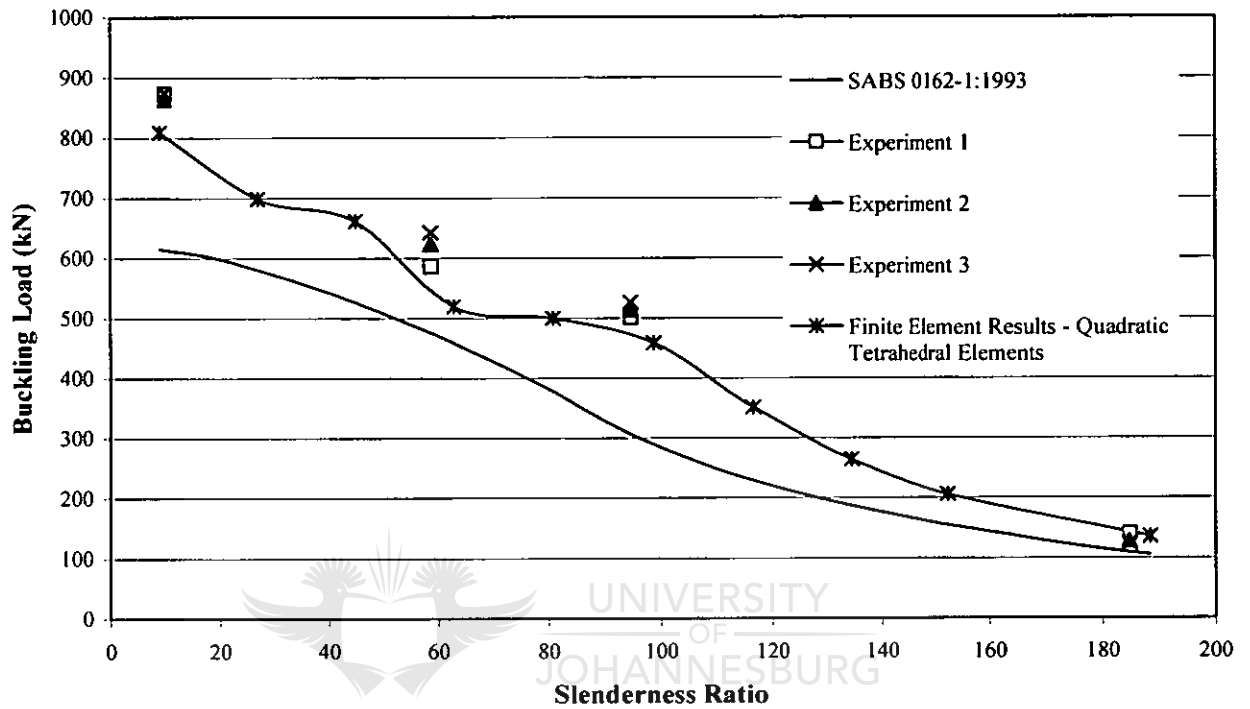


Figure 5.9: Comparison of FEM Results with Experimental Results

Examples of contour plots depicting von Mises stress for the two failure extremes are presented in Figure 5.10 and 5.11. The short column (200mm) failed by yielding of the material following by local buckling, while the slender column (2200mm) failed by overall flexural buckling.

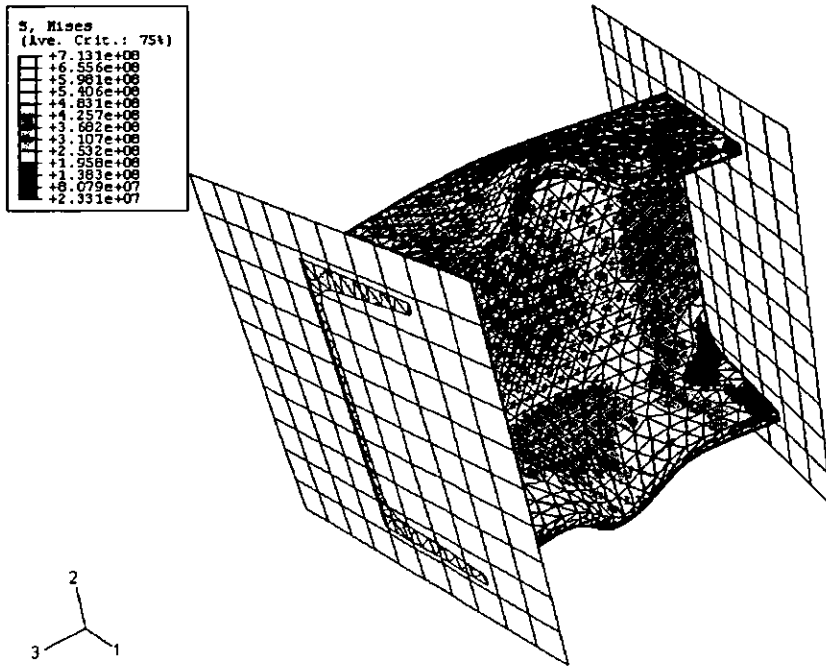


Figure 5.10: Example of a short column failed by yielding followed by Local Buckling

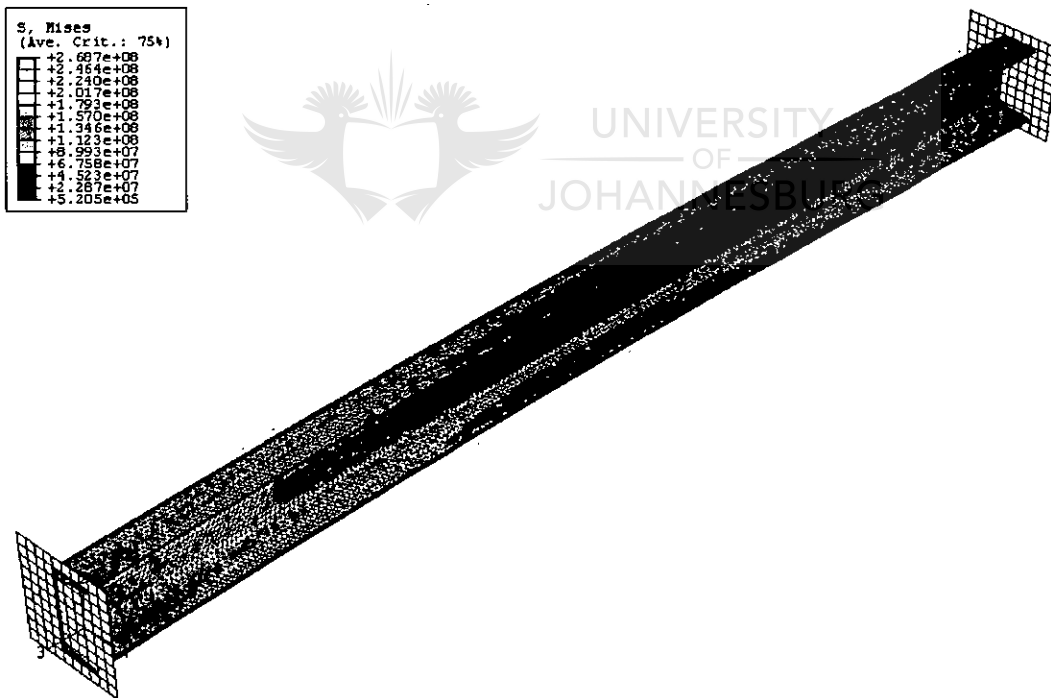


Figure 5.11: Example of a Slender Column Failing by Overall Flexural Buckling

5.3.1.1 Discussion

The above simulations were run in order to compare the numerical model available experimental data. The results of the Finite Element Analysis are a measure of the accuracy of the model. The above graph indicates that the Finite Element Results did not yield the exact same buckling loads as obtained by the experiments. For columns in the short and intermediate slenderness range, the Finite Element results are slightly less than the buckling loads obtained from the experiments. For columns in the slenderness range of $s/l = 94$, the FEM results are within approximately 11% of the experimental buckling loads. For very slender columns ($l/r = 150 - 200$), the approximation given by the Finite Element Analysis results correspond with the buckling loads obtained by the experiments. It can be concluded that the overall trend is accurately modelled.

5.3.2 Influence of Gradual Yielding Behaviour on Column Strength

One of the objectives of this study is to determine the influence of the gradual yielding behaviour of 3CR12 on column strength. To accomplish this, the same method of analysis was used for the Finite Element Analysis, with the exception of the material data. Once again, the material properties as obtained from the compression tests were taken and normalized to a yield stress of 300MPa, to enable the results to be directly comparable to the minimum prescribed by the SABS Code. However, the material data still portray the gradual yielding behaviour as exhibited by the actual material. In order to compare the Finite Element Results to a material with less gradual-yielding material behaviour, simulations were run with the exact same model, but with the material properties of 300WA, normalized to a yield stress of 300MPa. The material properties of the 300WA were determined by conducting stub column tests [38]. In order to graphically illustrate the more pronounced gradual yielding behaviour of 3CR12, a graph is plotted in which the 300WA stub column tests are compared to results from 3CR12 stub column tests (Figure 5.12) [38]. The results of the Finite Element Analysis are summarized as a column curve in Figure 5.13, together with the SABS Code, the Euler Column Curve and the 300WA results.

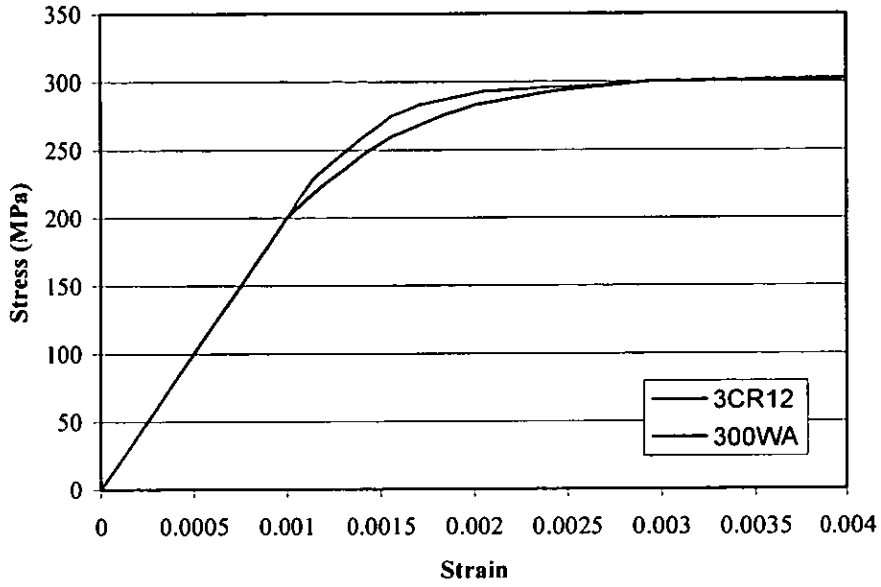


Figure 5.12: Comparison between 300WA and 3CR12 Stress-Strain Curves

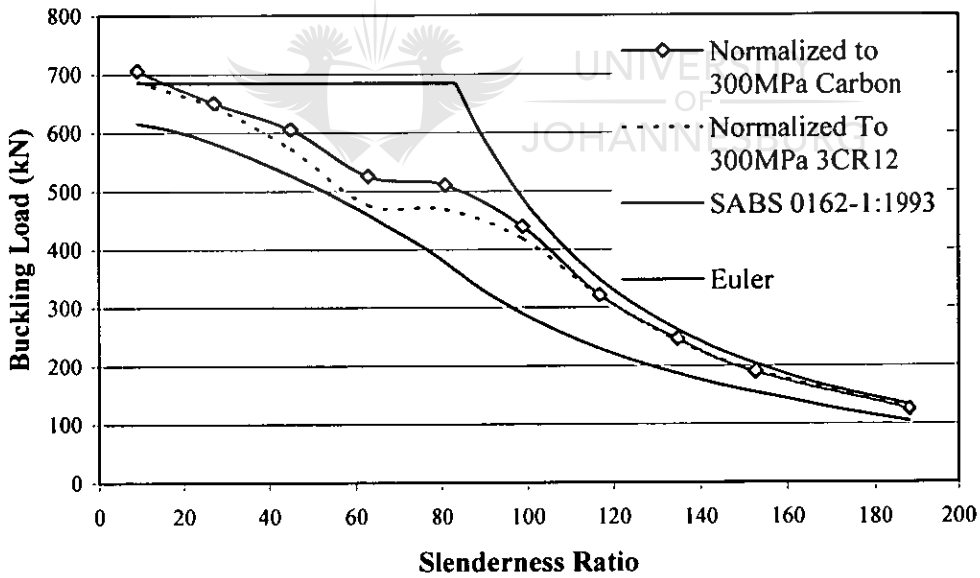


Figure 5.13: Column Strength of 3CR12 ($F_y = 300\text{MPa}$)

5.3.2.1 Discussion of Gradual Yielding Behaviour Results

From the resulting graph it is evident that the gradual yielding material behaviour of 3CR12 has a significant influence on column strength, especially in the intermediate slenderness range. The characteristic “dip” that was found with the experimental data is also reflected in the above results. This is the result of the lower localized tangent elastic modulus in the intermediate range between overall buckling and local buckling.

When compared to the Finite Element Results for 300WA, it can be seen that in the slenderness range of $s/l = 20$ to 100, the critical axial resistance of the 3CR12 columns are considerably less than the axial resistance of the 300WA columns. For columns long slenderness range ($s/l = 120 - 188$) the critical axial resistance of 3CR12, 300WA, coincide. For tall columns, in the slenderness range of $s/l = 155 - 188$, the values of both 3CR12 and 300WA are the same as predicted by Euler, which is expected.

It can therefore be concluded that the more pronounced gradual yielding behaviour of type 3CR12 corrosion resisting steel has a detrimental effect on the critical axial resistance of channel columns.

5.3.3 Influence of Initial Out-of-Straightness

As already noted earlier in the literature review, perfectly straight columns do not exist in reality. In this section, the influence of an initial out-of-straightness on the buckling load of the 3CR12 columns is investigated. The initial out-of-straightness was assumed to be that of a half-sine wave [28]. The behaviour of these columns was investigated using the same Finite Element Model used in the previous simulation, but in this case, the initial out-of-straightness was created by utilizing a half sinus wave, and superimposing this curvature onto the Finite Element Model. The material data was once again compression test data normalized to 300MPa. The curvature was obtained by modifying the nodes of the column in the input file (*.inp) for each simulation. Simulations were run for an initial out-of-straightness of $L/500$, $L/1000$ and $L/1500$. An initial out-of-straightness of $L/500$ would then typically imply a

maximum out-of-straightness at the center of the column of 0.4mm for the shortest column (200mm) and 4.4mm for the longest column (2200mm).

The results are graphically illustrated in the graphs below. (Figure 5.14-5.16)

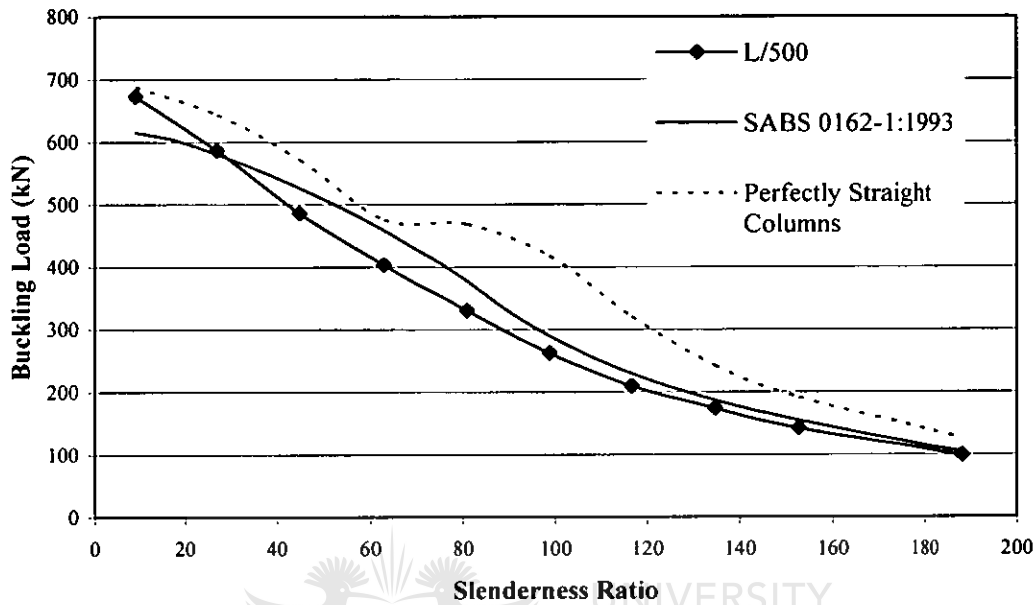


Figure 5.14: Column Curve for L/500

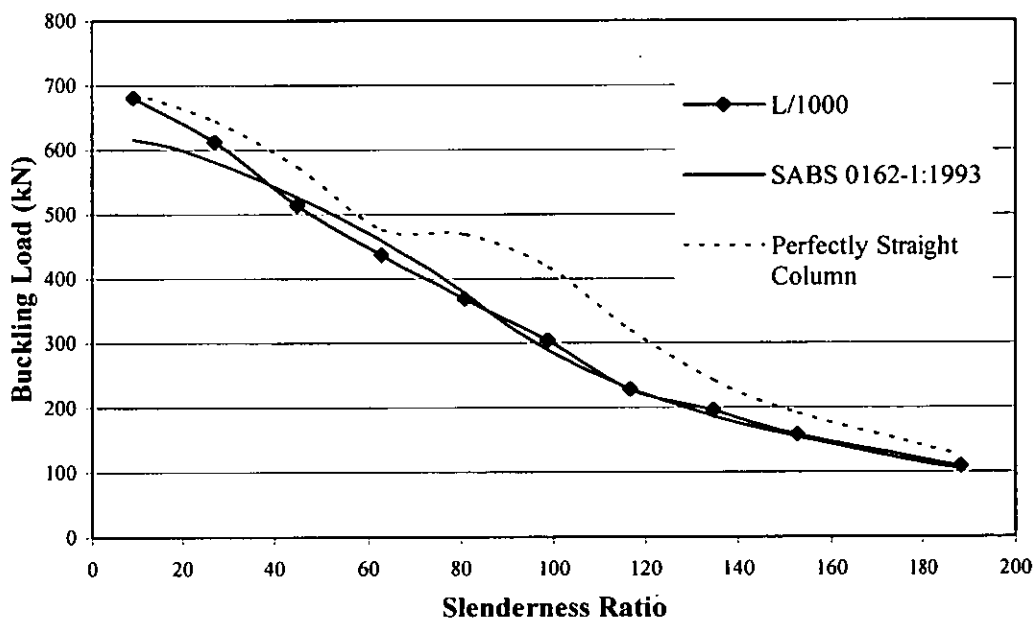


Figure 5.15: Column Curve for L/1000

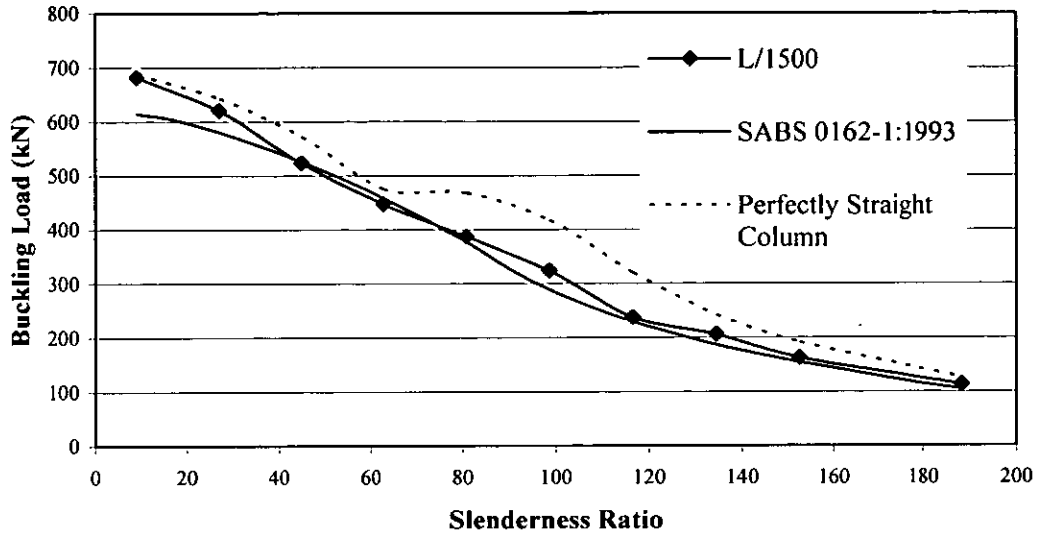


Figure 5.16: Column Curve for L/1500

To estimate whether an initial curvature has the same detrimental effect on the buckling load for columns with less gradual yielding material properties, simulations were done using the same Finite Element Models, but with the material properties of 300WA. The Figure below plots the results (Figure 5.17). A maximum allowable value of L/1000 was chosen for the simulations.

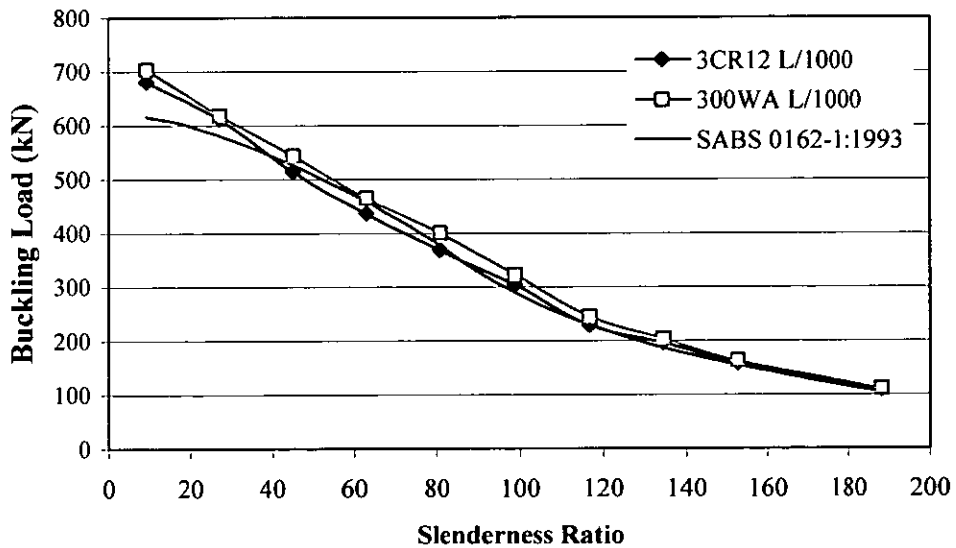


Figure 5.17: Column Curve L/1000 (300WA)

5.3.3.1 Discussion of Initial out-of-straightness Simulations

The results from the above simulations point toward an initial imperfection having a significant influence on the column strength. From the three imperfections simulated, the most pronounced decrease in strength can be seen for an initial imperfection of $L/500$. When the column curve for $L/500$ is compared to the column curve predicted by the SABS Code, it can be seen that the entire column curve lies beneath the curve, except for the two shortest columns (200mm and 600mm). The buckling load of the shortest column is not influenced by the initial imperfection, since the material properties causes the column to fail, and not by the applied load.

For columns with an initial out-of-straightness of $L/1000$ (the largest allowable) the situation improves slightly. Columns in the intermediate slenderness range ($s/l = 35$ to 80), lie below the minimum values prescribed by the code of practice. The results for slender columns (from $s/l = 134.5$) coincide with the results given by the code.

The column curve for columns containing an average initial out-of-straightness of $L/1500$ is mostly above the values prescribed by the code. The exception is for columns in the range of $s/l = 45$ to 80 , in which the code overestimates the critical axial resistance of these columns.

The last graph (Figure 5.17) plots the results for 300WA columns having an initial out-of-straightness of $L/1000$, together with the column curve for 3CR12 having a similar imperfection. From the graph it is evident that the effect of the initial curvature is more detrimental for 3CR12 columns than for 300WA columns. The values predicted by the SABS code of practice are just barely sufficient for 300WA. But for 3CR12, the code of practice underestimates the columns strength in the intermediate range.

Since the simulations for both 3CR12 and 300WA are similar except for the material properties, it can be concluded that the gradual yielding behaviour of the 3CR12 are responsible for the decrease in column strength in the intermediate range.

5.3.4 Influence of Eccentric Loading

To determine the influence eccentric loading will have on 3CR12 hot-rolled members, a series of simulations were conducted. Columns ranging in length from 200mm to 4200mm were simulated having applied loads at different eccentricities. Eccentric loading was modelled with the eccentricity varying up to 4mm either side of the centroid. The exact same model used to investigate the influence of gradual yielding behaviour was once again used, except that in this case, the point of loading are moved accordingly to introduce the eccentricities.

Since the axial load is moved from the centre of the cross-section, a bending-moment is introduced, and the member is no longer a pure column. This is due to the fact that part of the resistance is used to carry the axial load, and part the bending moment. [19]

The results of the simulations are shown below in Figure 5.18. This is a three-dimensional plot combining buckling load, length and eccentricity. Figure 5.19 gives a perpendicular view of the three-dimensional plot, to visualize the influence on each column length.

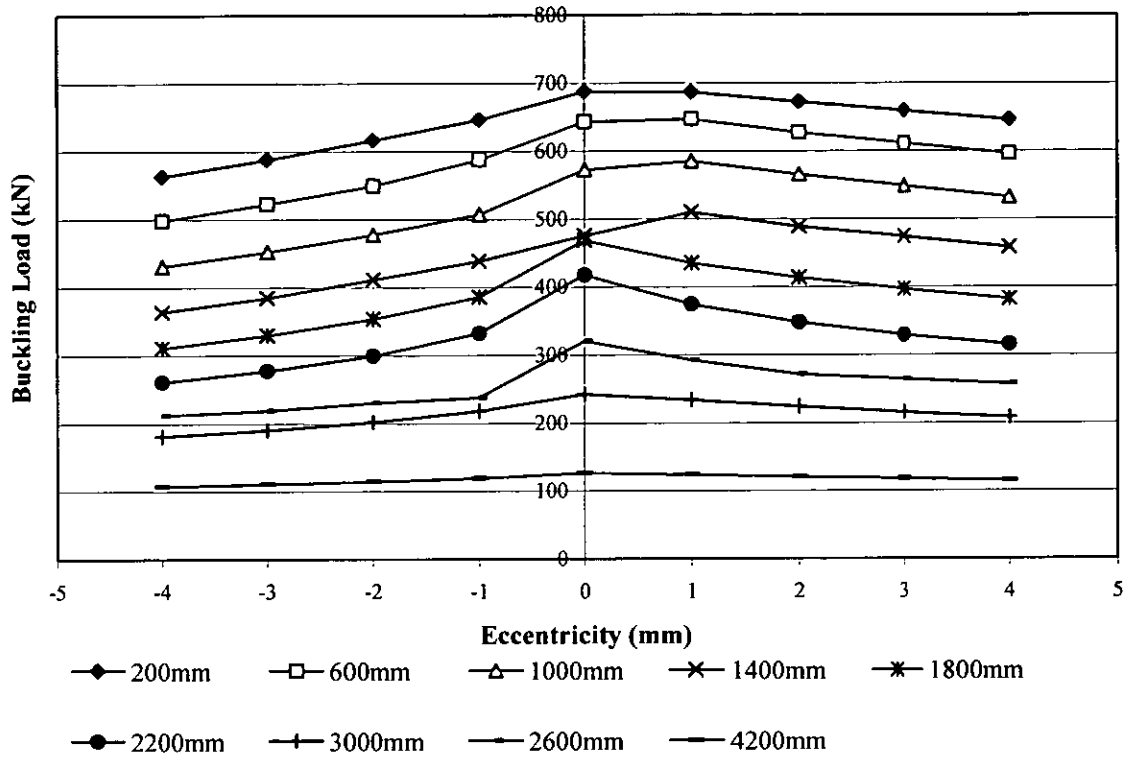


Figure 5.18: Perpendicular view of the three-dimensional plot

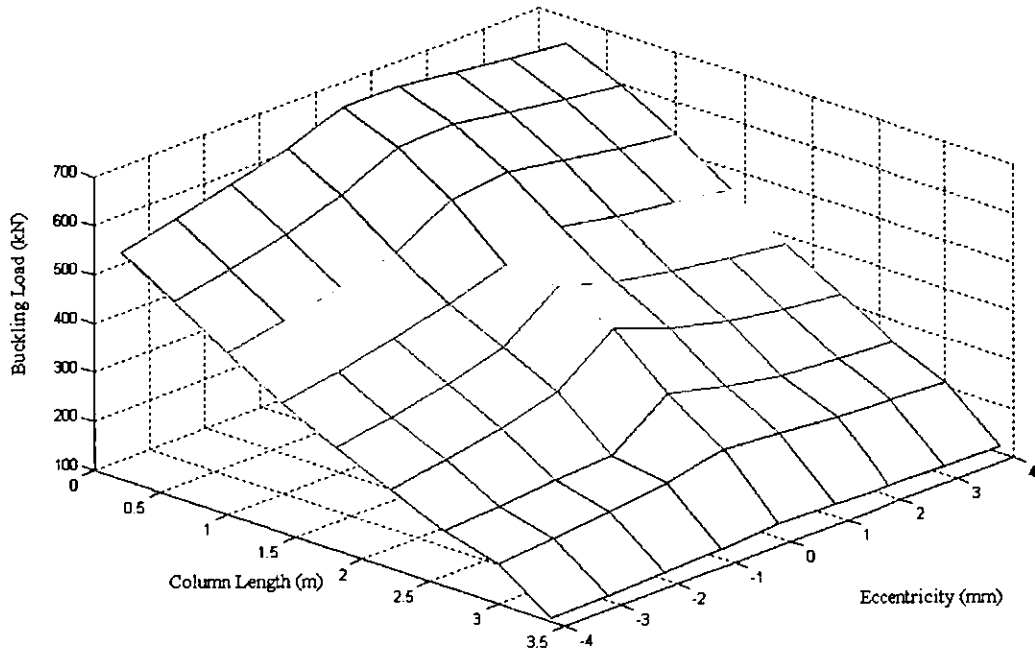


Figure 5.19: Three-dimensional plot of Eccentric Applied Load

5.3.4.1 Discussion of Eccentric Loading Results

From Figures 5.18 and 5.19 it is clear that eccentric loading has a noticeable influence on the buckling load of 3CR12 hot-rolled columns. The perpendicular plot indicates that the buckling strength decreases as the distance between the point of loading and the web of the channel section increases. This diminished buckling strength is caused by the flanges being thinner at the tips, and can therefore provide less resistance to buckling. Moving the point of loading closer to the web, the critical axial resistance decreases. This can be attributed to the non-linear behaviour of the material, which causes a reduction in stiffness at stresses above the proportional limit. This is only applicable to the cases where the point of loading is moved 1mm closer to the web. If the distance between the point of application and the web is further decreased the critical axial resistance diminishes even further, but not to the same extent as when the point of loading is moved in the opposite direction (towards the flange tips). For example, consider a 1000mm length column ($s/l = 44.8$). The buckling load is reduced from 572.6kN (loaded at the centroid) to 431.2 kN if the point of loading is moved 4mm closer to the flange tips, but is only reduced to 532.6 kN if the point is moved 4mm closer to the web section.

Another conclusion that can be drawn from the perpendicular plot (Figure 5.19) is that the influence of the eccentric loading becomes less pronounced as the slenderness ratio is increased.

5.3.5 Influence of Both Eccentric Loading and Initial Out-of-Straightness

Since it is possible that both eccentric loading as well as an initial out-of-straightness may occur in any particular column, it was decided to simulate this situation to determine the influence of these imperfections on the critical axial resistance. The columns have an initial out-of-straightness of $L/1000$, and were loaded 1mm closer to the flanges of the section. The results are plotted in the figure below. (Figure 5.20)

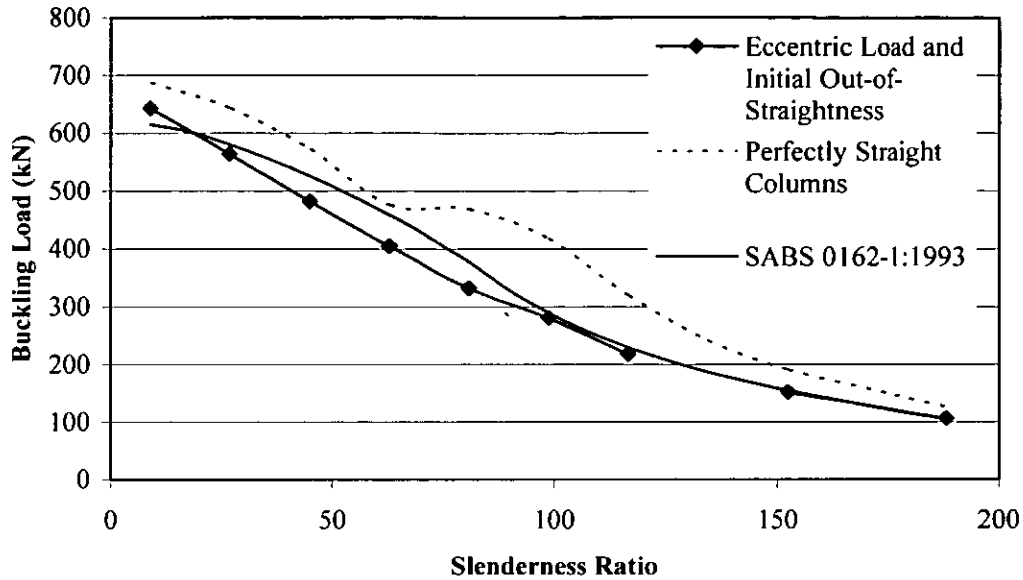


Figure 5.20: Influence of both Initial out-of-straightness and Eccentric Loading

5.3.5.1 Discussion of Results

The previous graph clearly indicates that the critical buckling load of a column with both an eccentric load and an initial imperfection are noticeably influenced. The most significant reduction in column strength can be seen in the intermediate column length range, ranging from a slenderness ratio of 8.97 to 98.65. For this range, the critical buckling loads are well below the minimum column curve prescribed by the SABS code. For tall columns, the strength was also reduced, but not as noticeably as for the intermediate columns. In this range, critical the buckling loads coincide with that prescribed by the SABS Code.

5.3.6 Influence of Residual Stresses on Column Strength

As a result of the cooling process used in manufacturing hot-rolled sections, the final columns almost always contain residual stresses. This scenario was modeled in ABAQUS by first dividing the channel section into 13 subsections as described in the previous chapter, and assigning different material properties to each section.

The material properties for each section were manipulated to represent the residual stresses by adjusting the yield stress for each section accordingly to represent the compressive or tensile residual stresses found experimentally. For example if a compressive residual stress of 30MPa was measured at a given point the local yield stress in this region was reduced from 300MPa to $(300 - 30) = 270$ MPa. For tensile residual stresses, the yield stress was increased accordingly. The rest of the model remained unchanged, implying that a 300MPa normalized stress-strain curve used and a perfectly straight column was modeled.

The results are summarized in the Figure below. (Figure 5.21). The SABS Code 0162-1:1993 are illustrated, as well as columns exhibiting only gradual yielding behaviour (normalized to a yield stress of 300MPa) and the critical axial resistance obtained for each column from ABAQUS.

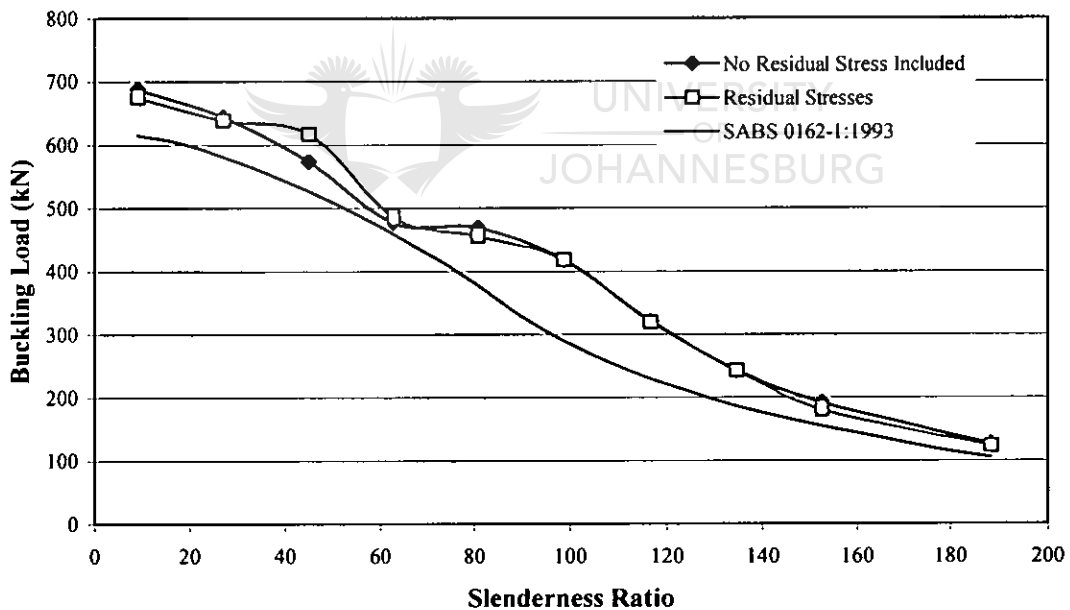


Figure 5.21: Influence of Residual Stress on Column Strength

5.3.6.1 Discussion of Residual Stress Simulations

Figure 5.21 indicates that the presence of residual stresses in the 3CR12 columns have an influence on the strength of the columns. The presence of residual stresses has shown to have both a beneficial as well as detrimental effect on the critical axial resistance. For short columns, the influence seems to be minimal, but for columns in the intermediate range ($s/l = 40$ to 60), the residual stresses have a more positive effect on the buckling strength of the columns, since the critical buckling load is slightly increased. For columns between $s/l = 60$ - 100 , the buckling load is once again reduced. This phenomenon may be attributed to the unsymmetrical distribution of the residual stresses throughout the section. The buckling load of columns in the elastic range is not influenced by the presence of residual stresses.

5.3.7 Effect of both Residual Stress and Initial Imperfection

In practice, columns with both residual stresses and initial imperfections are often encountered. To investigate the effect of this on the buckling load of the 3CR12 columns, the Finite Element Model from the previous Residual Stress simulations were utilized, but the nodes were modified to portray an initial out-of-straightness of a half-sinus wave. The simulations were conducted for an average initial out-of-straightness value of $L/1500$ (as obtained by Bjorhovde [23]) and the maximum allowed $L/1000$. Figure 5.22 illustrates the results.

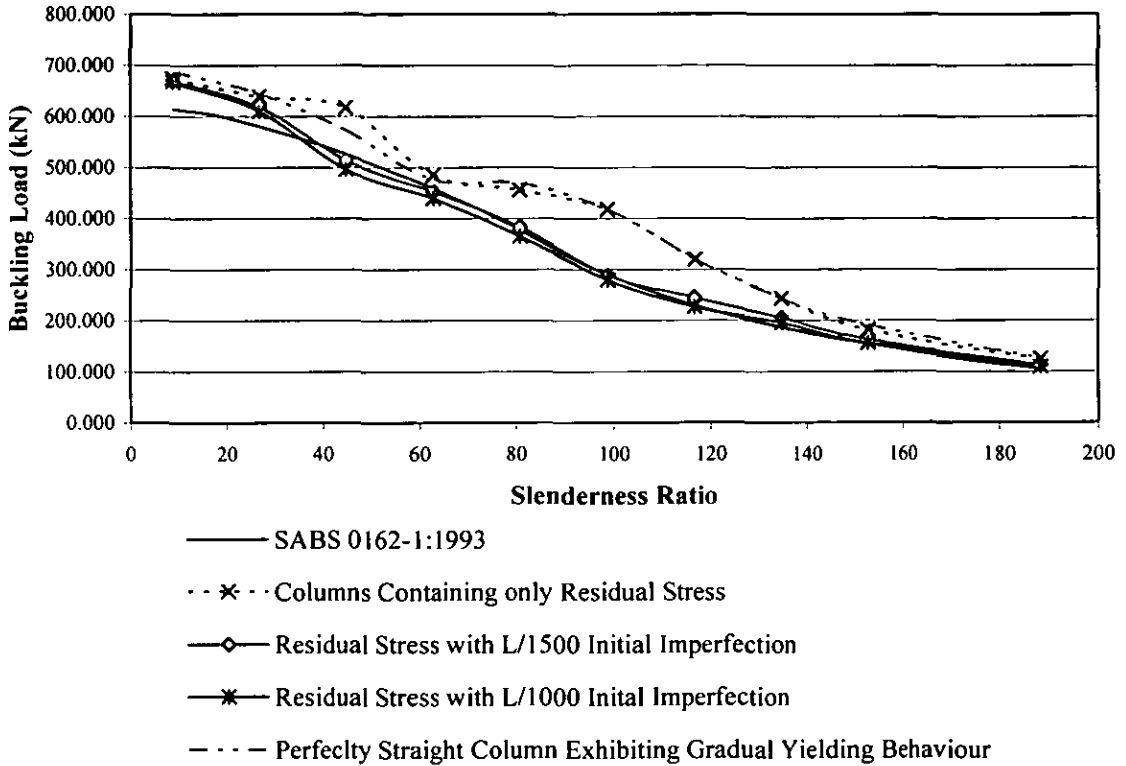


Figure 5.22: Columns Containing Residual Stresses and an Initial Curvature

5.3.7.1 Discussion of Results for Columns Containing Residual Stresses and an Initial Curvature

The above results indicate that internal residual stresses combined with initial curvature have a pronounced influence on the critical buckling load of 3CR12 columns. Except for the shortest column, 200mm, the entire column curve for both the average and maximum allowable initial out-of-straightness lies below the minimum column curve prescribed by the code of practice. When compared to the column curve for a perfectly straight column with only gradual yielding behaviour, it can be seen that the critical buckling load for each column is drastically reduced. The same can be said if the results are compared to columns containing only residual stresses.

6 CONCLUSIONS AND RECOMMENDATIONS

6.1 General Remarks

The purpose of this investigation was to determine the influence of the gradual yielding behaviour, the effect of geometric imperfections and residual stresses on the critical axial resistance of hot-rolled 3CR12 compression members. The section under analysis was a $152 \times 76 \times 18$ channel section. The investigation was conducted numerically by using the Finite Element Method. A non-linear Finite Element Code called ABAQUS was used to create the Finite Element Models of the hot-rolled columns. The material data utilized in the Finite Element Models were determined experimentally via compression tests. The sectioning method was used to establish the distribution of the residual stresses in the compression members. The Finite Element Results were compared to the SABS 0162-1:1993 code of practice. This chapter is a summary of all the conclusions from the investigation. Recommendations for possible future studies are also discussed.

6.2 Literature Review

Chapter 2 briefly discussed stainless steels, their properties and behaviour. A brief summary was also given on the applicable theory pertaining to axial compression members. Most importantly, previous research done on 3CR12 was discussed. Since hot-rolled sections are relatively new to the market, the amount of research available is still limited.

3CR12 hot-rolled sections were investigated by Bosch [1] for the use of structural steel members. Tensile and Compression tests conducted indicated that the material properties varied throughout the sections, which the author attributed to uneven cooling after the rolling process. It was concluded that the SSRC column curve and the Euler curve described the curve for the 3CR12 hot-rolled sections adequately. These curves were also found to be sufficient for columns with a small eccentricity.

A study conducted by Bredekamp [9] on hot-rolled and Built-up Stainless Steel Structural Members concluded that the gradual yielding behaviour of stainless steels causes a reduction in stiffness of the member if the stress exceeds the proportional limit. Since buckling is influenced by member stiffness, it was concluded that the material-nonlinearity is the most significant factor in the buckling of stainless steel columns.

6.3 Experimental Work

Compression tests conducted on the 300WA and 3CR12 hot-rolled columns indicated that the material properties vary significantly throughout the channel section.

Residual stresses were measured by the sectioning technique in both 300WA and 3CR12 hot-rolled sections. The results indicated that the 3CR12 sections did not behave as predicted by theory, since the two flanges exhibit conflicting behaviour, as well as the two corner sections, which should be in tension according to theory, but in this case both the corner sections contained compressive residual stresses. The 300WA sections however, behaved as predicted, with both corner sections containing tensile residual stresses.

6.4 Finite Element Analysis

A mesh analysis was conducted to determine a suitable element size to be used in the simulations. It was decided to mesh the 3CR12 columns with the smallest elements that could be practically used and that approached convergence. Therefore a 10mm quadratic tetrahedral element was utilized in the simulations, except for the tallest columns (3400mm and 4200mm), in which case the element size was increased to 20mm for practical reasons.

To determine the influence of the gradual yielding behaviour on the column strength, the experimentally obtained stress-strain graph was normalized to 300MPa, and compared to material data for 300WA, also normalized to 300MPa. A considerable reduction in column strength occurred in the intermediate slenderness range. The

“dip” found in the column curve from the experimental values were reflected in the Finite Element Analysis column curve.

The influence of an initial out-of-straightness was also investigated. For a column with a maximum allowable initial-out-straightness of $L/1000$, the SABS code of practice was underestimating the column strength in the intermediate slenderness range. Even for an average value of $L/1500$, certain buckling loads for columns in the intermediate slenderness range were underestimated by the SABS curve.

Eccentric Loading was simulated in ABAQUS for the columns. A three-dimensional plot as well as perpendicular plot illustrated that in almost all the cases the critical axial resistance is reduced, depending on the amount of eccentricity.

Combining an initial out-of-straightness with an eccentricity has a severe detrimental influence on the column strength. Except for the shortest column, the entire column curve is underestimated by the SABS code of practice.

In order to investigate the influence of residual stresses, the experimentally measured residual stresses were incorporated into the material properties of the column. The results indicated a slight deviation from the curve for a perfectly straight column in the intermediate slenderness range.

As is often the case in reality, columns with both residual stresses and initial out-of-straightness occur. This phenomenon was simulated and the results indicated that the critical buckling loads for almost all the columns are influenced extremely negatively, except for the shortest and tallest/most slender columns.

6.5 Overall Conclusion

Overall it can be concluded that ABAQUS simulations modeled the behaviour of the 3CR12 hot-rolled columns well. For perfectly straight columns with the minimum allowable yield strength of 300MPa prescribed by the code of practice, it seems that the code of practice is still sufficiently conservative for the design of 3CR12.

As for geometric imperfections, the Finite Element Method predicts negative results as far as comparison to the code of practice is concerned. In the intermediate slenderness range, the code of practice is overestimating the strength of the 3CR12 hot-rolled columns. It seems as if overall the combination of a geometric imperfection and the gradual yielding behaviour of the 3CR12 are overall detrimental to the strength of these columns. Since perfectly straight columns are a theoretical phenomenon only, it is therefore recommended that great caution be taken when using SABS 0162-1:1993 when designing for hot-rolled 3CR12 channel columns in the intermediate slenderness range. Comparing to 300WA columns the same basic behaviour regarding gradual yielding and initial out-of-straightness was observed but to a lesser degree than 3CR12.

6.6 Recommendations

It is recommended that the study be extended to include other hot-rolled sections, such as angles and I-beams, and other wide-flanges shapes in order to investigate the validity of the SABS code of practice for situations with geometric imperfections combined with a material nonlinearity.

In an attempt to improve the accuracy of the Finite Element Model, instead of using an average representative curve for the material data, the section can be subdivided into smaller sections with their respective material properties.

The residual stress distribution of the columns was unsymmetrical, and therefore it was difficult to make a sound conclusion from the Finite Element results. A symmetrical distribution should be investigated numerically in order to determine the influence of the residual stresses on the critical axial resistance more thoroughly.

REFERENCES

1. Bosch H.H. *Die strukturele gebruik van Warmgewalste Tipe 3CR12 Vlekvrye Staal*. M.Ing Thesis. Rand Afrikaans University. 1992
2. Budinski G. Budinski K. *Engineering Materials Properties and Selection 6th Edition*, Prentice Hall, Ohio, 1999
3. Dillon C.P. *Corrosion Resistance of Stainless Steels*, Marcel Dekker Inc, New York, 1995
4. British Standard, *Stainless Steels Part 3, Technical delivery conditions for semi-finished products, bars, rods and sections for general purposes*. EN 10088-3:1995
5. South African Stainless Steel Development Association, *Stainless Steel Buyers Guide*, 1995
6. Van Den Berg G.J. *The Torsional Flexural Buckling Strength of Cold-formed Stainless Steel Columns*. D.Ing Thesis, Rand Afrikaans University, November 1988.
7. *Columns Stainless Steel, Stainless Steel 3CR12 and Chromanite*. Pocket Guide.
8. The South African Institute of Steel Construction, *South African Steel Construction Handbook (Limit States Design)* , 1987
9. Bredenkamp P.J. van den Berg G.J. van der Merwe P., *Strength Prediction of Hot-rolled and Built-up Stainless Steel Structural Members*. Collected Papers

- of the Chromium Steels Research Group, Vol 5, 1998. Rand Afrikaans University.
10. Ramberg W, Osgood W.R. *Determination of Stress-strain Curves by Three Parameters*. National Advisory Committee on Aeronautics. Technical Note No. 902.
 11. Van der Merwe P, *Development of Design Criteria for Ferritic Stainless Steel Cold-formed Structural Members and Connections*. Ph.D Thesis, University of Missouri-Rolla. USA 1987.
 12. van den Berg G.J. *The behaviour of Cold-formed Stainless Steel Structural Members*. Collected Papers of the Chromium Steels Research Group, Vol 5, 1998, Rand Afrikaans University
 13. van den Bergh G.J. *The local buckling strength of partially stiffened Type 3CR12 stainless steel compression elements in Beam Flanges*, Collected Papers of the Chromium Steel Research group, Vol 5, 1998, Rand Afrikaans University
 14. American Society of Civil Engineers. *Specification for the design of Cold-formed Stainless Steel Structural Members*. ANSI/ASCE-8-90 1991
 15. DeGarmo E.P., Black. J.T. Kohser R.A. *Materials and Processes in Manufacturing 8th Edition*. John Wiley & Sons Inc New York 1999.
 16. SABS 0162-1:1993 *The Structural Use of Steel Part 1: Limit-State Design of Hot-rolled Steelwork*. The Council of South African Bureau of Standards. 1993
 17. Canadian Standard Association. *Limit-states design of steel structures*. CSA Standard Can-S16.1-M89

18. Mahachi J. *Design of Structural Steel Works in Southern Africa to SABS 0162*. Division of Building and Construction Technology, CSIR, Pretoria 1999.
19. Dowling, J.P., Harding J.E., Bjorhovde R., *Constructional Steel Design, an International Guide*, Elsevier Science Publishers, London, 1992
20. Chen W.F. Lui E.M. *Structural Stability, Theory and Implementation*, Elsevier Science Publishers, New York, 1987
21. Salmon C.G., Johnson J.E. *Steel Structures, Design and Behavior, 2nd Edition*, Harper & Row Publishers, New York, 1980
22. Tall L, *Structural Steel Design, 2nd Edition*, John Wiley & Sons, New York, 1974.
23. Bjorhovde R., *Deterministic and Probabilistic Approaches to the Strength of Steel Columns*. Ph.D Dissertation, Lehigh University, Bethlehem, Pa., May, 1972.
24. Yu W.W., *Cold-Formed Steel Design*, John Wiley & Sons, New York, 1985.
25. Galambos T.V. *Guide to Stability Design Criteria for Metal Structures, 5th Edition*, John Wiley & Sons, 1998
26. Allen H.G, Bulson P.S *Background to Buckling*, McGraw Hill Book Company, UK, 1980
27. Lay. M.G., Ward R. *Residual Stresses in Steel Sections*. Steel Construction Vol 3. 1969
28. Batterman R. Johnston B.G., *Behaviour and Maximum Strength of Metal Columns*, ASCE J. Structural Div. Vol 93, 1967

-
29. Fagan M.J. *Finite Element Analysis, Theory and Practice*, Longman Scientific & Technical, England, 1992
 30. Hibbitt, Karlsson and Sorensen, Inc, *Getting Started with Abaqus Standard*. Version 6.2, 2001
 31. Logan D.L. *A first Course in the Finite Element Method*, 3rd Edition. Brooks/Cole Thomson Learning, 2002.
 32. Young B. Yan J. *Finite Element Analysis and Design of fixed-ended plain channel columns*. Finite Element and Design, Vol 38, Elsevier, 2002
 33. Young B, Jintang Y, *Channel Columns Undergoing Local, Distortional, and Overall Buckling*. Journal of Structural Engineering, June 2002.
 34. Liang A. *Finite Element of Distortional Buckling of Cold-formed Stainless Steel Columns*, M.Ing Thesis, Rand Afrikaans University, April 2000
 35. Callister Jr. W.D., *Materials Science and Engineering an Introduction*, 4th Edition. John Wiley & Sons, New York, 1997
 36. American Society for Testing and Materials, *Annual Book of ASTM Standards*, Section 3, Metals Test Methods and Analytical Procedures. West Conshohocken, Penn 2001
 37. Klopper J.J. *The lateral Torsional Buckling Strength of Hot-Rolled 3CR12 Beams*. M.Ing Thesis, Rand Afrikaans University, May 2004
 38. Laubscher R.F., *An experimental and numerical investigation of the axial resistance of hot-rolled 3CR12 Columns*. Fourth South African Conference on Computational and Applied Mechanics, 2004
 39. Osgood W.R. *Corrections for lengths of columns tested between knife-edges*. Journal of the Aeronautical Society. Vol. 114. 1949.

APPENDIX A: Derivation of Euler Load

In order to derive the basic equation of a pinned-ended column, the following assumptions are made: [20]

- The member is perfectly straight
- The axial load is applied along the centroidal axis of the member.
- Before deformation, plane sections are plane, and remain plane after deformation
- Hook's law is obeyed by the column material.
- In order to approximate the curvature by a second derivate of the lateral displacement, it will be assumed that the deflection of the member is small.

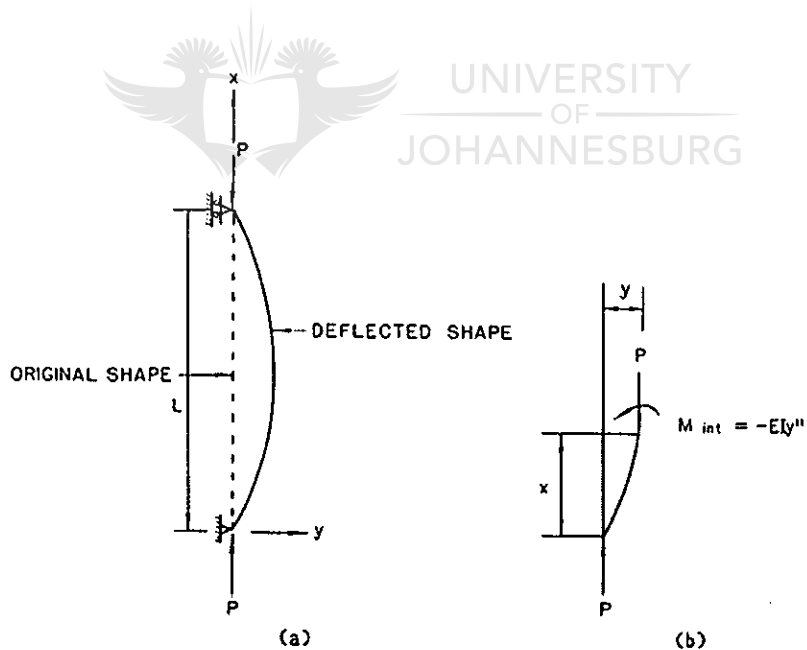


Figure A.1: Pinned-ended Column[20]

In figure A.1 a column is illustrated with both ends pinned, with the upper end free to move vertically. The column is loaded by an axial force P , which is applied along its centroidal axis.

The method of neutral equilibrium will be utilized to calculate the critical load. The column can be in equilibrium in both a straight and slightly bent form at the critical load.

Figure A.1 b shows a free body diagram of a segment of the column under investigation. For equilibrium, the free body diagram requires that:

$$-M_{int} + Py = 0 \quad \text{Eq. B.1}$$

M_{int} is the internal resisting moment and y is the lateral deflection of the segment.

The internal moment is defined as:

$$M_{int} = EI\Phi \quad \text{Eq. B.2}$$

E is Young's Modulus of the material, and I is the moment of inertia of the cross section. The value of EI is considered as the slope of the relation between the moment M_{int} and curvature $\Phi = 1/R$

The linear moment curvature can be derived from assumptions 3,4 and 5 as follows:

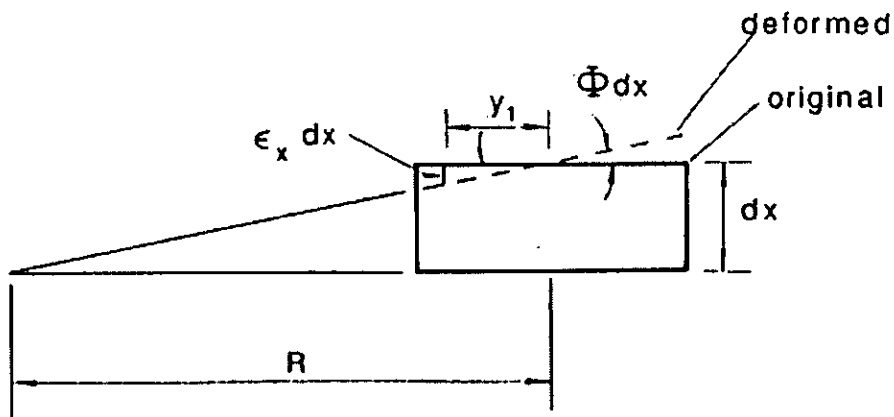


Figure B.1: Kinematics of a Column Segment[20]

In the figure on the previous page (Figure B.1), an infinitesimal segment of a column is illustrated. The segment is of length dx , with its deformed and undeformed positions shown. The kinematic relation is written as:

$$\frac{\varepsilon_x dx}{y_1} = \frac{dx}{R} \quad \text{Eq. B.3}$$

Or rewritten:

$$\varepsilon_x = \frac{y_1}{R} = y_1 \Phi \quad \text{Eq. B.4}$$

Where

ε_x = axial strain

R = radius of concentration

The axial stress is related to the axial strain from Hooke's Law:

$$\sigma_x = E\varepsilon_x \quad \text{Eq. B.5}$$

The internal moment M_{int} can be obtained by integrating the moment induced by the stress σ_x over the cross section.

$$M_{\text{int}} = \int_A y_1 \sigma_x dA \quad \text{Eq. B.6}$$

Substituting the kinematic equation (Eq. B.3) and stress-strain relation (Eq. B.5):

$$M_{\text{int}} = \frac{E}{R} \int_A y_1^2 dA \quad \text{Eq. B.7}$$

The moment of inertia I is given by $\int_A y_1^2 dA$, and $1/R$ is the curvature Φ .

The curvature Φ can be approximated by the second derivative of the lateral displacement:

$$\Phi = -\frac{d^2 y}{dx^2} = -y'' \quad \text{Eq. B.8}$$

The negative sign indicated that the range of change of the slope dy/dx of the deflected shape decreases as x increases.

The moment equation (Eq B.2) can now be written as:

$$M_{int} = -EIy'' \quad \text{Eq. B.9}$$

Substituting back into the equilibrium equation (Eq B.1) yields

$$EIy'' + Py = 0 \quad \text{Eq. B.10}$$

Using the notation

$$k^2 = \frac{P}{EI} \quad \text{Eq. B.11}$$

Equation B.10 can be rewritten as

$$y'' + k^2 y = 0 \quad \text{Eq. B.12}$$

The above equation is a second-order linear differential equation with constant coefficients. The general solution to this equation is:

$$y = A \sin kx + B \cos kx \quad \text{Eq. B.13}$$

Although there are three unknown variables, A, B and k, there are two independent boundary conditions:

$$\begin{aligned} y(0) &= 0 \\ y(L) &= 0 \end{aligned}$$

Substituting the first Boundary Conditions into Eq B.13,

$$B = 0$$

The second boundary Condition yields:

$$A \sin kL = 0 \quad \text{Eq. B.14}$$

The above equation is solved if $A = 0$ and/or $\sin kL = 0$

On order to obtain a nontrivial solution that also describes the equilibrium position of the column if it is slightly bent, Eq.B.14 can be satisfied if

$$kL = n\pi, \quad n = 1, 2, \dots$$

Or

$$k = \frac{n\pi}{L}$$

Solving for P from equation

$$P = \frac{n^2 \pi^2 EI}{L^2}$$

The critical load (P_{cr}) of the column is the value of P which corresponds to the smallest value of n . This load is also referred to as the Euler Load.



APPENDIX B: Results of Compression Tests

In this section the results of the compression test are shown. An individual graph is plotted for each of the 13 sections.

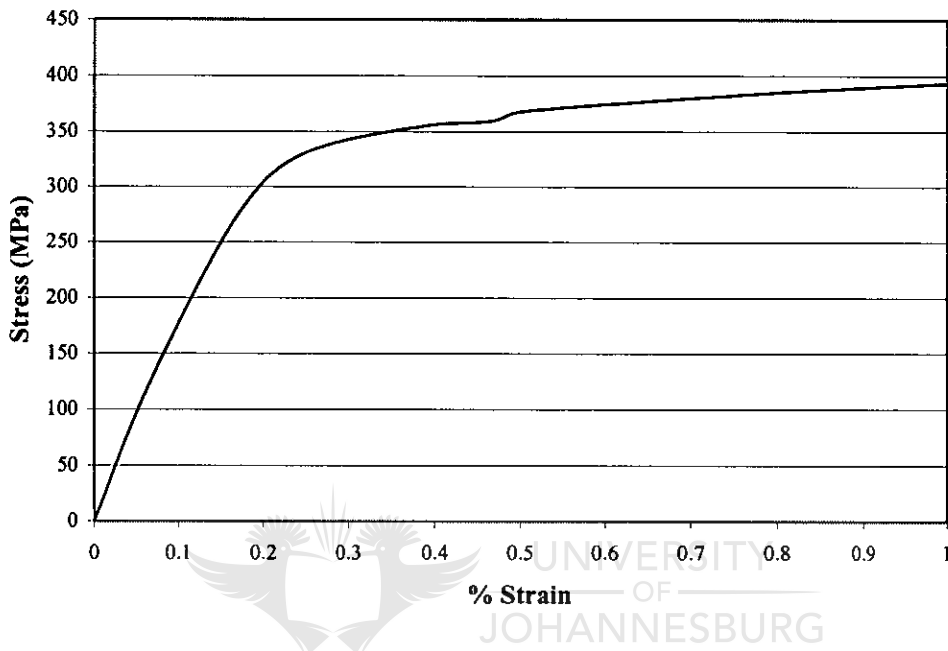


Figure B.1 Stress-Strain Curve for Section 1

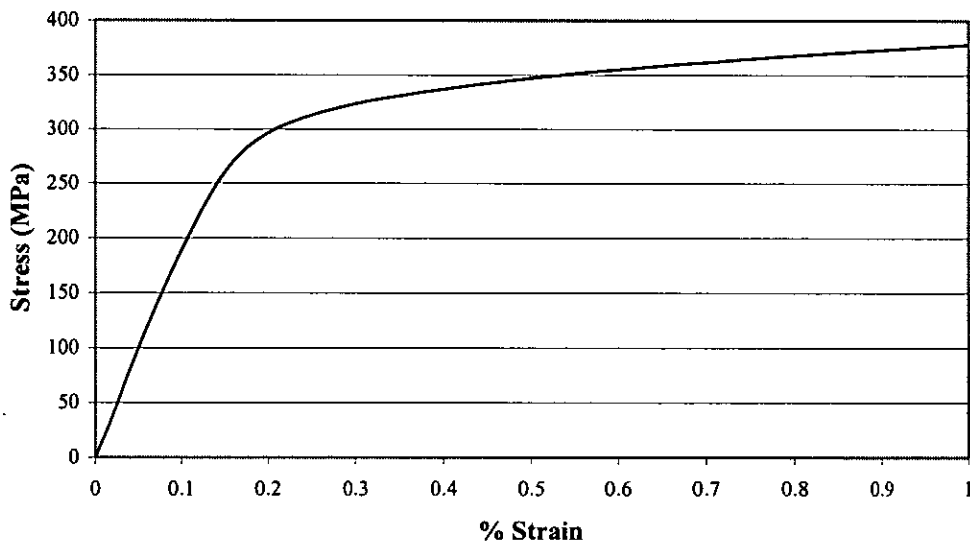


Figure B.2: Stress-Strain Curve for Section 2

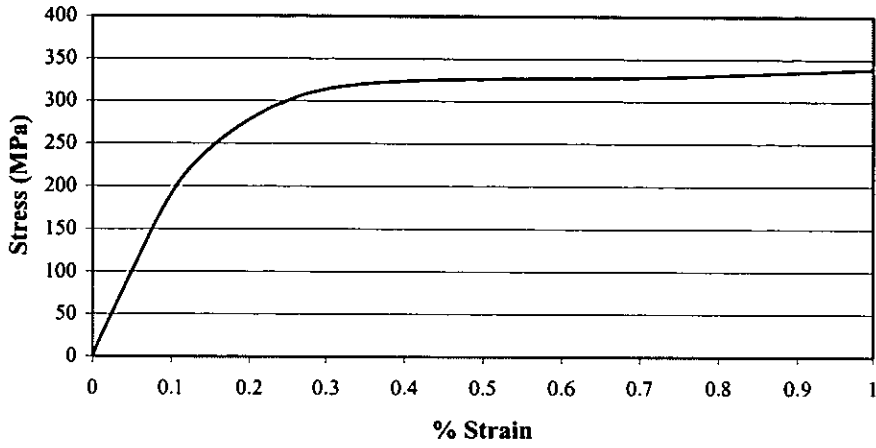


Figure B.3: *Stress-Strain Curve for Section 3*

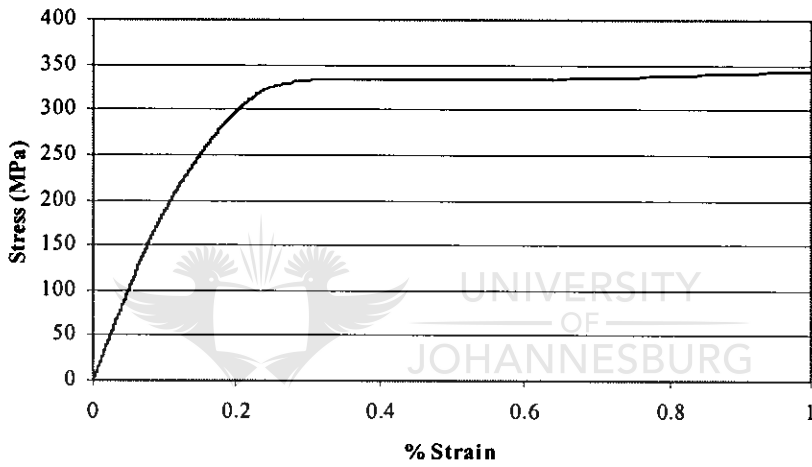


Figure B.4: *Stress-Strain Curve for Section 4*

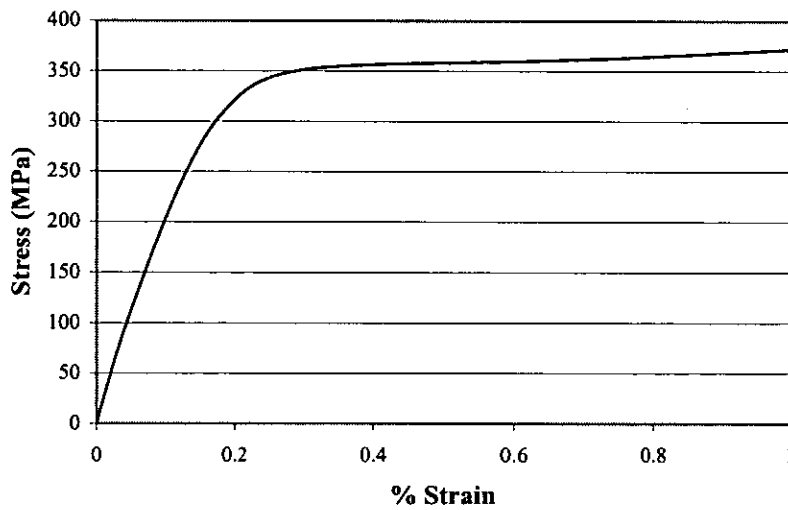


Figure B.5: *Stress-Strain Curve for Section 5*

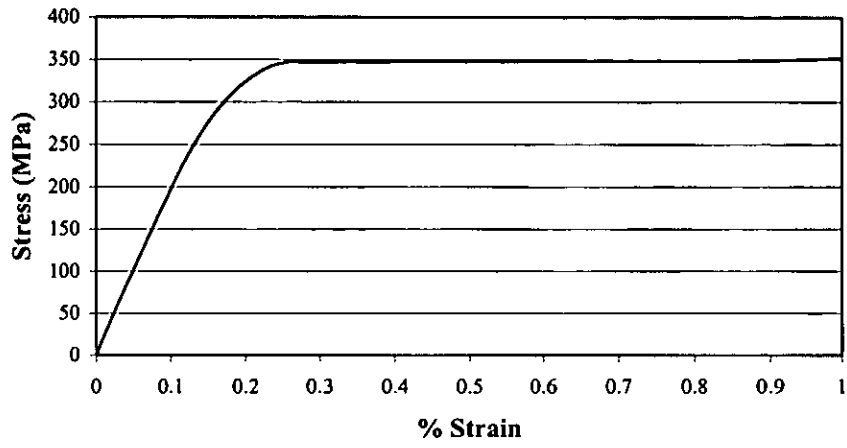


Figure B.6: *Stress-Strain Graph for Section 6*

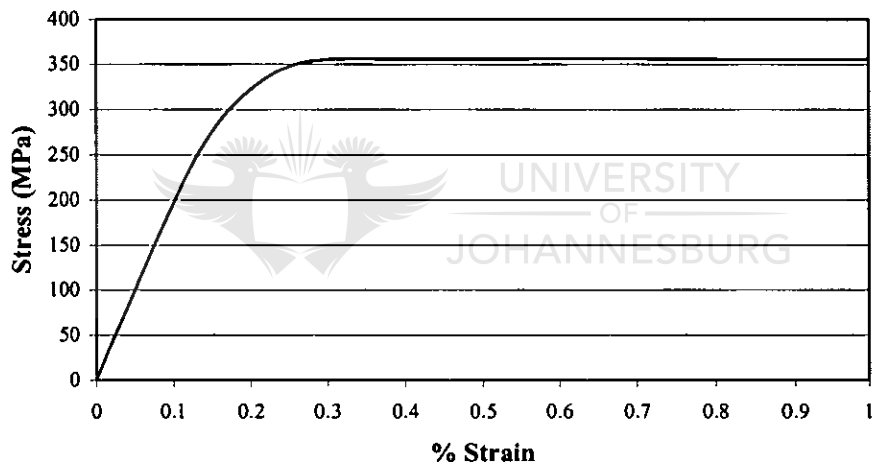


Figure B.7: *Stress-Strain Graph for Section 7*

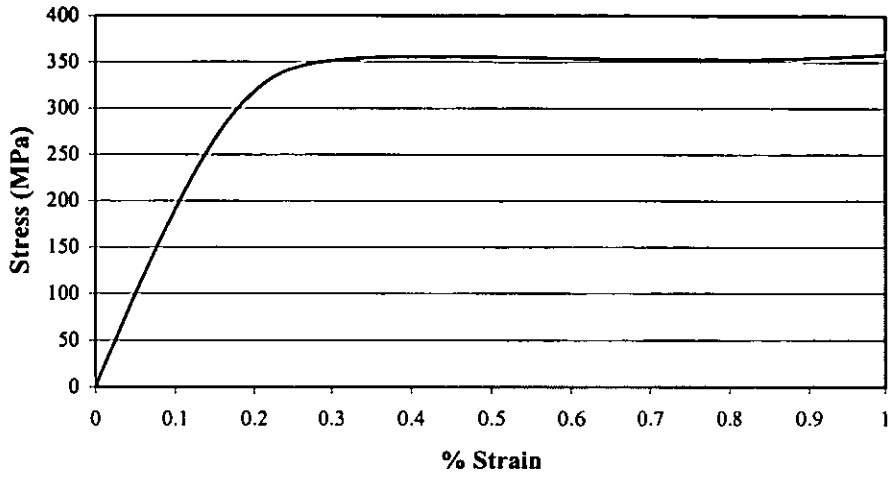


Figure B.8: *Stress-Strain Graph for Section 8*

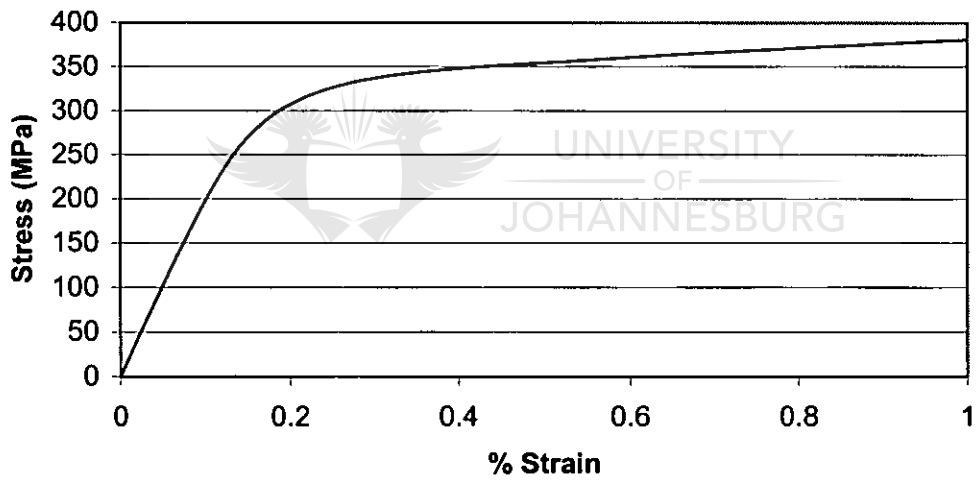


Figure B.9: *Stress-Strain Graph for Section 9*

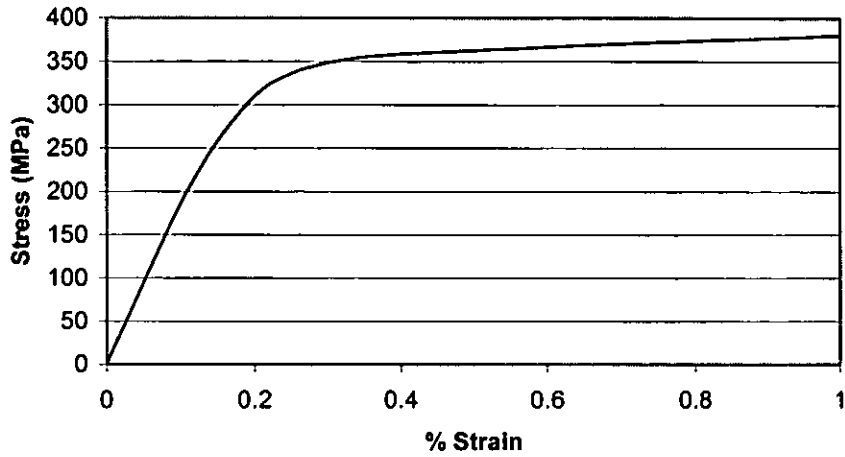


Figure B.10: *Stress-Strain Graph for Section 10*

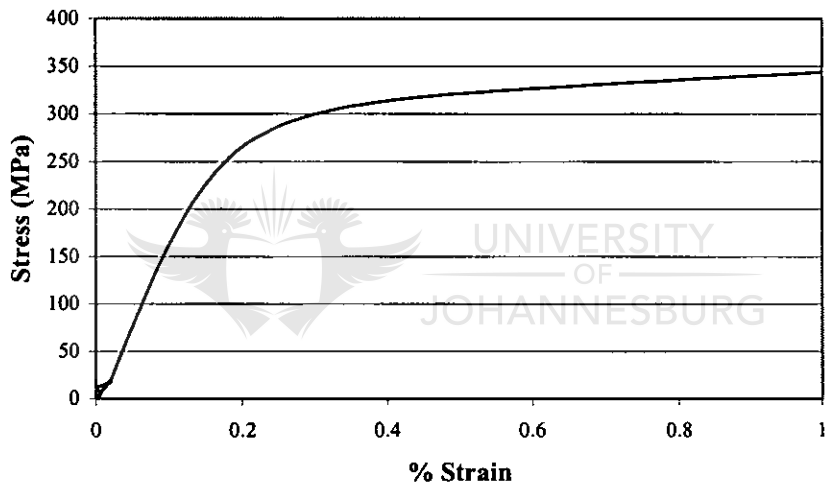


Figure B.11: *Stress-Strain Graph for Section 11*

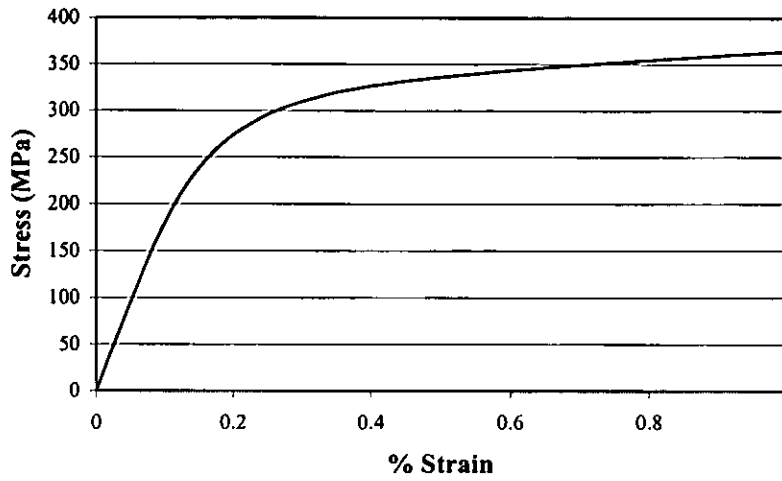


Figure B.12: *Stress-Strain Graph for Section 12*

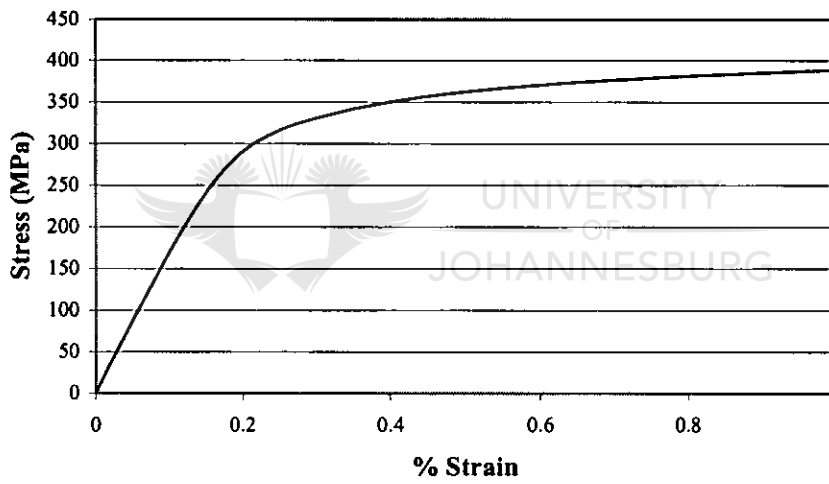


Figure B.13: *Stress-Strain Graph for Section 13*

APPENDIX C: Experimental Program

Experimental Work

Preparations Of Column Members

Iscor Longsteel Products provided all the 3CR12 sections. The carbon steel lengths were obtained from different suppliers (Iscor Longsteel Products and Highveld Stainless). All individual sections were obtained from the same batch and heat. The lengths were cut up into the required lengths that will cover the scope of the tests to be carried out.

The ends of each column were machined level (flat) on a milling machine. This was done to ensure that the load was uniformly applied across the entire surface area of the column while under compression.

Experimental Set-Up And Procedure



UNIVERSITY
OF
JOHANNESBURG

The load was measured by incorporating a loadcell into the set-up (Figure 1). A steel ball was placed between the loadcell and bottom adjustable plate. A second ball was positioned on top of the other adjustable plate. This was done to ensure that the column was supported in its weakest possible state (free rotation of the end-fixtures). Strain gauges were placed on the ends of each column. The strain gauges were monitored while 20% of the expected buckling load was applied.

The strain gauges would indicate if the load were not applied on the centroid of the column (each strain gauge should exhibit the same rate of change). Adjustments could then be made to ensure that the load was correctly applied. This was done by means of the adjustable plates. Load application was administered at no more than 1mm/min.

Results Of Column Tests

The overall effective length of the axial compression members was adjusted by taking the end-fixtures into account as described by Osgood [8]. This was achieved by adding the thickness of the adjustable plates and steel balls to the length of each member. The results of the channel column tests are shown in Table 1.

Table C.1: Axial compression test results: *Channel*152×76×18

<i>L/r</i>	3CR12				
	T1	T2	T3	<i>Avg (kN)</i>	SD
9.91	1054	1044	1054	1050.7	5.8
58.56	585.7	622.7	642.7	617.0	28.9
94.59	501	513.5	526	513.5	12.5
184.7	141	128	124	131.0	8.9

The material properties of 3CR12 hot-rolled sections in longitudinal compression are presented in Table 2.

Table C.2: Material Properties of 3CR12 in longitudinal compression

Channel	3CR12 (avg)
F_y (MPa)	327.5
F_p (MPa)	252.5
E_o (GPa)	209.7

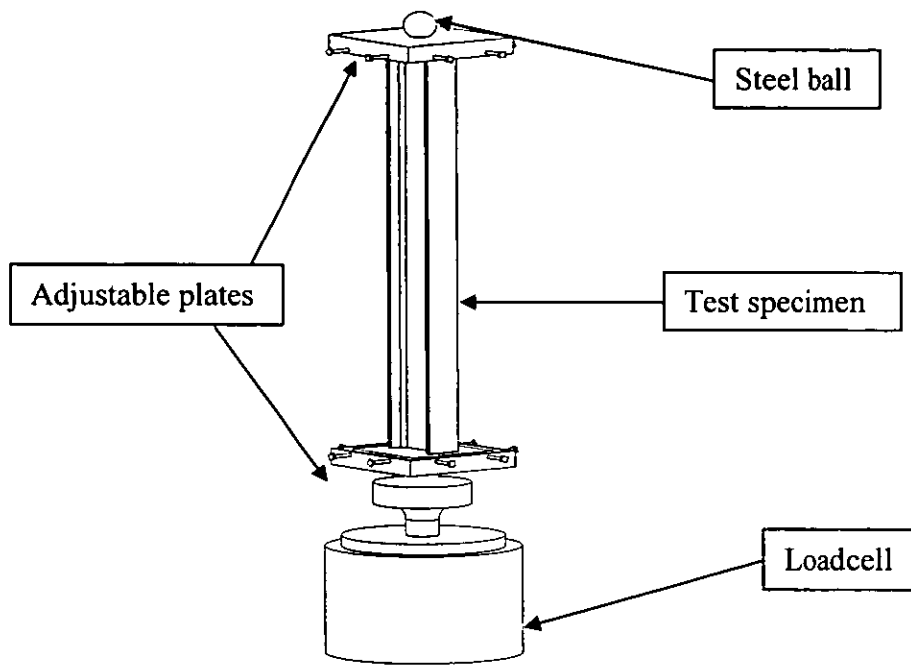


Figure C.1: Experimental Set-up



APPENDIX D: Example Input File

Below an example of a typical input file is shown. The nodes and elements have been removed in order to save space.

```

*Heading
** Job name: 200mm327MPa10mmQuadTets Model name: Model-1
*Preprint, echo=NO, model=NO, history=NO, contact=NO
**
** PARTS
**
*Part, name=P200mmchannel152x76x18
*End Part
**
*Part, name=bottom
*End Part
**
*Part, name=top
*End Part
**
**
** ASSEMBLY
**
*Assembly, name=Assembly
**
*Instance, name=P200mmchannel152x76x18-1, part=P200mmchannel152x76x18
*Node
  1,      0., 0.153999999, 0.200000003
  2,      0.,      0., 0.200000003
  3, 0.0754500031,      0., 0.200000003
  .....
*Element, type=C3D10M
  1, 1417, 1418, 1202, 626, 1580, 1579, 1578, 1582, 1581, 1583
  2, 1417, 608, 1419, 1418, 1586, 1585, 1584, 1580, 1587, 1588
  3, 1417, 421, 1419, 1420, 1590, 1589, 1584, 1592, 1591, 1593
  4, 1417, 373, 99, 1114, 1596, 1595, 1594, 1598, 1597, 1599

*Nset, nset=_PickedSet2, internal, generate
  1, 9518, 1
*Elset, elset=_PickedSet2, internal, generate
  1, 4951, 1
** Region: (Section-1:Picked)
*Elset, elset=_PickedSet2, internal, generate
  1, 4951, 1
** Section: Section-1
*Solid Section, elset=_PickedSet2, material=Material-1
  1.,
*End Instance
**
*Instance, name=bottom-1, part=bottom
  0.0216, 0.077, 0.
*Node
  1, -0.100000001, -0.100000001, 0.
  2, -0.0800000057, -0.100000001, 0.
  3, -0.0600000024, -0.100000001, 0.
  4, -0.0400000028, -0.100000001, 0.
  5, -0.0200000014, -0.100000001, 0.

```


6,	-6.20881735e-10,	-0.100000001,	0.
7,	0.0199999996,	-0.100000001,	0.
8,	0.0399999991,	-0.100000001,	0.
9,	0.0599999987,	-0.100000001,	0.
10,	0.0800000057,	-0.100000001,	0.
11,	0.100000001,	-0.100000001,	0.
12,	-0.100000001,	-0.0800000057,	0.
13,	-0.0799999982,	-0.0799999982,	0.
14,	-0.0600000024,	-0.0799999982,	0.
15,	-0.0399999991,	-0.0799999982,	0.
16,	-0.0199999996,	-0.0799999982,	0.
17,	0.,	-0.0799999982,	0.
18,	0.0199999996,	-0.0799999982,	0.
19,	0.0399999991,	-0.0799999982,	0.
20,	0.0599999987,	-0.0799999982,	0.
21,	0.0799999982,	-0.0800000057,	0.
22,	0.100000001,	-0.0800000057,	0.
23,	-0.100000001,	-0.0599999987,	0.
24,	-0.0799999982,	-0.0600000024,	0.
25,	-0.0600000024,	-0.0600000024,	0.
26,	-0.0399999991,	-0.0600000024,	0.
27,	-0.0199999996,	-0.0600000024,	0.
28,	0.,	-0.0600000024,	0.
29,	0.0199999996,	-0.0600000024,	0.
30,	0.0399999991,	-0.0600000024,	0.
31,	0.0599999987,	-0.0600000024,	0.
32,	0.0799999982,	-0.0600000024,	0.
33,	0.100000001,	-0.0600000024,	0.
34,	-0.100000001,	-0.0399999954,	0.
35,	-0.0799999982,	-0.0399999954,	0.
36,	-0.0600000024,	-0.0399999954,	0.
37,	-0.0399999991,	-0.0399999954,	0.
38,	-0.0199999996,	-0.0399999954,	0.
39,	0.,	-0.0399999954,	0.
40,	0.0199999996,	-0.0399999954,	0.
41,	0.0399999991,	-0.0399999954,	0.
42,	0.0599999987,	-0.0399999954,	0.
43,	0.0799999982,	-0.0399999991,	0.
44,	0.100000001,	-0.0400000028,	0.
45,	-0.100000001,	-0.0199999996,	0.
46,	-0.0799999982,	-0.0199999996,	0.
47,	-0.0600000024,	-0.0199999996,	0.
48,	-0.0399999991,	-0.0199999996,	0.
49,	-0.0199999996,	-0.0199999996,	0.
50,	0.,	-0.0199999996,	0.
51,	0.0199999996,	-0.0199999996,	0.
52,	0.0399999991,	-0.0199999996,	0.
53,	0.0599999987,	-0.0199999996,	0.
54,	0.0799999982,	-0.0199999996,	0.
55,	0.100000001,	-0.0200000014,	0.
56,	-0.100000001,	6.20881735e-10,	0.
57,	-0.0799999982,	0.,	0.
58,	-0.0600000024,	0.,	0.
59,	-0.0399999991,	0.,	0.
60,	-0.0199999996,	0.,	0.
61,	0.,	0.,	0.
62,	0.0199999996,	0.,	0.
63,	0.0399999991,	0.,	0.
64,	0.0599999987,	0.,	0.
65,	0.0799999982,	0.,	0.

66, 0.100000001, -6.20881735e-10, 0.
 67, -0.100000001, 0.0200000014, 0.
 68, -0.0799999982, 0.0199999996, 0.
 69, -0.0600000024, 0.0199999996, 0.
 70, -0.0399999991, 0.0199999996, 0.
 71, -0.0199999996, 0.0199999996, 0.
 72, 0., 0.0199999996, 0.
 73, 0.0199999996, 0.0199999996, 0.
 74, 0.0399999991, 0.0199999996, 0.
 75, 0.0599999987, 0.0199999996, 0.
 76, 0.0799999982, 0.0199999996, 0.
 77, 0.100000001, 0.0199999996, 0.
 78, -0.100000001, 0.0400000028, 0.
 79, -0.0799999982, 0.0399999991, 0.
 80, -0.0600000024, 0.0399999991, 0.
 81, -0.0399999991, 0.0399999991, 0.
 82, -0.0199999996, 0.0399999991, 0.
 83, 0., 0.0399999991, 0.
 84, 0.0199999996, 0.0399999991, 0.
 85, 0.0399999991, 0.0399999991, 0.
 86, 0.0599999987, 0.0399999991, 0.
 87, 0.0799999982, 0.0399999991, 0.
 88, 0.100000001, 0.0399999991, 0.
 89, -0.100000001, 0.0600000024, 0.
 90, -0.0799999982, 0.0599999987, 0.
 91, -0.0600000024, 0.0599999987, 0.
 92, -0.0399999991, 0.0599999987, 0.
 93, -0.0199999996, 0.0599999987, 0.
 94, 0., 0.0599999987, 0.
 95, 0.0199999996, 0.0599999987, 0.
 96, 0.0399999991, 0.0599999987, 0.
 97, 0.0599999987, 0.0599999987, 0.
 98, 0.0799999982, 0.0599999987, 0.
 99, 0.100000001, 0.0599999987, 0.
 100, -0.100000001, 0.0800000057, 0.
 101, -0.0800000057, 0.0799999982, 0.
 102, -0.0600000024, 0.0799999982, 0.
 103, -0.0399999991, 0.0799999982, 0.
 104, -0.0199999996, 0.0799999982, 0.
 105, 1.55220434e-10, 0.0799999982, 0.
 106, 0.0199999996, 0.0799999982, 0.
 107, 0.0399999991, 0.0799999982, 0.
 108, 0.0599999987, 0.0799999982, 0.
 109, 0.0800000057, 0.0799999982, 0.
 110, 0.100000001, 0.0800000057, 0.
 111, -0.100000001, 0.100000001, 0.
 112, -0.0800000057, 0.100000001, 0.
 113, -0.0599999987, 0.100000001, 0.
 114, -0.0399999991, 0.100000001, 0.
 115, -0.0199999996, 0.100000001, 0.
 116, 6.20881735e-10, 0.100000001, 0.
 117, 0.0200000014, 0.100000001, 0.
 118, 0.0400000028, 0.100000001, 0.
 119, 0.0600000024, 0.100000001, 0.
 120, 0.0800000057, 0.100000001, 0.
 121, 0.100000001, 0.100000001, 0.

*Element, type=R3D4

- 1, 1, 2, 13, 12
- 2, 2, 3, 14, 13
- 3, 3, 4, 15, 14



4, 4, 5, 16, 15
5, 5, 6, 17, 16
6, 6, 7, 18, 17
7, 7, 8, 19, 18
8, 8, 9, 20, 19
9, 9, 10, 21, 20
10, 10, 11, 22, 21
11, 12, 13, 24, 23
12, 13, 14, 25, 24
13, 14, 15, 26, 25
14, 15, 16, 27, 26
15, 16, 17, 28, 27
16, 17, 18, 29, 28
17, 18, 19, 30, 29
18, 19, 20, 31, 30
19, 20, 21, 32, 31
20, 21, 22, 33, 32
21, 23, 24, 35, 34
22, 24, 25, 36, 35
23, 25, 26, 37, 36
24, 26, 27, 38, 37
25, 27, 28, 39, 38
26, 28, 29, 40, 39
27, 29, 30, 41, 40
28, 30, 31, 42, 41
29, 31, 32, 43, 42
30, 32, 33, 44, 43
31, 34, 35, 46, 45
32, 35, 36, 47, 46
33, 36, 37, 48, 47
34, 37, 38, 49, 48
35, 38, 39, 50, 49
36, 39, 40, 51, 50
37, 40, 41, 52, 51
38, 41, 42, 53, 52
39, 42, 43, 54, 53
40, 43, 44, 55, 54
41, 45, 46, 57, 56
42, 46, 47, 58, 57
43, 47, 48, 59, 58
44, 48, 49, 60, 59
45, 49, 50, 61, 60
46, 50, 51, 62, 61
47, 51, 52, 63, 62
48, 52, 53, 64, 63
49, 53, 54, 65, 64
50, 54, 55, 66, 65
51, 56, 57, 68, 67
52, 57, 58, 69, 68
53, 58, 59, 70, 69
54, 59, 60, 71, 70
55, 60, 61, 72, 71
56, 61, 62, 73, 72
57, 62, 63, 74, 73
58, 63, 64, 75, 74
59, 64, 65, 76, 75
60, 65, 66, 77, 76
61, 67, 68, 79, 78
62, 68, 69, 80, 79
63, 69, 70, 81, 80



UNIVERSITY
OF
JOHANNESBURG

64, 70, 71, 82, 81
 65, 71, 72, 83, 82
 66, 72, 73, 84, 83
 67, 73, 74, 85, 84
 68, 74, 75, 86, 85
 69, 75, 76, 87, 86
 70, 76, 77, 88, 87
 71, 78, 79, 90, 89
 72, 79, 80, 91, 90
 73, 80, 81, 92, 91
 74, 81, 82, 93, 92
 75, 82, 83, 94, 93
 76, 83, 84, 95, 94
 77, 84, 85, 96, 95
 78, 85, 86, 97, 96
 79, 86, 87, 98, 97
 80, 87, 88, 99, 98
 81, 89, 90, 101, 100
 82, 90, 91, 102, 101
 83, 91, 92, 103, 102
 84, 92, 93, 104, 103
 85, 93, 94, 105, 104
 86, 94, 95, 106, 105
 87, 95, 96, 107, 106
 88, 96, 97, 108, 107
 89, 97, 98, 109, 108
 90, 98, 99, 110, 109
 91, 100, 101, 112, 111
 92, 101, 102, 113, 112
 93, 102, 103, 114, 113
 94, 103, 104, 115, 114
 95, 104, 105, 116, 115
 96, 105, 106, 117, 116
 97, 106, 107, 118, 117
 98, 107, 108, 119, 118
 99, 108, 109, 120, 119
 100, 109, 110, 121, 120



UNIVERSITY
 OF
 JOHANNESBURG

```
*Node
    122,      0.,      0.,      0.
*Nset, nset=bottom-1-RefPt_, internal
122,
*Elset, elset=bottom-1, generate
    1, 100, 1
*End Instance
**
*Instance, name=top-1, part=top
    0.0216,    0.077,    0.2
*Node
    1, -0.100000001, -0.100000001,    0.
    2, -0.0800000057, -0.100000001,    0.
    3, -0.0600000024, -0.100000001,    0.
    ....
*Element, type=R3D4
    1, 1, 2, 13, 12
    2, 2, 3, 14, 13
    3, 3, 4, 15, 14
    4, 4, 5, 16, 15
.....
*Node
    122,      0.,      0.,      0.
```

```

*Nset, nset=top-1-RefPt_, internal
122,
*Elset, elset=top-1, generate
1, 100, 1
*End Instance
**
*Nset, nset=Set-1, instance=bottom-1
122,
*Nset, nset=_PickedSet14, internal, instance=top-1
122,
*Nset, nset=_PickedSet15, internal, instance=bottom-1
122,
*Elset, elset=_PickedSurf9_SNEG, internal, instance=top-1, generate
1, 100, 1
*Surface, type=ELEMENT, name=_PickedSurf9, internal
_PickedSurf9_SNEG, SNEG
*Elset, elset=_PickedSurf10_S4, internal, instance=P200mmchannel152x76x18-1
1134, 1437, 1570, 2011, 2159, 2806, 4408, 4907, 4910, 4915
*Elset, elset=_PickedSurf10_S3, internal, instance=P200mmchannel152x76x18-1
543, 561, 802, 1095, 1114, 1336, 1475, 1477, 1478, 1680, 1684, 1703, 1705, 1805, 1860, 1982
1985, 1987, 1997, 2039, 2158, 2288, 2383, 2810, 2814, 3173, 3314, 3333, 3506, 3572, 3579, 3894
4089, 4901, 4905
*Elset, elset=_PickedSurf10_S1, internal, instance=P200mmchannel152x76x18-1
304, 1548, 1893, 2617, 2961, 3178, 3242, 3803, 3950, 4625, 4667, 4685, 4904
*Elset, elset=_PickedSurf10_S2, internal, instance=P200mmchannel152x76x18-1
1898, 4900, 4902
*Surface, type=ELEMENT, name=_PickedSurf10, internal
_PickedSurf10_S4, S4
_PickedSurf10_S3, S3
_PickedSurf10_S2, S2
_PickedSurf10_S1, S1
*Elset, elset=_PickedSurf11_SPOS, internal, instance=bottom-1, generate
1, 100, 1
*Surface, type=ELEMENT, name=_PickedSurf11, internal
_PickedSurf11_SPOS, SPOS
*Elset, elset=_PickedSurf12_S1, internal, instance=P200mmchannel152x76x18-1
1125, 1572, 1586, 2241, 2268, 2322, 2364, 3299, 3466, 3589, 4076, 4341, 4578, 4929
*Elset, elset=_PickedSurf12_S3, internal, instance=P200mmchannel152x76x18-1
527, 530, 647, 648, 650, 836, 840, 986, 1177, 1293, 1535, 1571, 1621, 1882, 1969, 2014
2028, 2676, 2746, 2954, 3268, 3304, 3597, 3817, 4770
*Elset, elset=_PickedSurf12_S4, internal, instance=P200mmchannel152x76x18-1
1044, 1996, 2323, 2569, 2684, 2765, 2865, 3027, 3179, 4024, 4267, 4342
*Elset, elset=_PickedSurf12_S2, internal, instance=P200mmchannel152x76x18-1
2022, 2029, 2277, 2336, 2398, 2482, 2879, 3747, 4457, 4593
*Surface, type=ELEMENT, name=_PickedSurf12, internal
_PickedSurf12_S1, S1
_PickedSurf12_S3, S3
_PickedSurf12_S4, S4
_PickedSurf12_S2, S2
*Elset, elset=_PickedSurf13_S4, internal, instance=P200mmchannel152x76x18-1
1088, 1143, 1199, 1314, 1421, 1425, 1505, 1516, 1520, 1521, 1533, 1555, 1598, 1700, 1710, 1714
1733, 1741, 1813, 1873, 1897, 1899, 2220, 2238, 2242, 2253, 2265, 2286, 2363, 2398, 2438, 2491
2660, 2676, 2745, 2820, 2848, 3026, 3050, 3051, 3070, 3071, 3194, 3203, 3215, 3239, 3247, 3249
3407, 3409, 3432, 3442, 3598, 3640, 3664, 3720, 3732, 3894, 3938, 3939, 3957, 3979, 3990, 3994
4022, 4085, 4187, 4200, 4304, 4392, 4404, 4555, 4577, 4600, 4602, 4615, 4635, 4636, 4644, 4653
4670, 4672, 4688, 4715, 4718, 4729, 4741
*Elset, elset=_PickedSurf13_S3, internal, instance=P200mmchannel152x76x18-1
453, 456, 479, 642, 1179, 1221, 1270, 1273, 1369, 1370, 1371, 1373, 1586, 1664, 1687, 1724
1807, 1811, 1849, 1913, 1914, 1926, 1992, 2017, 2046, 2245, 2256, 2258, 2277, 2319, 2321, 2324
2326, 2328, 2362, 2387, 2402, 2406, 2408, 2413, 2414, 2417, 2439, 2441, 2443, 2447, 2482, 2485

```

2609, 2824, 2861, 2866, 2873, 2879, 3009, 3022, 3038, 3041, 3045, 3054, 3059, 3107, 3141, 3145
 3156, 3169, 3183, 3199, 3201, 3207, 3211, 3213, 3220, 3237, 3244, 3251, 3267, 3281, 3426, 3466
 3473, 3625, 3627, 3629, 3631, 3645, 3673, 3682, 3685, 3689, 3699, 3703, 3709, 3725, 3763, 3765
 3766, 3914, 3947, 3971, 4007, 4024, 4028, 4044, 4168, 4184, 4224, 4265, 4269, 4273, 4276, 4279
 4296, 4325, 4338, 4340, 4606, 4613, 4659, 4661, 4665, 4679, 4680, 4689, 4702, 4708, 4723, 4740
 4832, 4889

*Elset, elset= _PickedSurf13_S1, internal, instance=P200mmchannel152x76x18-1

843, 1058, 1247, 1248, 1354, 1504, 1580, 1584, 1599, 1651, 1720, 1722, 1730, 1736, 1815, 1853
 1870, 1903, 1904, 1909, 1918, 1934, 2015, 2040, 2227, 2232, 2239, 2267, 2269, 2274, 2281, 2367
 2389, 2403, 2419, 2421, 2455, 2473, 2503, 2538, 2566, 2585, 2632, 2644, 2663, 2679, 2744, 2870
 2876, 3013, 3019, 3020, 3033, 3036, 3042, 3048, 3064, 3076, 3277, 3356, 3430, 3460, 3461, 3470
 3588, 3615, 3662, 3697, 3707, 3727, 3746, 3767, 3881, 3898, 3958, 3967, 3975, 3981, 4005, 4083
 4089, 4090, 4174, 4178, 4185, 4188, 4225, 4241, 4251, 4283, 4284, 4300, 4310, 4346, 4408, 4428
 4499, 4552, 4612, 4614, 4639, 4647, 4654, 4676, 4678, 4704, 4706, 4721, 4724, 4730, 4901, 4947

*Elset, elset= _PickedSurf13_S2, internal, instance=P200mmchannel152x76x18-1

47, 214, 932, 951, 1057, 1059, 1076, 1083, 1091, 1095, 1114, 1115, 1141, 1160, 1175, 1428
 1508, 1514, 1582, 1654, 1715, 1723, 1734, 1735, 1800, 1818, 1837, 1891, 1908, 1924, 1925, 1938
 2075, 2085, 2095, 2097, 2167, 2251, 2257, 2285, 2354, 2422, 2461, 2496, 2497, 2515, 2654, 2662
 2669, 2814, 2874, 2999, 3016, 3035, 3039, 3046, 3068, 3083, 3168, 3187, 3189, 3195, 3227, 3233
 3256, 3257, 3259, 3326, 3387, 3395, 3404, 3412, 3457, 3508, 3596, 3621, 3626, 3636, 3639, 3650
 3674, 3833, 3852, 3946, 3970, 3996, 4021, 4051, 4095, 4154, 4195, 4277, 4287, 4291, 4299, 4315
 4334, 4343, 4348, 4351, 4394, 4520, 4559, 4598, 4626, 4660, 4700, 4713, 4728, 4908, 4911, 4912
 4915, 4942, 4948

*Surface, type=ELEMENT, name=_PickedSurf13, internal

_PickedSurf13_S4, S4

_PickedSurf13_S3, S3

_PickedSurf13_S2, S2

_PickedSurf13_S1, S1

*Rigid Body, ref node=bottom-1.bottom-1-RefPt_, elset=bottom-1.bottom-1

*Rigid Body, ref node=top-1.top-1-RefPt_, elset=top-1.top-1

** Constraint: Constraint-1

*Tie, name=Constraint-1, adjust=yes, no thickness

_PickedSurf10, _PickedSurf9

** Constraint: Constraint-2

*Tie, name=Constraint-2, adjust=yes, no thickness

_PickedSurf12, _PickedSurf11

*End Assembly

**

** MATERIALS

**

*Material, name=Material-1

*Density

7800.,

*Elastic

2.097e+11, 0.3

*Plastic

2.00769e+08, 0.

2.07777e+08, 4.78548e-05

2.1456e+08, 9.57096e-05

2.21083e+08, 0.000143564

2.27337e+08, 0.000191419

2.33404e+08, 0.000239274

2.39227e+08, 0.000287129

2.44752e+08, 0.000334984

2.50023e+08, 0.000382838

2.55056e+08, 0.000430693

2.59839e+08, 0.000478548

2.64357e+08, 0.000526403

2.68647e+08, 0.000574258

2.72729e+08, 0.000622112

2.76592e+08, 0.000669967
2.80241e+08, 0.000717822
2.83673e+08, 0.000765677
2.86938e+08, 0.000813532
2.89977e+08, 0.000861387
2.92821e+08, 0.000909241
2.9547e+08, 0.000957096
2.97933e+08, 0.00100495
3.00194e+08, 0.00105281
3.02295e+08, 0.00110066
3.04227e+08, 0.00114851
3.05984e+08, 0.00119637
3.07608e+08, 0.00124423
3.09073e+08, 0.00129208
3.10429e+08, 0.00133994
3.1169e+08, 0.00138779
3.12833e+08, 0.00143564
3.1389e+08, 0.0014835
3.14853e+08, 0.00153135
3.15772e+08, 0.00157921
3.16623e+08, 0.00162706
3.17408e+08, 0.00167492
3.18156e+08, 0.00172277
3.18886e+08, 0.00177063
3.19587e+08, 0.00181848
3.20262e+08, 0.00186634
3.20872e+08, 0.00191419
3.21456e+08, 0.00196205
3.22014e+08, 0.0020099
3.22535e+08, 0.00205776
3.2303e+08, 0.00210561
3.2351e+08, 0.00215347
3.23968e+08, 0.00220132
3.24405e+08, 0.00224918
3.24832e+08, 0.00229703
3.2524e+08, 0.00234489
3.2562e+08, 0.00239274
3.25983e+08, 0.00244059
3.26335e+08, 0.00248845
3.26673e+08, 0.00253631
3.27001e+08, 0.00258416
3.27318e+08, 0.00263201
3.27632e+08, 0.00267987
3.27932e+08, 0.00272772
3.28229e+08, 0.00277558
3.28514e+08, 0.00282343
3.28776e+08, 0.00287129
3.29025e+08, 0.00291914
3.29271e+08, 0.002967
3.29511e+08, 0.00301485
3.2974e+08, 0.00306271
3.29966e+08, 0.00311056
3.30185e+08, 0.00315842
3.30399e+08, 0.00320627
3.30612e+08, 0.00325413
3.30822e+08, 0.00330198
3.31028e+08, 0.00334984
3.31286e+08, 0.00339769
3.31564e+08, 0.00344555
3.31838e+08, 0.0034934



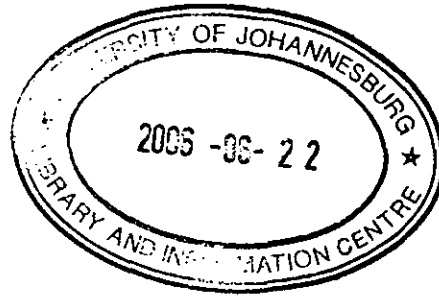
UNIVERSITY
OF
JOHANNESBURG

3.32109e+08, 0.00354126
3.3244e+08, 0.00358911
3.32709e+08, 0.00363696

```
** -----  
**  
** STEP: Step-1  
**  
*Step, name=Step-1, nlgeom=YES  
*Static  
1., 1., 1e-05, 1.  
**  
** BOUNDARY CONDITIONS  
**  
** Name: BC-1 Type: Displacement/Rotation  
*Boundary  
_PickedSet14, 1, 1  
_PickedSet14, 2, 2  
** Name: BC-2 Type: Displacement/Rotation  
*Boundary  
_PickedSet15, 1, 1  
_PickedSet15, 2, 2  
_PickedSet15, 3, 3  
_PickedSet15, 6, 6  
**  
** LOADS  
**  
** Name: Load-1 Type: Pressure  
*Dsload  
_PickedSurf13, P, 49.476  
**  
** OUTPUT REQUESTS  
**  
*Restart, write, frequency=1  
**  
** FIELD OUTPUT: F-Output-1  
**  
*Output, field, variable=PRESELECT  
**  
** HISTORY OUTPUT: H-Output-1  
**  
*Output, history  
*Node Output, nset=Set-1  
RF1, RF2, RF3, RM1, RM2, RM3  
*End Step  
** -----  
**  
** STEP: Step-2  
**  
*Step, name=Step-2, nlgeom=YES, inc=200  
*Dynamic,alpha=-0.05,haftol=100000.  
0.01,1.,1e-05,1.  
**  
** BOUNDARY CONDITIONS  
**  
** Name: BC-1 Type: Displacement/Rotation  
*Boundary  
_PickedSet14, 3, 3, -0.05  
**  
** OUTPUT REQUESTS  
**
```




```
*Restart, write, frequency=1
**
** FIELD OUTPUT: F-Output-1
**
*Output, field, variable=PRESELECT, frequency=1
**
** HISTORY OUTPUT: H-Output-1
**
*Output, history, frequency=1
*Node Output, nset=Set-1
RF1, RF2, RF3, RM1, RM2, RM3
*End Step
```



UNIVERSITY
OF
JOHANNESBURG